Thermal Conductivity Determination of Octadecane and Eicosane near Phase Transition for Solid Specimen Prepared Subject to Controlled Freezing and Explaining the "Anomalous" Measurements in Terms of Solid-Solid Transition

by

MD Shafkat Bin Hoque

A thesis submitted to the Graduate Faculty of
Auburn University
in partial fulfillment of the
requirements for the Degree of
Master of Science

Auburn, Alabama
August 4, 2018

Keywords: eicosane, octadecane, phase change, rotator phase, thermal conductivity, transient plane source technique.

Approved by

Jay M. Khodadadi, Chair, Professor of Mechanical Engineering
Roy Knight, Associate Professor of Mechanical Engineering
Daniel Harris, Associate Professor of Mechanical Engineering

Abstract

The effects of the freezing time and vacuum oven time (degasification time) associated with processing of two paraffins specimen, i.e. octadecane ($C_{18}H_{38}$) and eicosane ($C_{20}H_{42}$) on the temperature-dependent thermal conductivity in solid phase have been studied. Two distinct freezing routes, i.e. ice-water and liquid nitrogen routes have been utilized to control the freezing time of eicosane and octadecane specimen (melting temperatures of 37 ^{o}C and 26.5 ^{o}C, respectively) in a novel experimental setup. Four vacuum oven times (0, 5, 10 and 20 hours) have been utilized during the preparation process of the two materials for both freezing routes. In order to relate the rate of progress of the freezing front to the freezing time, a one-dimensional heat transfer model associated with the proposed experimental configuration was developed. The freezing/solidification time of the octadecane and eicosane specimen initially decreases with the vacuum oven time until 10 hours is reached, after which it increases for both processing routes. Theoretical predictions of the dimensionless thickness of the solidifying specimen (ε^{+}) as a function of t^{+} were generally in great agreement with the visually-observed quantities. Thermal conductivity of the solid octadecane specimen from 11.5 ^{o}C to 24.8 ^{o}C and eicosane specimen from 20.9 ^{o}C to 35.5 ^{o}C are evaluated for samples prepared following the ice-water and liquid nitrogen routes and all vacuum oven times by means of the transient plane source method. Thermal conductivity of both paraffins associated with the liquid nitrogen route are smaller than the ice-water route in most cases, however deviation of this behavior is recorded for nearly all vacuum oven times. Thermal conductivity of octadecane and eicosane exhibited enhanced values for both ice-water and liquid nitrogen routes and four degasification times as the temperatures of the specimen nears the solid-liquid phase transition points. This behavior recorded for both eicosane and octadecane is explained by inclusion of solid-solid phase transition characterized by possession of a greater thermal conductivity than the solid phase just below the solid-liquid phase transition in a computational model of the simplified transient hot-wire method by utilizing the ANSYS Fluent code. The greater thermal conductivity associated with the solid-solid phase transition causes the thermal conductivity to ascend with respect to temperature before the solid-liquid phase transition point similar to the climb in the experimental results of both octadecane and eicosane proving that rotator phase can be responsible for the recorded trends.

Acknowledgments

First of all, I would like to express my sincerest gratitude to Professor Jay M. Khodadadi for his guidance and mentorship during my graduate study at Auburn University. I would also like to thank Professors Daniel Harris and Roy Knight for serving on my MS thesis committee.

I want to thank the US Department of Energy for financially supporting my research under Grant No: DE-SC0002470. I appreciate the financial support provided by the Department of Mechanical Engineering of Auburn University in the form of teaching assistantship.

I also want to thank Mahdi Nabil, Rabih Al Ghossein and Dr. Naseem Ansari for their advice. The advice of Dr. Ansari helped me in my computational modeling of the role of the rotator phase on thermal conductivity. Mr. Nabil and Mr. Al Ghossein provided their assistance during various stages of my thesis and I am grateful for that.

A portion of the experimental part of my thesis was completed at the Chemistry and Biochemistry Department of Auburn University. I want to thank Dr. Jimmy Mills and his graduate students for allowing me to use their lab space and instruments. Dr. Thomas Burch of the Mechanical Engineering Department of Auburn University provided me an anemometer during the experimental part of my thesis and I appreciate his help very much.

I also want to acknowledge the contributions of my lab mates: Dourna Jamshideasli, Yi Zeng, Wenwen Ye, and Egemen Caglar. They have all helped me at various stages of my thesis. Lastly, I would also like to thank my family members for their support throughout my graduate education at Auburn University.

Finally, permissions were obtained for all artworks reproduced from prior published work of others.

Table of Contents

List of Tables

List of Figures

List of Abbreviations

AFM	Atomic Force Microscope
DSC	Differential Scanning Calorimetry
FTIR	Fourier Transformation Infrared Spectroscopy
GNP	Graphite Nanoplatelet
OS	Oleoyl Sarcosine
PA	Palmitic Acid
PCM	Phase Change Materials
PW	Paraffin Wax
SEM	Scanning Electron Microscope
SS	Steady State
TEM	Transmission Electron Microscope
TES	Thermal Energy Storage
THW	Transient Hot Wire
TPS	Transient Plane Source

List of Symbols

a	Radius of the Wire, m
b	Radius of the Cylidrical Bar, m
C_p	Specific Heat, J/kgK
D_h	Hydraulic Diameter, m
g	Gravitational acceleration, m/s^2
G	Heat Generation inside the Wire, W/m^3
h	Heat Transfer Coefficient, W/m^{2}K
H	Initial Thickness of the Processed Liquid Sample, m
k	Thermal Conductivity, W/mK
l	Length, m
L_f	Latent Heat or Heat of Fusion, J/kg
Nu	Nusselt Number, i.e. $\frac{hl}{k_{fluid}}$
Pr	Prandtl Number, i.e. $C_p\mu / k$
q	Strength of the Heat Source, W/m
r	Radius, m
Ra	Rayleigh Number, i.e. $\frac{g\beta(T_{Surface}-T_{sink})l^3}{\nu\alpha}$
Re	Reynolds Number, i.e. uD_h / ν
t	Time, sec

t^+	Non-dimensional Freezing Time, Defined by Equation 3.2d
t_{TPS}	Heating Time Period in the Transient Plane Source Method, sec
T	Temperature, ^{o}C or K
u	Velocity of the Hot Air Flow, m/s

Greek Symbols

α	Thermal Diffusivity, m^2/s
β	Volumetric Thermal Expansion Coefficient, K^{-1}
ε^+	Non-dimensional Thickness of the Solidifying Layer of the Specimen, Defined by Equation 3.2c
ε_T	Difference Between the Melting and Initial Temperatures ($T_m - T_i$), ^{o}C
ε'_T	Difference Between the Rotator Phase and Initial Temperatures ($T_R - T_i$), ^{o}C
μ	Dynamic Viscosity, $N.s/m^2$
v	Kinematic Viscosity, m^2/s
ρ	Density, kg/m^3
τ_m	Time Instant When Solid Eicosane Adjacent to the Wire Starts to Melt, sec
τ_p	Time Duration of Heat Discharge of the Hot Wire, sec

Subscripts

I	Initial
l	Liquid
m	Melting
R	Rotator Phase

s	Solid
w	Wire

Chapter 1 Introduction

1.1 Background, Objectives and Motivation of the Current Thesis

Throughout the latter half of the last century, fossil fuels especially coal and oil were the major sources of energy around the world. Such levels of consumption of fossil fuels have not slowed down. For example, according to Hawken (2010) between 2000 and 2008, 20 percent of all the oil consumed since its discovery in 1856 was burned (240 billion barrels). Extensive use of the fossil fuels for energy production are not without drawbacks. In recent years, across the globe much attention has been focused on the adverse effects of utilization of fossil fuels on human health and the environment. Moreover, the continued usage of fossil fuels to meet the increasing energy demand of everyday life has caused significant depletion in the existing fossil fuel reserves and greater release of waste heat to the environment (Papapetrou et al., 2018). Due to these reasons, there has been a constant rise in the demand for renewable sources of energy over the last few decades. However, the problems associated with the renewable energy sources, especially solar and wind energy are their low efficiencies and unpredictable output. Cost-effective, robust and environment-friendly energy storage can be a possible solution to the uncertainty associated with the output of these renewable energy sources and thermal energy storage (TES) has been established as a crucial part of the available energy storage processes in recent years (Rathod and Banerjee, 2013).

Physical and chemical processes are the two general approaches that can be used for storing thermal energy as exhibited in Figure 1.1 (Mehling and Cabeza, 2008). Physical processes work by varying the temperature of the system (sensible heat storage) or by phase transition (latent heat storage) (Mehling and Cabeza, 2008, Nabil, 2013, Al Ghossein, 2015). Chemical processes work by transformation of material structures at the molecular level influenced by outside factors in order to absorb or release energy (Al Ghossein, 2015). One important consideration is that both the physical and chemical processes must be reversible to store thermal energy (Mehling and Cabeza, 2008). One advantage of latent heat storage systems is that they possess greater storage density in contrast to sensible heat storage systems and are therefore preferable (Rathod and Banerjee, 2013, Fang et al., 2015, Zalba et al., 2003, Sharma et al., 2009).

In recent years, phase change materials (PCM) have been widely studied for latent heat storage. Sharma et al. (2009) provided a detailed categorization of the currently-used phase change materials as exhibited in Figure 1.2. Rathod and Banerjee (2013) carried out a review study of various phase change materials and stated that paraffins (C_nH_{2n+2}) possess several preferable properties including high latent heat, no supercooling, and chemical stability in contrast to other PCM. Because of these reasons, in the present research project, we have chosen two n-alkanes, namely eicosane ($C_{20}H_{42}$) and Octadecane ($C_{18}H_{38}$). However, one of the main problems associated with the use of paraffins for latent heat storage is their low thermal conductivity (Rathod and Banerjee, 2013). Because of this reason, a great number of researchers have used thermal conductivity promoters with paraffins to remedy this shortcoming (Table 1.1). However, to date very few studies have been found where the effect of the cooling rate applied during solid sample preparation on the thermal conductivity of phase change materials were investigated.

In the present study, a scheme of controlling the cooling rate during solidification of specimen was explored and a mathematical model was developed to relate various parameters relevant to freezing of a phase change material following a one-dimensional (1-D) heat transfer route. Freezing time and thermal conductivity of eicosane and octadecane were studied experimentally for four different vacuum oven heating periods (0, 5, 10 and 20 hours) and two different solidification processes. A possible rationale was also provided to explain the "anomalous" enhanced thermal conductivity measurements observed close to the melting temperatures of the paraffins utilized.

1.2 Short overview of the current investigation

Chapter one referred to the objectives, inspiration and background of the thesis. In chapter two, ten publications are reviewed to establish the state-of-the-art on how the thermal conductivities of pure eicosane and octadecane vary with temperature. Chapter three covers the details of the experimental study including description of the experimental setup and instruments, sample preparation procedure and a 1-D model. Thermal conductivity measurement techniques are then discussed in general and special focus is placed on the adopted TPS method. Analysis of the experimental thermal conductivity results and the validity of the adopted processing approach are also provided at the end of chapter three. In chapter four, the results obtained from a numerical model are presented to provide an explanation for the observed "anomalous" enhancement of thermal conductivity near the melting points of eicosane and octadecane. Finally, chapter five contains the synopsis and key findings of the thesis.

Table 1.1. Four types of thermal conductivity promoters (nanowire, nanoparticles, nanotubes and nanoplatelets) applied by researchers with paraffins (C_nH_{2n+2}) taken from ten different studies.

Authors	Thermal conductivity promoters	Paraffins
Fan (2011)	Copper oxide (CuO) nanoparticles	Cyclohexane (C_6H_{12}) and eicosane ($C_{20}H_{42}$)
Nabil and Khodadadi (2013)	Copper oxide (CuO) nanoparticles	Eicosane ($C_{20}H_{42}$)
Al Ghossein (2015)	Silver (Ag) nanoparticles	Eicosane ($C_{20}H_{42}$)
Wang et al. (2009)	Multi-walled carbon nanotubes (MWNTs)	Paraffin wax (PW)
Wang et al. (2010a)	Al_2O_3 nanoparticles	Paraffin wax (PW)
Angayarkanni and Philip (2015)	Copper nanowire, multiwalled carbon nanotubes and graphene nanoplatelets	n-hexadecane ($C_{16}H_{34}$)
Fang et al. (2013)	Graphene nanoplatelets (GNPs)	Eicosane ($C_{20}H_{42}$)
Motahar et al. (2014)	Mesoporous silica ($MPSiO_2$) nanoparticles	n-octadecane ($C_{18}H_{38}$)
Ho and Gao (2009)	Al_2O_3 nanoparticles	n-octadecane ($C_{18}H_{38}$)
Águila et al. (2018)	Copper oxide (CuO) nanoparticles	Octadecane ($C_{18}H_{38}$)

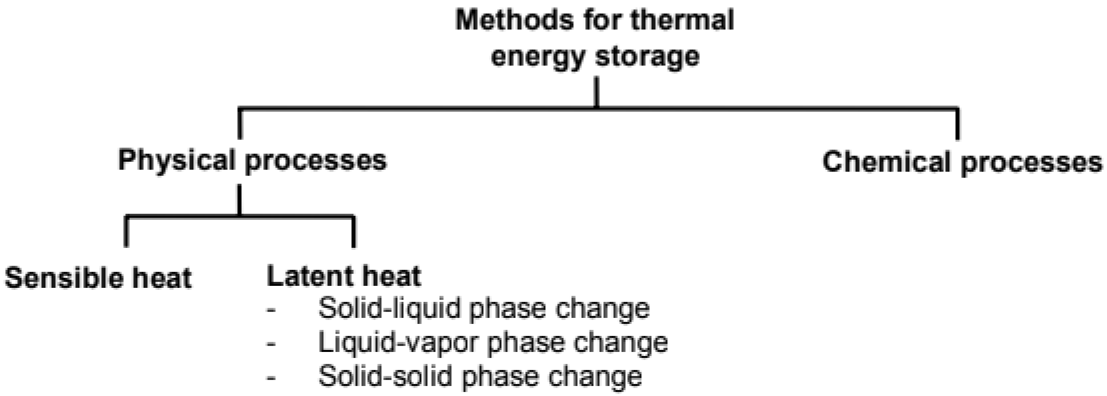

Figure 1.1. Different techniques that are used for storing of thermal energy (Mehling and Cabeza, 2008).

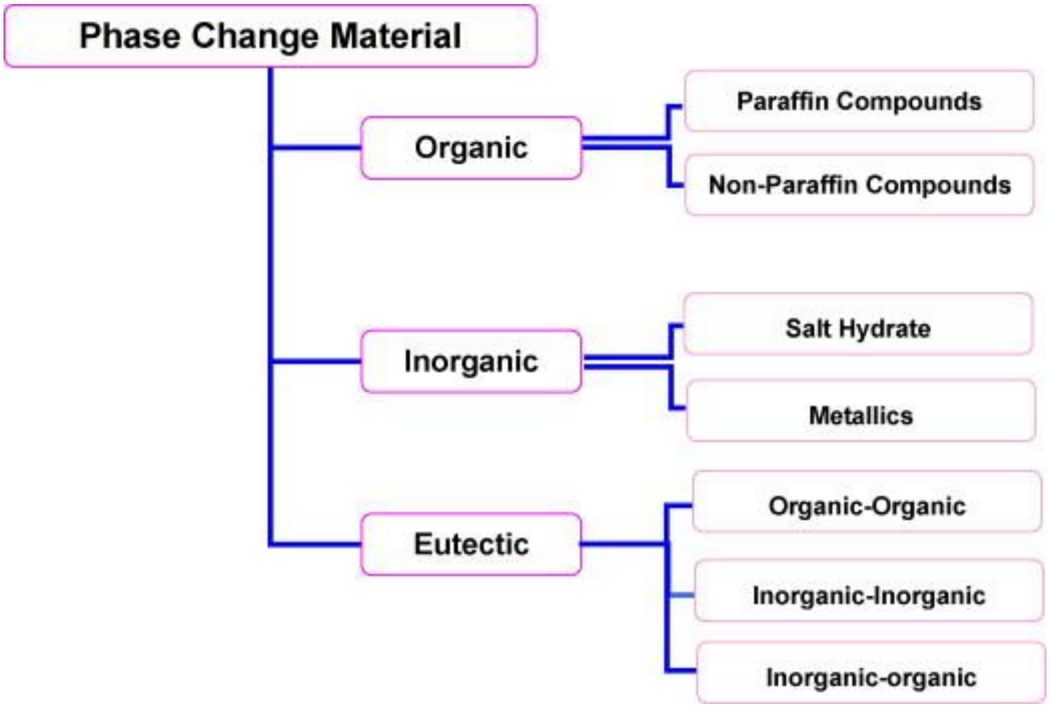

Figure 1.2. Detailed categorization of the currently-used phase change materials (Sharma et al., 2009).

Chapter 2 Review of Previous Publications on the Thermal Conductivity of Octadecane and Eicosane in Liquid and Solid Phases Determined Using the Transient and Steady-State Methods

This Chapter specifically emphasizes reviewing 11 publications that investigated various thermophysical properties of pure octadecane, eicosane and their composites including nanoadditives in both liquid and solid phases. Among the many properties discussed in these papers, we have given significant importance to the temperature-dependent thermal conductivity of pure octadecane and eicosane in their solid state near the phase transition temperature. At the end of the chapter, three tables have been prepared to compile the findings from different publications regarding the dependence of thermal conductivity of octadecane and eicosane with respect to temperature.

2.1 Previous publications on the thermal conductivity of octadecane and eicosane with respect to temperature in both liquid and solid phases determined using the transient and steady-state methods

Powell et al. (1961) used a guarded-plate instrument to measure the thermal conductivity of entrapped air-free n-octadecane (Eastman Kodak Co., Kodak Limited) samples with two different thicknesses (2 and 3 mm) in both liquid and solid states. The thermal conductivity values determined for two thicknesses were similar and based on this, the authors concluded that the instrument could be used to evaluate the thermal conductivity of any material in liquid state and noticeable molecular orientation was not present.

Griggs and Yarbrough (1978) studied the thermal conductivity values of 95% pure n-hexadecane ($C_{16}H_{34}$), n-nonadecane ($C_{19}H_{40}$), 99% pure n-heptadecane ($C_{17}H_{36}$), n-eicosane ($C_{20}H_{42}$) and n-octadecane ($C_{18}H_{38}$) using two different measurement systems based on the steady-state methods. The first thermal conductivity measuring system (TCMS1) (Dyer and Griggs, 1975, Dyer, 1975) was applied to investigate the cases of solid hexadecane and nonadecane, while system two (TCMS2) (Mehlon, 1977, 1979a, 1979b) was applied to investigate heptadecane, eicosane, and octadecane. In both thermal conductivity measuring systems, conductivity values of the samples were calculated utilizing the Fourier's law and the errors in the results were ± 20% and ± 30% for TCMS1 and TCMS2, respectively. The TCMS1 approach produced a thermal conductivity value of 0.265 W/mK at 273.9 K for n-nonadecane, while TCMS2 produced values of 0.209 W/mK and 0.375 W/mK at 293 K for n-heptadecane and n-eicosane, respectively.

Yarbrough and Kuan (1983) experimentally evaluated temperature-dependent thermal conductivity values of five paraffins in their solid phase using a steady-state method. The following paraffins (C_nH_{2n+2}) were examined in this study: tetradecane ($C_{14}H_{30}$), pentadecane ($C_{15}H_{32}$), heptadecane ($C_{17}H_{36}$), octadecane ($C_{18}H_{38}$) and eicosane ($C_{20}H_{42}$). The authors utilized an unguarded radial heat-flow instrument where the annular space between a copper tube (inner radius 0.00997 m, span 0.80 m) and a stainless steel tube (outer radius 0.003175 m, span 0.84 m) was filled with 99% pure liquid samples. The temperature difference across the solidified sample in the annular space was measured using eleven thermocouples and the uncertainty related to this measuring process was the main cause of experimental uncertainty which ranged up to ±14%. The results revealed that for all five paraffins, thermal conductivity values changed proportionally with the number of carbon atoms and inversely with temperature.

Similar to Griggs and Yarbrough (1978) and Yarbrough and Kuan (1983), Stryker and Sparrow (1990) carried out an experimental study on the properties, i.e. thermal conductivity, density and solid-liquid phase transition temperature of solid eicosane ($C_{20}H_{42}$) utilizing the steady-state method. The authors utilized a spherical cell (inside diameter of 0.0762 m and outside diameter of 0.1524 m) where the solidification of 99% pure liquid eicosane took place in the annular space across which the temperature difference was measured. A vacuum pump was utilized in order to create vacuum during eicosane sample preparation process and it was revealed that the thermal conductivity did not exhibit alterations with respect to temperature for samples prepared without vacuum, whereas opposite of this behavior was recorded for samples prepared applying vacuum. The authors also recorded that the density of the samples prepared applying vacuum changed without any pattern with respect to solidification temperature and due to the existence of extra voids possessed a smaller value in contrast to the samples prepared without vacuum which did not exhibit alterations with respect to solidification temperature.

Ho and Gao (2009) prepared nanofluids by emulsifying Al_2O_3 nanoparticles (Nanotech, Kanto Chemical Co. Inc., JAPAN) at 5 and 10 wt% loadings in liquid n-octadecane (solid-liquid phase transition point of 26.5 ^oC, Zeeland Chemicals, USA) using sonication to study their latent heat, density, phase transition behavior, dynamic viscosity and thermal conductivity. Utilization of a Decagon Devises KD2 thermal analyzer (Pullman, WA) for determining the thermal conductivity of pure octadecane and nanofluids revealed that a non-linear relation existed between the registered values of the thermal conductivity and Al_2O_3 nanoparticle concentrations (Figure 2.1). It was noticed from differential scanning calorimetry (DSC) analysis that the solid-liquid phase transition points remained almost constant despite addition of nanoparticles. While with the addition of

Al_2O_3 nanoparticles, density and viscosity of the nanofluids rose, the latent heat of fusion dropped when compared to pure octadecane.

Nabil and Khodadadi (2013) prepared dispersions of eicosane (solid-liquid phase change temperature 37 ^oC) and CuO nanoparticles (radius 2.5~7.5 nm, Clary and Mills, 2011), subjected the dispersions to three separate paths of freezing and studied the thermal conductivity of the eicosane-CuO nanocomposites with respect to temperature and nanoparticle concentrations. Utilizing sodium oleate ($C_{18}H_{33}O_2Na$) solely as a surfactant (Clary and Mills, 2011), 0, 1, 2, 3.5, 5, 6.5, 8 and 10 wt% of CuO nanoparticles were added to eicosane by means of stirring at 80 ^oC, prior to degasification at -40 kPa gage and 65 ^oC (Fan, 2011). After that, the first group of specimen was kept at the ambient temperature, the second group was kept on an ice-water bath layer and the last group was kept in an unplugged oven in order to achieve phase transition to solid from liquid subject to varying time durations. Application of the transient plane source (TPS) method revealed that while variation of temperature did not seem to have any influence on the thermal conductivity of the solid specimen below 33 ^oC, after this distinct temperature, thermal conductivity exhibited spikes (Figure 2.2 that shows data from samples prepared following the ambient temperature route). The authors also recorded that the thermal conductivity behavior was controlled by the solidification paths and for 3.5, 5, 6.5, 8 and 10 wt% specimen, this behavior was non-monotonic with respect to nanoparticle concentrations.

Fang et al. (2013) carried out a similar study as of Nabil and Khodadadi (2013) but with eicosane ($C_{20}H_{42}$) and graphene nanoplatelets (GNP). They utilized eicosane with purity greater than 99 wt% (TCI Co, Ltd, CHINA) and GNP with purity higher than 99.5 wt% (stated diameter of 5-10 µm, Chengdu Organic Chemicals Co., Ltd, CHINA) without any additional refinement. Both the eicosane and GNP were placed in a vacuum environment maintained at 105 ^oC for 12 hours before

GNP were dispersed in eicosane at 0, 1, 2, 5, and 10 wt% mass fractions by rigorous stirring at 60 ^{o}C for half an hour utilizing a hot plate magnetic stirrer, after which intensive sonication was used for 30 minutes. The authors used different instruments such as scanning electron microscope (SEM, Hitachi SU-70, Tokyo, JAPAN), transmission electron microscope (TEM, JEOL JEM-1230), differential scanning calorimeter (Netzsch DSC 200 F3, Selb, GERMANY) and atomic force microscope (AFM, Veeco Miltimode) to characterize the pure eicosane, pure GNPs, and the composite samples. Utilization of the transient plane source method with the help of a Hot Disk Thermal Constants Analyzer (TPS 2500S, Hot Disk AB, SWEDEN) for determining the thermal conductivity revealed that from 10 ^{o}C to 30 ^{o}C, the thermal conductivities of the samples did not change much with temperature (Figure 2.3). At higher mass fractions (5 and 10 wt%), the reason of the noticed change in thermal conductivity values with respect to temperature might be the higher degree of uncertainties related to the method of sample preparation. As the temperature became closer to the melting temperatures, the thermal conductivity values of all samples increased remarkably (Figure 2.4). For different mass fractions, these increases were parallel indicating that the spike in thermal conductivity was linked to the solid eicosane component of the composites. The authors attributed this to the change of crystalline structures and increased molecular vibrations when the solid-liquid phase change becomes imminent.

Motahar et al. (2014) studied two thermophysical properties, i.e. thermal conductivity and viscosity of octadecane/MPSiO$_2$ nanocomposites prepared by dispersing mesoporous silica (MPSiO$_2$) nanoparticles (size 350±100 nm) in n-octadecane (99% pure, solid-liquid phase transition temperature 27.5 ^{o}C). To obtain the samples, MPSiO$_2$ nanoparticles of 1, 3 and 5 wt% loadings were mixed with degassed liquid octadecane at 50 ^{o}C, followed by stirring and sonication. A thermal constants analyzer (TPS 2500, Hot Disk AB, SWEDEN) was utilized for determining the thermal conductivity of pure octadecane and composites in solid (5–25 °C) and liquid state (30–55 °C) at 5 °C temperature increments as exhibited in Figure 2.5. This instrument uses the transient plane source method and the results revealed that the relation between the thermal conductivity and the $MPSiO_2$ mass fraction for the solid and liquid states of the composite were non-monotonic and monotonic, respectively. The authors used a viscometer (LVDV-II+ Brookfield programmable viscometer, Middleboro, MA) to determine viscosity at three different temperatures (35 °C, 45 °C and 55 °C) and found that viscosity of liquid octadecane and composites descended with temperature and ascended with $MPSiO_2$ mass fraction.

Vélez et al. (2015) experimentally investigated several thermophysical properties such as thermal conductivity, thermal diffusivity, density, melting point, and latent heat of three 99% pure paraffins (n-hexadecane, n-octadecane and n-eicosane) obtained from Sigma-Aldrich (St. Louis, MO). The authors used a densimeter (Ludwig Schneider, Wertheim, GERMANY) to determine density, a transient multi-current hot wire technique (Vargaftik, 1975, Holmen et al., 2002, and Peñas et al., 2008, de Zárate et al., 2010, Assael et al., 1991) to determine the thermal conductivity and thermal diffusivity, and differential scanning calorimetry (DSC1 instrument, Mettler Toledo, Leicester, UNITED KINGDOM) technique for evaluating the melting and crystallization points, and heat of melting and crystallization. DSC analysis of all three paraffins revealed that while during solidification hexadecane and octadecane exhibited only liquid-solid phase transition, eicosane exhibited liquid-solid phase transition immediately followed by solid-solid phase transition because of its structural transformation after crystallization was complete (de Zárate et al., 2010, Briard et al., 2003, and Xie et al., 2008). It was noticed that thermal properties like the melting and crystallization points, heat of melting and crystallization of the examined paraffins depended on their number of carbon atoms and exhibited a direct proportionality relationship. While the reported thermal conductivity values of the solid state hexadecane ($C_{16}H_{34}$) and eicosane ($C_{20}H_{42}$) did not exhibit significant change before approaching the solid-liquid phase transition points, thermal conductivity values of solid octadecane ($C_{18}H_{38}$) and liquid hexadecane and eicosane reduced with raising of the measurement temperature.

Al Ghossein et al. (2017) used silver (Ag) nanoparticles as a thermal conductivity promoter with eicosane ($C_{20}H_{42}$) and studied the influences of temperature, nanoparticle mass fractions, and freezing time on the thermal conductivity behavior of the eicosane-Ag nanocomposites. In presence of Oleoyl Sarcosine (OS), 0, 1, 2, 3.5, 5, 6.5, 8 and 10 wt% of silver nanoparticles were dispersed in liquid eicosane solely by stirring (Darvin et al., 2016) followed by solidification in individual aluminum molds. First set of liquid specimen solidified on an ice-water bath, second set solidified at the room temperature and third set solidified in an unplugged oven with corresponding freezing times of 3 minutes, 30 minutes and 3 hours, respectively. Application of the transient plane source method clearly revealed that the change of thermal conductivity homogeneously matched the change of the registered freezing time and temperature for the specimen. One crucial discovery of this study was the sudden spike in the registered thermal conductivity in the 30-35 ^{o}C range for the eicosane and eicosane-Ag specimen (Figure 2.6 that shows data from samples prepared following the ambient temperature route). Differential scanning calorimetry analysis revealed that the experimental solid-liquid phase transition temperature of eicosane was 37 ^{o}C and it reduced by 0.2 ^{o}C, 0.5 ^{o}C, 1.1 ^{o}C, 1.5 ^{o}C, 1.9 ^{o}C, 2.5 ^{o}C, and 3.5 ^{o}C with 1, 2, 3.5, 5, 6.5, 8 and 10 wt% of silver nanoparticle concentrations, respectively. The experimentally-revealed latent heat value of eicosane was 241 J/g and reductions by 12, 33, 49, 64, 94, 107 and 162.7 J/g corresponding to 1, 2, 3.5, 5, 6.5, 8 and 10 wt% silver nanoparticle concentrations, respectively were noticed.

Águila et al. (2018) used ultrasonic stirring and sonication to disperse different concentrations (2.5, 5 and 10 w/v% denoted by the authors as the weight per volume fraction) of surface-modified CuO nanoparticles (radius 37.5 nm, density 6400 kg/m^3 (Bashirnezhad et al., 2015, Elsebay et al., 2016)) in 99% pure liquid Octadecane (solid-liquid phase change temperature 28-30 ^{o}C, Sigma-Aldrich, St. Louis, MO) to prepare three nanofluids. Use of sodium oleate as a stabilizer (Li and Chang, 2004) proved successful for 120 minutes during which viscosity and thermal conductivity values of the base PCM and nanofluids were determined. The authors utilized the transient hot-wire technique (THW) for determining the thermal conductivity values of nanofluids in the range 30–40 ^{o}C and pure octadecane in the range 30–50 ^{o}C. As observed in Figure 2.7, thermal conductivity values of the three examined nanofluids changed inversely with temperature and proportionally with CuO nanoparticle loadings. Viscosity determined by a Brookfield model DV2T-LV viscometer (Middleboro, MA) revealed that an inverse non-linear relation existed between viscosity and temperature for all three nanofluids and the base PCM.

2.2. Analysis and interpretation of the thermal conductivity data of octadecane and eicosane with respect to temperature collected from the reviewed publications

With the aid of the "GetData Graph Digitizer" software (http://getdata-graph-digitizer.com/), thermal conductivity data as a function of temperature of solid octadecane, liquid octadecane and solid eicosane were collected from different studies and summarized in Tables 2.1, 2.2 and 2.3, respectively. Thermal conductivity variations of solid octadecane, liquid octadecane and solid eicosane with respect to temperature collected from different studies determined by the transient and steady-state methods are also exhibited in Figures 2.8, 2.9 and 2.10, respectively. From Table 2.1 and Figure 2.8, it is observed that the thermal conductivity of solid octadecane adopted from five different studies differ widely with the lowest values exhibited by Powell et al. (1961). Table

2.2 and Figure 2.9 exhibit that the thermal conductivity of liquid octadecane adopted from five different studies differ widely with lowest values recorded by Ho and Gao (2009). From Table 2.3 and Figure 2.10, it is clear that unlike solid and liquid octadecane, thermal conductivity of solid eicosane adopted from seven different studies are in agreement with an enhancement recorded near the solid-liquid phase transition point (37 ^{o}C, Al Ghossein, 2015) by several authors.

2.3 Rationale behind the present investigation

Whereas Stryker and Sparrow (1990) stands out as a well-designed experiment in relation to solid sample preparation for their steady-state measurements, Nabil (2013) and Al Ghossein (2015) initiated their approach to process solid disk-like specimen for TPS-based determination of thermal conductivity. In the current investigation, we have studied the influence of the freezing time during preparation of the solid octadecane and eicosane specimen on the thermal conductivity with a specific focus near the solid-liquid phase transition. The measurements were performed using the transient plane source method and the experimental results were generally found to be consistent with the results from the reviewed publications as exhibited in the later part of the thesis. Specific new findings in relation to the proposed solid specimen processing approach will be highlighted.

Table 2.1 Thermal conductivity values of solid octadecane (melting temperature of 26.5 ^oC, Ho and Gao, 2009) with respect to temperature reported in five different studies inspected using both the transient and steady-state methods.

	Powell et al. (1961)	**Griggs and Yarbrough (1978)**	**Yarbrough and Kuan (1983)**	**Motahar et al. (2014)**	**Vélez et al. (2015)**
Thermal conductivity method	N/A	SS	SS	TPS	THW
Temperature (^oC)	*k* (W/mK)	*k* (W/mK)	*k* (W/mK)	*k* (W/mK)	*k* (W/mK)
-14.05					0.361
-11.58					0.359
-9.11					0.358
-6.65					0.354
-4.18					0.347
-1.71					0.338
-0.47					0.327
0.45					0.344
3.23					0.329
3.05			0.340		
5				0.374	
5.7					0.329
6.52			0.329		
8.17					0.335
9.21	0.195		0.328		
9.33					
10				0.373	
10.642					0.324
11.73			0.326		
13.11					0.319
14.68			0.318		
15				0.369	
15.88					0.317
16.11	0.193				
20		0.374		0.365	
21.08	0.189				
21.66	0.2				
23.97	0.191				
24.26	0.197				
25		0.358		0.37	

Table 2.2 Thermal conductivity of liquid octadecane (melting temperature of 26.5 ^{o}C, Ho and Gao, 2009) with respect to temperature reported in five different studies using the transient methods.

	Powell et al. (1961)	**Ho and Gao (2009)**	**Motahar et al. (2014)**	**Vélez et al. (2015)**	**Águila et al. (2018)**
Thermal conductivity method	N/A	THW	TPS	THW	THW
Temperature (^{o}C)	*k* (W/mK)	*k* (W/mK)	*k* (W/mK)	*k* (W/mK)	*k* (W/mK)
30		0.129	0.153		
31.86	0.153				
35		0.129	0.151		0.141
35.318				0.149	
39.51	0.152				
40		0.129	0.151		0.132
40.24				0.149	
40.32	0.152				
41.14	0.152				
45		0.131	0.149		0.137
45.05					
49.75	0.152				
50		0.129	0.146		0.130
50.019				0.148	
54.96				0.147	
55		0.127	0.143		
59.41	0.151				
59.911				0.147	
60		0.121		0.147	
64.92				0.146	
69.9				0.146	
74.81				0.147	

Table 2.3 Thermal conductivity of solid eicosane (melting temperature of 37 ^{o}C, Al Ghossein, 2015) with respect to temperature reported in seven different studies inspected using both the transient and steady-state methods.

	Griggs and Yarbrough (1978)	**Yarbrough and Kuan (1983)**	**Stryker and Sparrow (1990) [Without vacuum, water bath]**	**Nabil and Khodadadi (2013) [Oven solidification route]**	**Fang et al. (2013)**	**Vélez et al. (2015)**	**Al Ghossein (2015) [Oven solidification route]**
Thermal conductivity method	SS	SS	SS	TPS	TPS	THW	TPS
Temperature (^{o}C)	*k* (W/mK)	*k* (W/mK)	*k* (W/mK)	*k* (W/mK)	*k* (W/mK)	*k* (W/mK)	*k* (W/mK)
-14.04						0.439	
-11.57						0.436	
-9.41						0.452	
-6.94						0.451	
-4.47						0.455	
-1.99						0.451	
0.79						0.448	
2.1		0.413					
3.26						0.439	
5.7		0.393					
5.73						0.443	
8.2						0.434	
9.65		0.392					
10				0.4505	0.414		0.4502
10.53			0.416				
10.68						0.439	
12.78		0.355					
12.84						0.428	
15				0.4528	0.403		0.4546
15.07			0.421				
15.62						0.425	
16.16		0.344					
18.09						0.414	
19.51		0.341					
19.69			0.421				
20	0.375			0.4597	0.3964		0.4554
20.56						0.388	
23.03						0.378	

24.59			0.421				
25	0.359			0.4513	0.388		0.4522
25.82						0.362	
27.98						0.335	
28.23			0.418				
30	0.339			0.4530	0.408		0.4533
31					0.437		0.4546
32				0.4519			0.4522
32.24			0.418				
33				0.4551	0.696		0.4551
33.75			0.414				
34	0.313			0.4789	1		0.4789
35				0.6317	1.392		0.6228

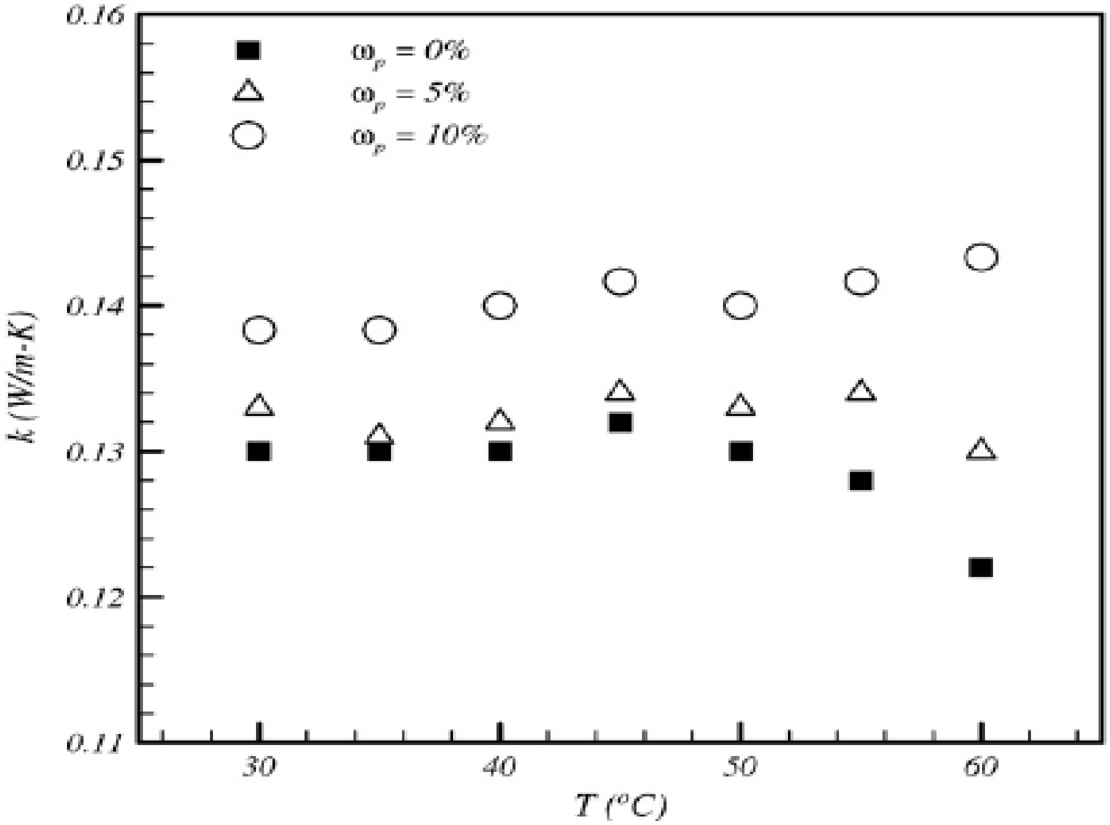

Figure 2.1. Temperature-dependent thermal conductivity of pure octadecane (melting temperature of 26.5 °C, Ho and Gao, 2009) and octadecane/Al_2O_3 nanofluids for two concentrations of Al_2O_3 nanoparticles determined by a Decagon Devises KD2 thermal analyzer (Ho and Gao, 2009).

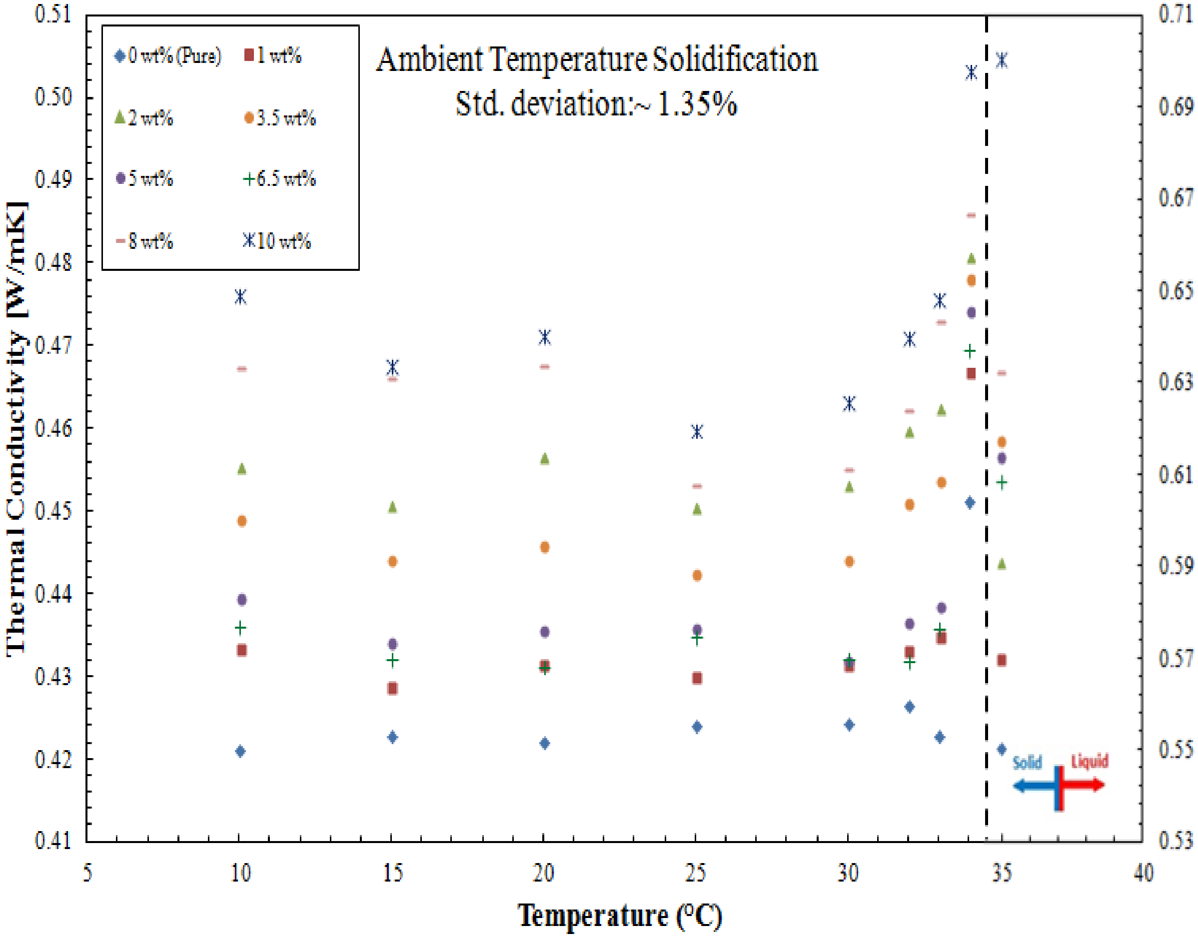

Figure 2.2. Thermal conductivity of eicosane-CuO specimen with respect to temperature for 0, 1, 2, 3.5, 5, 6.5, 8 and 10 wt% of CuO nanoparticles below the solid-liquid phase transition temperature determined by a Hot Disk Thermal Constants Analyzer (ambient temperature solidification path) (Nabil and Khodadadi, 2013).

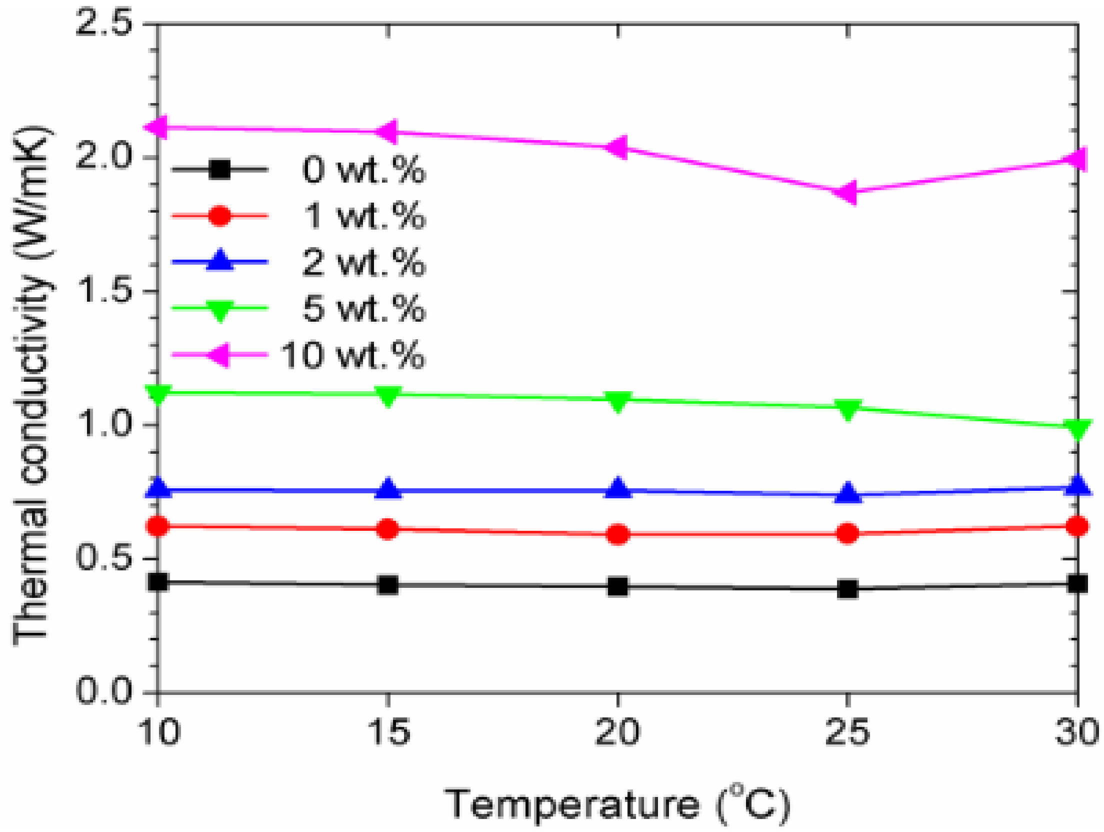

Figure 2.3. Temperature-dependent thermal conductivity of pure eicosane (melting temperature of 37 °C, Fang et al., 2013) and eicosane/GNP nanocomposites in their solid state for five mass fractions (0, 1, 2, 5, and 10 wt%) of GNP determined by the transient plane source technique (Fang et al., 2013).

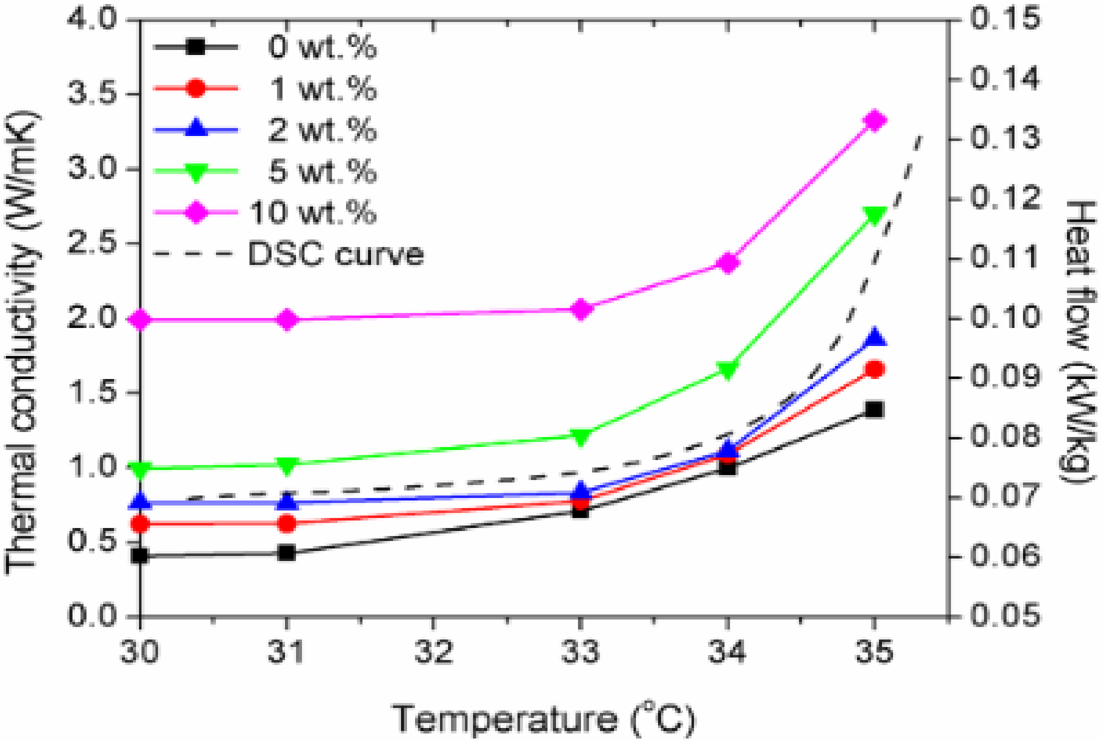

Figure 2.4. Temperature-dependent thermal conductivity of pure eicosane (melting temperature of 37 °C, Fang et al., 2013) and eicosane/GNP nanocomposites in solid state below the solid-liquid phase change temperature for five mass fractions (0, 1, 2, 5, and 10 wt%) of GNP determined by the transient plane source technique (Fang et al., 2013).

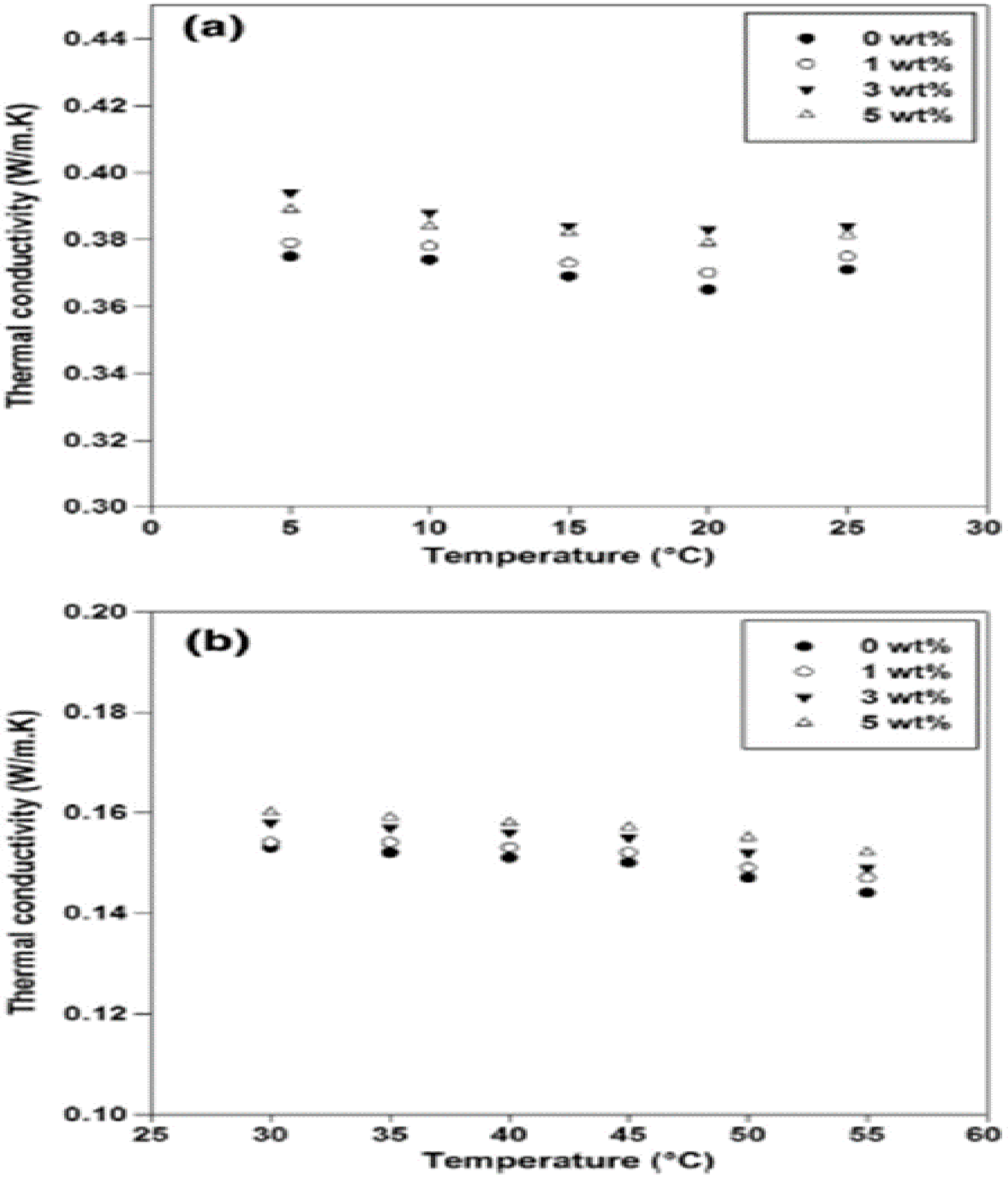

Figure 2.5. Temperature-dependent thermal conductivity of pure octadecane (melting temperature of 27.5 ^{o}C, Motahar et al., 2014) and octadecane/MPSiO$_2$ nanocomposite samples for three MPSiO$_2$ loadings in (a) solid state and (b) liquid state determined by the transient plane source technique (Motahar et al., 2014).

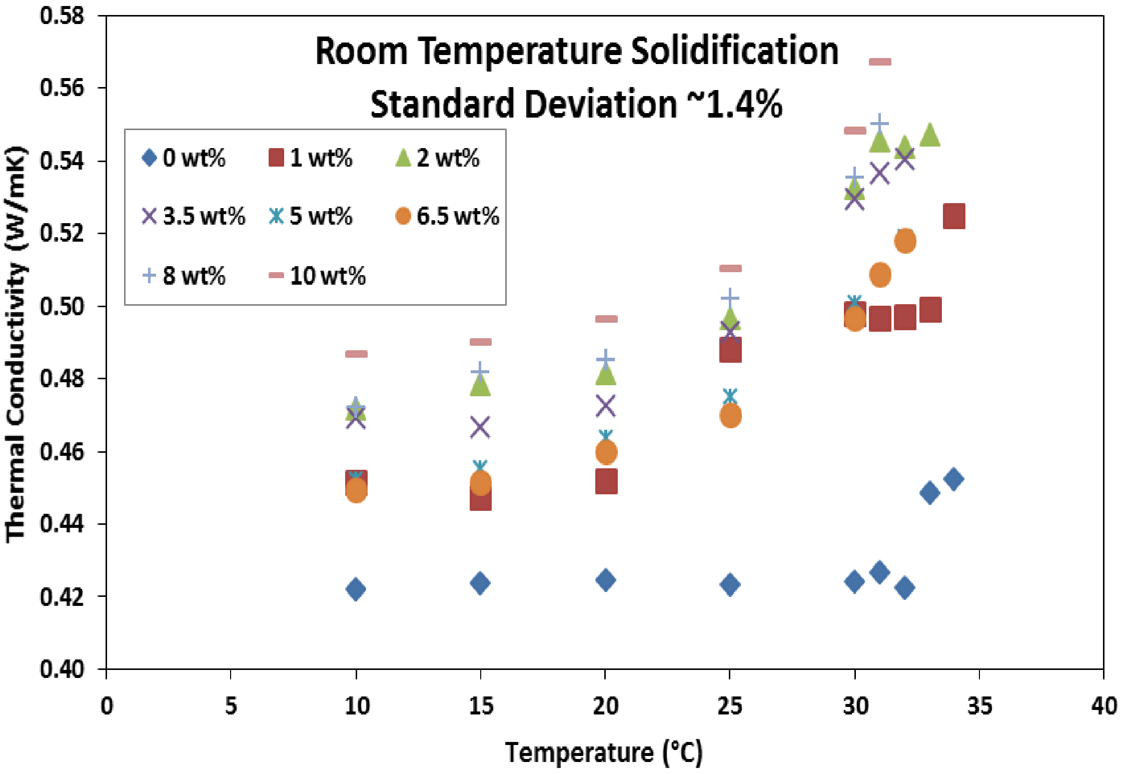

Figure 2.6. Temperature-dependent thermal conductivity of pure eicosane (melting temperature of 37 °C, Al Ghossein et al., 2017) and eicosane-Ag specimen for 0, 1, 2, 3.5, 5, 6.5, 8 and 10 wt% of silver nanoparticles below the solid-liquid phase transition temperature evaluated by a Hot Disk Thermal Constants Analyzer (Room temperature solidification) (Al Ghossein et al., 2017).

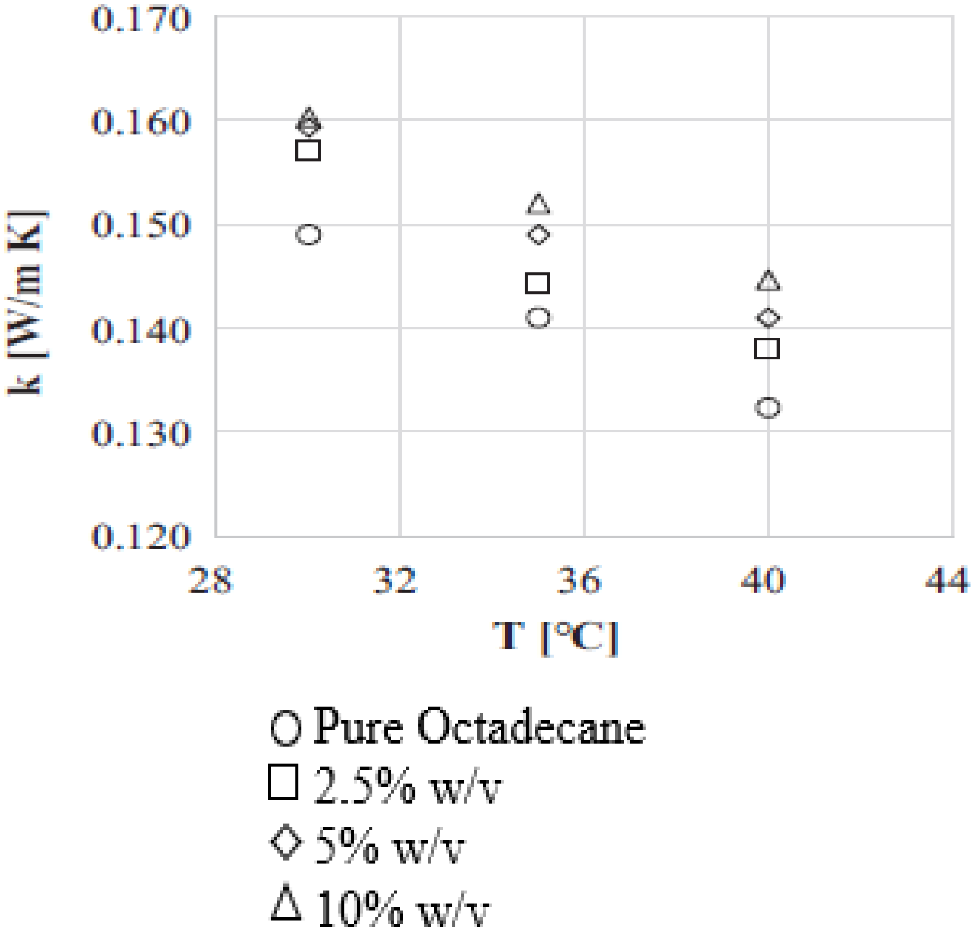

Figure 2.7. Temperature-dependent thermal conductivity of pure octadecane (melting temperature of 28-30 °C, Águila et al., 2018) and octadecane/CuO nanofluids for three concentrations (%w/v or weight per volume fraction) of CuO nanoparticles determined by the transient hot-wire technique (Águila et al., 2018).

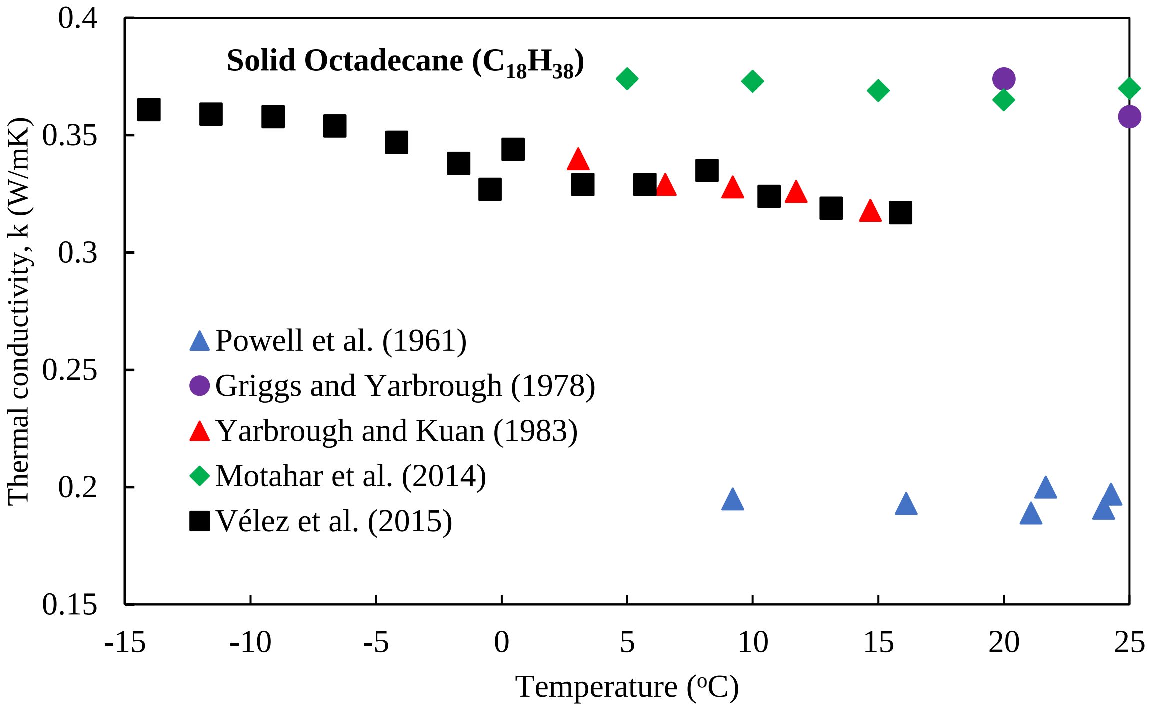

Figure 2.8. Temperature-dependent thermal conductivity of solid octadecane (melting temperature of 26.5 °C, Ho and Gao, 2009) adopted from five different studies using both the transient and steady-state methods.

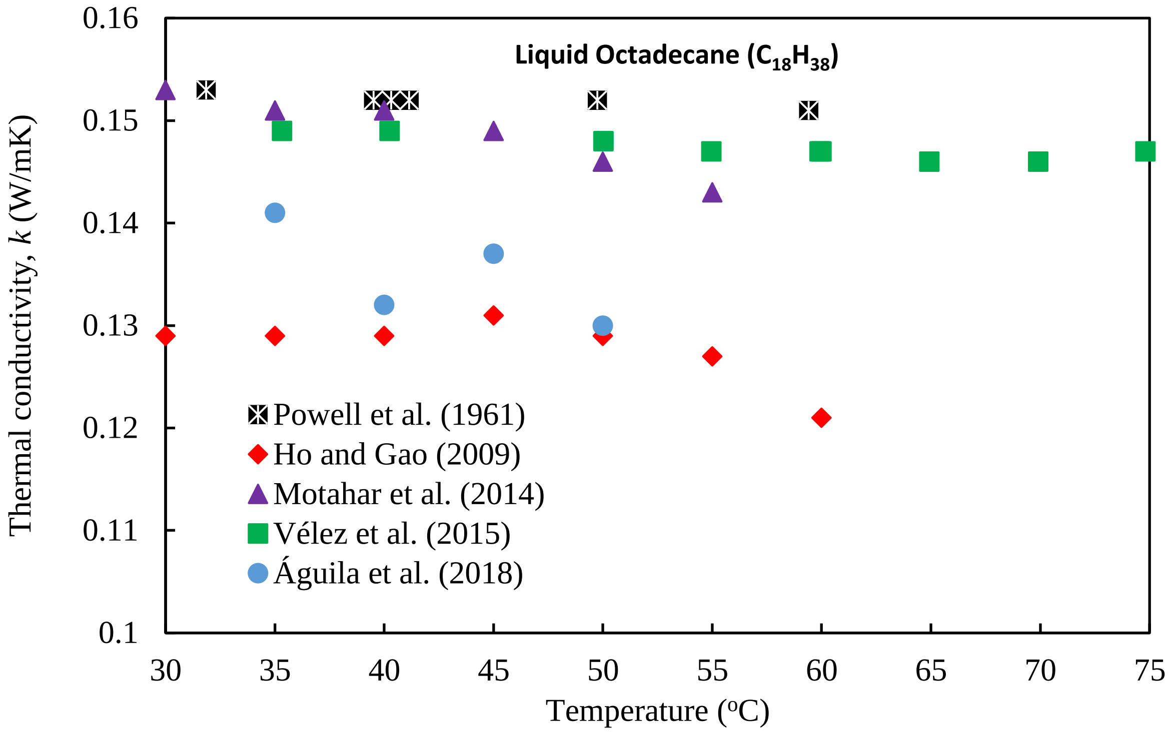

Figure 2.9. Temperature-dependent thermal conductivity of liquid octadecane (melting temperature of 26.5 °C, Ho and Gao, 2009) adopted from five different studies using various transient methods.

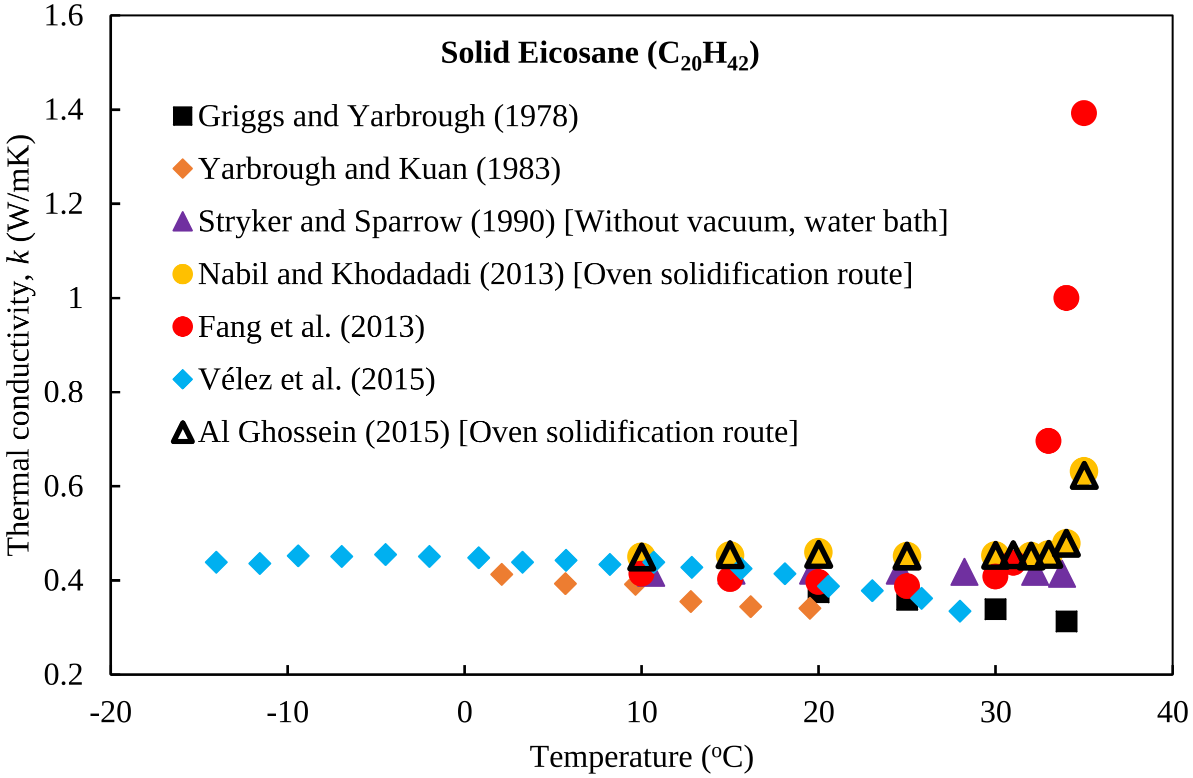

Figure 2.10. Temperature-dependent thermal conductivity of solid eicosane (melting temperature of 37 °C, Al Ghossein, 2015) adopted from seven studies using both transient and steady-state methods.

Chapter 3 Determination of Thermal Conductivity of Octadecane and Eicosane Solid Specimen Prepared under Controlled Freezing by Ice-Water and Liquid Nitrogen Routes

In this chapter, a specially-designed experimental setup utilized for preparation of solid disk-like specimen and the associated mathematical theory behind its operation are discussed. The procedures for sample preparation, description of the instruments and thermal conductivity measurement techniques are discussed in great detail. At the end of the chapter, experimental results of the current investigation are presented. Analysis and possible explanations of the trends of the experimental findings are also discussed at the end of this chapter.

3.1 Rationale for the adopted sample preparation route

Nabil (2013) stands out as the first study in which pairs of solid disk specimen were prepared to be processed for thermal conductivity measurements using the transient plane source method. In summary, composites of eicosane/copper oxide nanoparticles were prepared by stirring of the mixture at first with subsequent degasification (Fan, 2011) after which solidification/freezing of the nanocomposites was accomplished by subjecting the mixtures to three distinct freezing paths. These three paths were identified as firstly the ice-water bath solidification route, secondly the oven solidification route and thirdly the ambient solidification route. In effect, phase transition to solid specimen from liquid samples was achieved by varying the time durations of freezing for samples that underwent uncontrolled multi-dimensional solidification. Soon thereafter, Al Ghossein (2015) followed generally similar steps working with eicosane/silver nanoparticle mixtures which was stirred (Darvin et al., 2016) at first and then subjected to nearly identical three solidification paths as Nabil (2013) in order to prepare the solid specimen. These three distinct freezing approaches featured multiple paths of heat extraction from the liquid specimen and heat losses were possible in all directions. In order to maintain consistency during processing of octadecane and eicosane solid specimen in the current investigation, we have established a process similar to the ones applied by the above described researchers with certain exceptions aimed at facilitating utilization of a novel experimental configuration. In all three solidification routes utilized by Nabil (2013) and Al Ghossein (2015) in order to prepare the eicosane solid specimen, three possible heat transfer paths were present (Figure 3.1), whereas the experimental configuration of the current investigation ensured one-dimensional heat transfer during the preparation of octadecane and eicosane solid specimen.

3.2. Experimental setup utilized to control the freezing time of pure octadecane and eicosane solid specimen

The experimental setup that was utilized in order to control the freezing/solidification time of pure octadecane and eicosane solid specimen following a one-dimensional heat extraction scheme is given in Figure 3.2. A Holmes® heater (current: 12.5 amps, power: 1500 W, and voltage: 120 V, Jarden Consumer Solutions, Boca Raton, FL, as shown in Figure 3.3) (Holmes® Heater, Owner's Guide, 2013) was used for establishing hot air flow through a test-section (Figure 3.2a). A 10×10 inch and 22-inch-long cardboard box that served as the test-section was used to guide the hot air flow to the surrounding laboratory atmosphere. Aluminum molds containing molten composites were then placed on a copper stage cold-plate that coincided with the bottom wall of the test-section (Figure 3.2b) and were exposed to hot air stream flowing above. The air velocities and temperatures for various settings of the heater unit were recorded using an anemometer (Climate measuring instrument, probes and accessories, Testo Inc., Sparta, NJ) (Testo 480, Climate

Measuring Instrument, Instruction manual, 0970 4800 en 05 V01.05 en-GB and, testo, wheel measuring head 100 mm, application information, 0970 0473 en 01). The copper stage cold-plate served as part of the path for heat removal from the specimen to be discussed below. A dewar (Pope Scientific 8621, capacity of 1.9 L, depth of 0.19 m and height of 0.252 m) was utilized for storing liquid nitrogen or ice-water that served as the sink in the system (Figure 3.4). A vented wooden cap (diameter of 6 inch and width of 0.75 inch) utilized to cover the dewar had a center hole of 1.5 inch diameter (Figure 3.5) and a path was designed for nitrogen vapors to leave the dewar. Through this center hole, a copper rod of 1.5 inch diameter and 7.25 inch length (Figure 3.6) was utilized to transfer heat from the aluminum mold to the heat sink containing either ice-water or liquid nitrogen. The top end of the copper rod with greater diameter coincided with the bottom wall of the test-section and served as the stage for placing the aluminum molds. The dewar flask was supported independently from the test-section by using a robust cardboard box.

3.3. One-dimensional model utilized to derive relations between the dimensionless specimen thickness and associated freezing time of octadecane and eicosane solid specimen prepared using the ice-water and liquid nitrogen routes

A schematic diagram of the model of the multi-component heat extraction unit proposed here is shown in Figure 3.7. In summary, one-dimensional flow of heat from the high temperature of the wind tunnel (T_∞) to the low temperature of the cold liquid stored in the dewar ($T_{sink} < T_\infty$) is channeled through the PCM, aluminum and copper layers. Neglecting shrinkage of the PCM upon phase change, the PCM layer of thickness H is assumed to consist of two layers associated with the liquid (thickness of ($H - \varepsilon$)) and solid (time-varying thickness of ε) components. In Figure 3.7, symbols h_o, k_l, k_s, l_{Al}, k_{Al}, l_{Cu}, k_{Cu}, h_{sink}, ρ and L_f stand for constants that designate heat transfer coefficient of hot air flow above the solidifying PCM, thermal conductivity of liquid PCM, thermal conductivity of solid PCM, length of the aluminum layer, thermal conductivity of aluminum, length of the copper layer, thermal conductivity of copper, heat transfer coefficient of the sink, density of the PCM, and latent heat of the PCM, respectively.

Similar to Kreith (1967), through invoking a number of resistors in series (Figure 3.8), the expression of heat flowing between the two ends is:

$$\frac{q}{A} = \frac{T_{\infty} - T_{sink}}{\frac{1}{h_o} + \frac{L - \varepsilon}{k_l} + \frac{\varepsilon}{k_s} + \frac{l_{Al}}{k_{Al}} + \frac{l_{Cu}}{k_{Cu}} + \frac{1}{h_{sink}}} \quad (3.1)$$

The two resistors at the two ends are associated with heat convection to the media maintained at the two extreme temperatures, whereas the remaining resistors are based on conductive paths. We assume that the latent heat of freezing is far more dominant that the heat capacity of the subcooled solidifying layer. Siegel (1977) argues that this is valid if $L_f / (C_p(T_m - T_{sink}))$ is greater than 1.5. In our experiment, for the ice-water as the heat sink fluid and eicosane as the specimen, the value of $L_f / (C_p(T_m - T_{sink}))$ is 3.47. The heat flow rate responsible for extracting latent heat of fusion necessary for solidification is then given by:

$$\frac{q}{A} = \rho L_f \frac{d\varepsilon}{dt} \quad (3.2)$$

with the time derivative of variable thickness of the solidifying layer standing for the volume rate of solid formation per unit area. Effectively, the solid-liquid interface is at the melting point of the PCM (Kreith, 1967) and the top two resistors are negligible.

Combining relations (3.1) and (3.2) leads to:

$$\frac{T_m - T_{sink}}{\frac{\mathcal{E}}{k_s} + \frac{l_{Al}}{k_{Al}} + \frac{l_{Cu}}{k_{Cu}} + \frac{1}{h_{sink}}} = \rho L_f \frac{d\mathcal{E}}{dt}$$

$$\left(\frac{\mathcal{E}}{k_s} + \frac{l_{Al}}{k_{Al}} + \frac{l_{Cu}}{k_{Cu}} + \frac{1}{h_{sink}}\right) d\mathcal{E} = \frac{T_m - T_{sink}}{\rho L_f} dt$$

$$\frac{1}{h_{sink}}\left(1 + \frac{\mathcal{E}h_{sink}}{k_s} + \frac{l_{Al}h_{sink}}{k_{Al}} + \frac{l_{Cu}h_{sink}}{k_{Cu}}\right) d\mathcal{E} = \frac{T_m - T_{sink}}{\rho L_f} dt$$

We now introduce the dimensionless parameters M^+, P^+ and ε^+ defined as follows:

$$\frac{l_{Al}h_{sink}}{k_{Al}} = M^+ \tag{3.2a}$$

$$\frac{l_{Cu}h_{sink}}{k_{Cu}} = P^+ \tag{3.2b}$$

$$\frac{\mathcal{E}\, h_{sink}}{k_s} = \mathcal{E}^+ \tag{3.2c}$$

The last relation is the dimensionless thickness of the solidifying layer. Thus:

$$\frac{h_{sink}}{k_s} d\mathcal{E} = d\mathcal{E}^+,$$

$$d\mathcal{E} = \frac{k_s}{h_{sink}} d\mathcal{E}^+$$

$$\frac{1}{h_{sink}}(1 + M^+ + P^+ + \mathcal{E}^+)\frac{k_s}{h_{sink}} d\mathcal{E}^+ = \frac{T_m - T_{sink}}{\rho L_f} dt$$

The appropriate dimensionless time (t^+) then emerges as follows:

$$\frac{(T_m - T_{sink})h_{sink}^2}{\rho L_f k_s} t = t^+ \tag{3.2d}$$

$$\frac{(T_m - T_{sink})h_{sink}^2}{\rho L_f k_s} dt = dt^+$$

$$(1 + M^+ + P^+ + \mathcal{E}^+)d\mathcal{E}^+ = \frac{(T_m - T_{sink})h_{sink}^2}{\rho L_f k_s} dt$$

Leading to:

$$(1 + M^+ + P^+)d\mathcal{E}^+ + \mathcal{E}^+ d\mathcal{E}^+ = dt^+$$

Upon integrating from the start of heat extraction at initial time zero to any time instant t^+:

$$\int_0^{\mathcal{E}^+} (1 + M^+ + P^+)d\mathcal{E}^+ + \int_0^{\mathcal{E}^+} \mathcal{E}^+ d\mathcal{E}^+ = \int_0^{t^+} dt^+$$

$$(1 + M^+ + P^+)\mathcal{E}^+ + \frac{(\mathcal{E}^+)^2}{2} = t^+$$

$$(\mathcal{E}^+)^2 - 2t^+ + 2(1 + M^+ + P^+)\mathcal{E}^+ = 0$$

$$\mathcal{E}^+ = -(1 + M^+ + P^+) \pm \sqrt{(1 + M^+ + P^+)^2 + 2t^+}$$

At $t = 0$ there was only liquid PCM and solidification did not start yet, so the negative sign was not considered and the above equation becomes:

$$\mathcal{E}^{+} = -(\,1 + M^{+} \, + P^{+}) + \sqrt{(\,1 + \, M^{+} \, + P^{+})^{2} + 2t^{+}} \qquad (3.3)$$

We now introduce the following parameter that combines processing parameters associated with the heat sink, copper layer and aluminum layer:

$$S^{+} = 1 + M^{+} + P^{+}$$

Note that this parameter will always be greater than 1. During practical preparation of the specimen, one needs to evaluate this parameter. Appendix A of this thesis provides the highlights of the approach. For instance, the heat transfer coefficients for the hot air wind tunnel (h_o) and the liquid sink (h_{sink}) were estimated to be 1.778 W/m^2K and 401 W/m^2K for eicosane and ice-water route, respectively.

Finally, the dimensionless expression for dependence of the thickness of the solidifying layer (ε^{+}) on time (t^{+}) is:

$$\varepsilon^{+} = - S^{+} + \sqrt{(S^{+})^{2} + 2t^{+}} \qquad (3.4)$$

Variations of ε^{+} with t^{+} for different S^{+} values of 1, 2, 3, 4 and 5 are shown in Figure 3.9. With the aid of this model, one can predict the instantaneous thickness of the solidifying layer at any time instant. Conversely, starting with a known layer of liquid PCM, the time duration required for complete freezing of the specimen when $\varepsilon = H$ can be predicted. Appropriateness of this simple model in relation to observations of the proposed processing technique will be discussed later.

3.4 Preparation processes of pure octadecane and eicosane solid specimen

We obtained 99% pure eicosane ($C_{20}H_{42}$) and Octadecane ($C_{18}H_{38}$) from Sigma-Aldrich (St. Louis, MO) and used both materials without additional refinement in this study. The thermophysical properties of eicosane are as follows: melting temperature of 37 ^{o}C (Al Ghossein, 2015), solid volumetric mass density of 840 kg/m^3, liquid volumetric mass density of 789 kg/m^3, latent heat of 247.5 kJ/kg, and boiling point of 345.1 ^{o}C as adopted from Al Ghossein (2015), Al Ghossein et al. (2017) and Freund et al. (1982). Following properties of Octadecane have been adopted from Vélez et al. (2015), Ho and Gao (2009): melting point of 26.5 ^{o}C, and latent heat of 243.68±0.096 kJ/kg. To prepare the eicosane and octadecane solid samples, similar processes used by Al Ghossein (2015) and Nabil (2013) were followed with certain changes that were intended to lead to samples prepared following the proposed current one-dimensional heat extraction process. These materials are in solid state at room temperature and were melted by raising the temperature by means of a Hotplate/Stirrer (VWR, Randor, PA, current: 10 amps, power: 1000 W). Liquid samples of both materials were kept at 80 ^{o}C for 30 minutes (Figure 3.10a) and then poured in Aluminum molds (diameter 0.0254 m and height 0.009525 m) containing aluminum foils (VWR International, Randor, PA) of similar dimensions and immediately placed in a heated vacuum oven (Fisher Scientific, Isotemp®, Vacuum Oven, Model 281A) that was held at 0 kPa gage pressure (Figure 3.10b). For eicosane, the vacuum oven was set at 40 ^{o}C and for Octadecane, the vacuum oven was set at 48 ^{o}C. The vacuum oven times were varied among 0, 5, 10 and 20 hours to study the effects of degasification period of the specimen on the thermal conductivity of the materials. After the designated time periods, the samples were taken out of the vacuum oven and placed on the copper stage of the experimental setup discussed in section 3.2 (Figure 3.10c). To ensure one-dimensional heat transfer during preparation of the solid specimen, the heater was set to generate air at a temperature higher than the melting points of the respective PCM. For eicosane, the heater was set at 38.7 ^{o}C (about 2 ^{o}C above the solid-liquid phase transition point of 37 ^{o}C, Al Ghossein, 2015), whereas for octadecane, the heater was set at 34.2 ^{o}C (about 8 ^{o}C above the solid-liquid phase transition point of 26.5 ^{o}C, Ho and Gao, 2009). To study the effects of the cooling rate of the specimen on the thermal conductivity of the solid samples, two different liquids were used in the dewar that served as the heat sink, namely:

1. Liquid Nitrogen (approximate sink temperature/boiling temperature of the sink fluid taken to be -195.63 ^{o}C) (Gilmore and Donabedian, 2003),
2. Ice-water bath (approximate sink temperature/solid-liquid phase transition temperature of the sink fluid: 0 ^{o}C).

In all cases, we waited 20 minutes after pouring liquid N_2 and ice-water in the dewar flask. The solidification times of the pure octadecane and eicosane samples were determined visually using a stopwatch (Figure 3.11). Note that the liquid sample was transparent as seen in Figure 3.11a and upon freezing a progressing opaque appearance was observed (Figure 3.11b-c). It should be noted that an inaccuracy associated with bias of the observer can be introduced in this observation. In all cases, the solidification times of the samples following the liquid N_2 route were significantly lower than the ice-water route, as discussed below. As the transient plane source technique requires ensuring no air gap between the heater/sensor probe and the solid samples, the disk-shaped specimen were leveled using coarse aluminum oxide sandpapers (60 grit, 3M, St. Paul, MN) after the aluminum foils were separated from the molds and the samples were taken out of the foils. A weight machine (maximum capacity: 0.21 kg, Ohaus Corporation, Pine Brook, NJ) was utilized to measure the mass of the octadecane and eicosane solid specimen which varied from 3.5 to 4 grams.

3.5 Description of the available techniques for thermal conductivity determination

Steady-state methods and quite well-established transient method (Assael et al., 2010, Wakeham and Assael, 1999) are the two broad classes of techniques that are used for determining thermal conductivity of materials in various phases and a brief description of these techniques is given below:

3.5.1 Short description of the steady-state methods

As reviewed in the previous chapter, the steady-state methods have been used by Griggs and Yarbrough (1978), Yarbrough and Kuan (1983) and Stryker and Sparrow (1990) for measuring thermal conductivity of n-alkane paraffins. However, the steady-state methods have a major disadvantage related to upholding a strict requirement for a long time duration during which the stable temperature difference across the sample needs to reach the steady-state condition before a measurement can be performed.

3.5.2 Brief description of the transient methods

In utilizing the transient methods, measurements can be taken over a very short period of time making this method more convenient in practice. Because of this reason, researchers have utilized various forms of the transient methods in order to evaluate thermal conductivity. For example, Nabil and Khodadadi (2013), Al Ghossein (2015), Motahar et al. (2014), and Fang et al. (2013) used the transient plane source technique. Vélez et al. (2015) and Ho and Gao (2009) used the transient hot wire technique, whereas Wang et al. (2008) used the transient-short-hot-wire (TSHW) technique to determine thermal conductivity.

3.6. Description of the thermal conductivity determination process of pure solid octadecane and eicosane solid specimen

We employed the transient plane source method by means of a Hot Disk Thermal Constant Analyser (TPS 500, ThermTest Inc., CANADA) to order to determine the temperature-dependent thermal conductivity of the octadecane and eicosane solid specimen prepared following the liquid nitrogen and ice-water routes for four vacuum oven times. The information presented in this part of the thesis, i.e. the description of thermal conductivity determination principles for the pure octadecane and eicosane specimen and corresponding equipment were taken from the instruction manual of Hot Disk Thermal Constants Analyser (ThermTest Inc, Fredericton, CANADA). In order to calibrate the thermal constant analyser, two stainless steel specimen provided by the manufacturer was carefully tested five times at 22.5 ^{o}C and the recorded average thermal conductivity was 13.952 W/mK (deviation of 0.7% when compared to the manufacturer-tested value of 13.85 W/mK reported by Nabil, 2013 and Nabil and Khodadadi, 2013). The hot disk sensor utilized in the current investigation for both eicosane and octadecane specimen was made of nickel foil, had the dual role of simultaneously being the thermometer and the heat source, had a Kapton insulation, a diameter of 6.378mm, and could be employed over a broad span of temperature with an uppermost limit at 573 K. We employed the sensor with the 6.378 mm diameter in contrast to the sensor with 12.806 mm diameter because of the relatively short dimensions (thickness 0.009525 m and diameter 0.0254 m) of the eicosane and octadecane specimen (Al Ghossein, 2015, Al Ghossein et al., 2017). The theory supporting operation of the TPS technique requires eicosane and octadecane disk specimen of infinite radius and thickness and since this requirement is physically unattainable, great importance was placed to safeguard that the energy released from the sensor stayed within the solid specimen throughout the entire heating time. To assure this, we assigned the measurement recording time and the applied heating power in such a way that the TPS 500-computed probing depth (Δ_p) for each case never surpassed the available probing depth. According to the manufacturer's manual, the computed probing depth is determined according to:

$$\Delta_p = 2\sqrt{\alpha\, t_{TPS}} \tag{3.5}$$

with symbols α and t_{TPS} designating the thermal diffusivity of the specimen and input heating time, respectively, whereas the available probing depth for each specimen is the thickness of the solid disk specimen that was about 6 mm.

.According to the manufacturer, the lowermost limit of the time gap between two subsequent test runs must be about 36 times the applied recording time and as the measurement times varied from 10 to 20 seconds in our experiments, we waited 20 minutes between two consecutive test runs at a specific measurement temperature in order to assure consistency among all eicosane and octadecane solid specimen tested. Among the 200 temperature ascension values generated by the TPS 500 for each test, we dismissed the first ten and last ten points when determining thermal conductivity as these 20 points can be corrupted by the specific heat of the hot disk sensor and relatively shorter dimensions of the eicosane and octadecane solid specimen.

In preparing the samples to determine the thermal conductivity of the solid specimen as a function of temperature, specimen of octadecane and eicosane were placed on top of aluminum plates (Lytron Co., Model CP20G01, Woburn, MA) (Nabil, 2013, Nabil and Khodadadi, 2013, Al Ghossein, 2015, Al Ghossein et al., 2017). These plates were hydraulically-supplied by distilled water flowing through plastic tubes connected to a circulating bath equipped with a programmable controller (PN:TC-502P-115, Hz/A: 60/12, Brookfield, Middleboro, MA) (Nabil, 2013, Nabil and Khodadadi, 2013, Al Ghossein, 2015, Al Ghossein et al., 2017, Brookfield, circulating baths with programmable controller, operators manual, 2009).

A top screw, two side screws, a metal plate at the bottom and another plate at the top were employed in order to level the hot disk sensor with respect to the specimen and to put pressure on the specimen-sensor-specimen arrangement so that the sensor did not slip when consecutive test runs were administered at a designated measurement temperature. The plastic tubes and the entire configuration (Figure 3.12) were carefully covered by means of Styrofoam to confirm that heat loss to the laboratory environment was kept to a minimum and the temperature intentionally set for the bath circulation unit and the temperature of solid specimen were as close as possible. A calibrated thermocouple was carefully inserted inside the specimen-sensor-specimen arrangement as exhibited in Figure 3.12 and the temperature of the octadecane and eicosane solid specimen were recorded by the output of the following equipment (linked to the thermocouple): USB-TC, Measurement Computing, location: Norton, MA. Four thermocouples were calibrated by means of ice-water and liquid nitrogen in the Department of Chemistry and Biochemistry and the generated errors were negligible (±0.05%) in all cases justifying their utilization in current investigation. Once the bath input temperature was decided, temperatures of the solid specimen were recorded after 60, 70, 80 and 90 minutes and it was revealed that the resultant temperatures deviated from the designated temperature of the bath circulator (Table 3.1). The difference between the assigned bath circulator temperature and the measurement temperature ranged between 1.5 and 0.5 ^{o}C in a nearly monotonically-decaying fashion as the assigned bath circulator temperature was raised. As the recorded temperatures obtained after these four distinct waiting time periods were almost identical to each other as exhibited in Table 3.1, we concluded that the steady-state was established for the specimen and the average of the four temperatures were taken as the measurement temperature of the solid specimen. The thermal conductivity of octadecane was inspected at bath circulator assigned temperatures of 10, 15, 20, 21, 22, 23, and 24 ^{o}C, whereas for eicosane, the measurement temperatures were 20, 30, 32, 33, 34, and 35 ^{o}C.

3.6.1. Sensitivity to applied pressure to the specimen/sensor sandwich system

To examine any possible influence of the applied contact pressure on temperature-dependent thermal conductivity of octadecane and eicosane solid specimen, a piece of paper (0.075 kg/m^2, Staples, Framingham, MA) was placed between the top metal plate and screw to verify that they were barely touching, after which the screw was carefully rotated by 0, 90, 180, 270 and 360 degrees. This practice was carried out at 16.2 ^{o}C and 22.9 ^{o}C for the solid specimen of eicosane associated with the ice-water route and 0 hour vacuum oven time and the results revealed that the thermal conductivity did not exhibit any remarkable alterations after 180 degrees resulting in all analysis being done at 360 degrees in order to maintain consistency (Table 3.2 and Figure 3.13).

3.7. Analysis and interpretation of the freezing data for octadecane and eicosane solid specimen prepared by the liquid nitrogen and ice-water routes for four vacuum oven times

As exhibited clearly in Table 3.3 and Figure 3.14, for the octadecane and eicosane solid specimen prepared by both the ice-water and liquid nitrogen routes, freezing time changes non-monotonically with the elapsed vacuum oven time (degasification time). Freezing times descend as the vacuum oven time is varied from 0 hour to 5 hours and then ascend when the degasification time varies from 5 hours to 10 hours for almost all the studied cases. One exception is exhibited for the octadecane specimen prepared by the ice-water route where the lowest value of the freezing time is recorded at 10 hours vacuum oven time. We have not further investigated any reasons for this non-monotonic behavior of the freezing time with respect to degasification time, however one reason can be the presence of micron size air bubbles in liquid octadecane and eicosane (Nabil, 2013, Nabil and Khodadadi, 2013, Al Ghossein, 2015, Al Ghossein et al., 2017). Air possesses lower thermal conductivity (0.02623 W/mK at 27 ^{o}C as reported by Kadoya et al., 1985) than liquid octadecane and eicosane (mentioned at Table 2.2, and Vélez et al., 2015, respectively) that can prevent effective heat transfer during freezing in both liquid nitrogen and ice-water routes. We have theorized that when the vacuum oven time is 5 hours, the amount of micron size air bubbles in liquid octadecane and eicosane is lowest for almost all the studied cases resulting in improved heat transfer and consequent shortest recorded freezing times. Furthermore, greater vacuum oven times did not serve to remove the existing micron size air bubbles and agglomeration of the bubbles might have led to generation of micron size air layers preventing improvement of heat transfer and causing slower freezing in both liquid nitrogen and ice-water routes.

Figure 3.15 exhibits the dependence of the experimentally-evaluated non-dimensional parameter $H\,h_{sink} / k_s$ on the dimensionless freezing time t^+ for the eicosane (Table 3.4) and octadecane (Table 3.5) specimen associated with both ice-water and liquid nitrogen routes. In preparing these dimensionless quantities, current experimentally-determined thermal conductivities of the respective solid specimen at three temperatures along with the pertinent data needed for non-dimensionalization (Appendix A) were used. It is observed that for each of the paraffins, the visually-observed t^+ and the corresponding parameters $H\,h_{sink} / k_s$ associated with the liquid nitrogen route are distinctly greater than the ice-water route. This is due to the reason that the non-dimensional freezing time (t^+) depends on the temperature difference between the solid-liquid phase transition point and heat sink (i.e. $T_m - T_{sink}$) and this difference is greater for the liquid nitrogen route. Figures 3.16, 3.17, 3.18 and 3.19 exhibit the comparison between the experimental parameter $H\,h_{sink} / k_s$ and theoretical ε^+ values (Equation 3.4) for the eicosane ice-water, eicosane liquid nitrogen, octadecane ice-water and octadecane liquid nitrogen routes, respectively. In each Figure, a least-squares-based linear curve fit to $H\,h_{sink} / k_s$ is also presented along with the resulting correlation and the coefficient of determination (R^2). The S^+ values for the eicosane ice-water, eicosane liquid nitrogen, octadecane ice-water and octadecane liquid nitrogen routes (evaluated with the aid of quantities highlighted in Appendix A) are 1.19, 1.3, 1.19 and 1.3, respectively. The experimental and theoretical data presented in Figures 3.16-3.19 are in generally good agreement. The linear curve-fits to the experimental data associated with the eicosane ice-water, eicosane liquid nitrogen, octadecane ice-water and octadecane liquid nitrogen routes have slope values of 0.1368, 0.0611, 0.1334 and 0.0556 and R^2 coefficients of determination values of 0.9906, 0.998, 0.9925 and 0.9978, respectively.

The novel experimental configuration utilized in the current investigation results in nearly identical theoretical and experimental values for the thickness of the solidifying layer for both octadecane and eicosane associated with the ice-water and liquid nitrogen routes. Therefore, it can be employed for preparing consistent set of solid specimen for utilization with the TPS system.

3.8. Analysis and interpretation of the thermal conductivity of octadecane and eicosane solid specimen prepared by liquid nitrogen and ice-water routes for four vacuum oven times

Thermal conductivity of solid eicosane specimen with respect to temperature (20.9 ^{o}C to 35.5 ^{o}C) for both liquid nitrogen and ice-water routes and four vacuum oven times of current investigation are exhibited in Table 3.6. For vacuum oven time of 0 and 10 hours, thermal conductivity associated with the liquid nitrogen route is always smaller than the ice-water route, whereas for 5 and 20 hours of vacuum oven time, this distinct trend is disobeyed for three specific instances (34.8 ^{o}C for 5 hours vacuum oven time and 34.8 ^{o}C and 35.5 ^{o}C for 20 hours vacuum oven time). Thermal conductivity at a given measurement temperature varied irregularly without any recognizable pattern in relation to the vacuum oven time and freezing time of the eicosane specimen for each of the two preparation routes. As the measurement temperature nears the solid-liquid phase transition point, thermal conductivity of all eicosane specimen associated with both liquid nitrogen and ice-water routes and four vacuum oven times exhibited enhancement with the largest recorded value being 0.7065 W/mK. This “anomalous” behavior will be discussed further below in relation to solid-solid transition. Al Ghossein (2015) and Vélez et al. (2015) both studied the solid-solid phase transition in eicosane by the DSC analysis and their results revealed that during the solidification of eicosane, solid-solid phase transition could be detected, whereas during the melting of eicosane, DSC analysis did not exhibit any evidence of solid-solid phase transition (Kolesnikov and Syunyaev, 1985, de Zárate et al., 2010). It should be noted that DSC measurements are critically dependent on the heating rate as reported by Lazaro et al. (2013). The heating rates reported by Al Ghossein (2015), Vélez et al. (2015), and Kolesnikov and Syunyaev (1985) during their experiments were 5 ^{o}C/min, 2 ^{o}C/min and 1 ^{o}C/min, respectively.

Thermal conductivity of solid octadecane specimen with respect to temperature (11.5 ^{o}C to 24.8 ^{o}C) for both liquid nitrogen and ice-water routes and four vacuum oven times are exhibited in Table 3.7. At eight instances (20.9 ^{o}C for 0 and 5 hours of vaccum oven time, 20.9 ^{o}C, 22.9 ^{o}C, 23.8 ^{o}C and 24.8 ^{o}C for 10 hours of vacuum oven time, 23.8 ^{o}C and 24.8 ^{o}C for 20 hours of vacuum oven time), the thermal conductivity of ocdecane specimen associated with the liquid nitrogen route is greater than the ice-water route. For the remaining 20 cases, thermal conductivity of octadecane specimen associated with the liquid nitrogen route is smaller than the ice-water route. Similar to eicosane, thermal conductivity changes irregularly without any observed pattern in relation to the vacuum oven time and freezing time of the octadecane specimen for each of the two processing routes. As the measurement temperature gets closer to the solid-liquid phase transition point, thermal conductivity of all octadecane specimen associated with both liquid nitrogen and ice-water routes and four vacuum oven times exhibit enhancements with the highest recorded value being 0.704 W/mK.

Figure 3.20 exhibits the thermal conductivity of eicosane solid specimen taken from Table 3.6, whereas in Figure 3.21 the same data are shown for two different ranges of temperature (10-30 and 30-37 ^{o}C) in order to provide greater clarity. Reference thermal conductivity data of Al Ghossein (2015), Nabil and Khodadadi (2013) for eicosane associated with their “oven solidification routes” are provided in Figures 3.20, whereas “ambient” and “ice-water bath” solidification route data of Nabil and Khodadadi (2013) are also reproduced in Figure 3.21. From Figure 3.21, it is observed that the difference between the thermal conductivity values associated with the ice-water route and liquid nitrogen route for a specific vacuum oven time in the current investigation is not on the same scale as the difference between the ambient solidification and ice-water bath solidification route recorded by Nabil and Khodadadi (2013). From the left part of Figure 3.21, we can observe that the highest and lowest differences between the thermal conductivity values of any two routes were usually around 0.05 and 0.02 W/mK in the case of Nabil and Khodadadi (2013), whereas in current investigation, the differences between ice-water and liquid nitrogen routes varies from around 0.05 to 0.0035 W/mK.

Data of Table 3.7 are plotted in Figures 3.22 and 3.23 for octadecane along with the reference data of Motahar et al. (2014). From the left part of Figure 3.23, we can observe that the thermal conductivity values associated with both ice-water and liquid nitrogen routes are higher than the values reported by Motahar et al. (2014) with the closest values exhibited at 5 hours vacuum oven time associated with the liquid nitrogen route.

3.9. Key findings of the relations among thermal conductivity values and preparation of octadecane and eicosane solid specimen under controlled freezing by ice-water and liquid nitrogen routes

A novel experimental configuration has been developed to ensure one-dimensional heat extraction during the freezing process of liquid octadecane and eicosane specimen by the liquid nitrogen and ice-water routes. Visually-determined freezing time changes non-monotonically with the elapsed vacuum oven times (0 hour, 5 hours, 10 hours and 20 hours) for both eicosane and octadecane specimen with the lowest freezing time recorded at either 5 or 10 hours. Variation of the dimensionless depth of the solidifying layer (ε^+) with t^+ depends on the value of S^+ that ranged between 1.19 and 1.3 for the eicosane and octadecane specimen prepared by both liquid nitrogen and ice-water routes. Visually-observed dimensionless thickness of the solid specimen agreed very well with the theoretical predictions.

Application of the transient plane source method revealed that the thermal conductivity of the solid paraffins associated with both liquid nitrogen and ice-water routes and four vacuum oven times exhibit enhancements when the specimen temperature becomes close to the solid-liquid phase transition point. For a particular vacuum oven time, the thermal conductivities of the paraffin specimen associated with the liquid nitrogen route are smaller than the ice-water route for the majority of the cases, though opposite of this trend is also recorded on several instances (three for eicosane and eight for octadecane).

Table 3.1. Deviation of temperature of the eicosane specimen associated with the liquid nitrogen route and 0 hour vacuum oven time from bath circulator assigned temperature after 60, 70, 80 and 90 minutes inspected by thermocouples placed in the specimen-sensor-specimen arrangement (upper limit of standard deviation is 0%).

Bath circulator assigned temperature (^{o}C)	Temperature of the eicosane specimen after 60 minutes (^{o}C)	Temperature of the eicosane specimen after 70 minutes (^{o}C)	Temperature of the eicosane specimen after 80 minutes (^{o}C)	Temperature of the eicosane specimen after 90 minutes (^{o}C)	Mean temperature of the eicosane specimen (^{o}C)
10	11.5	11.5	11.5	11.5	11.5
15	16.2	16.2	16.2	16.2	16.2
20	20.9	20.9	20.9	20.9	20.9
21	21.9	21.9	21.9	21.9	21.9
22	22.9	22.9	22.9	22.9	22.9
23	23.8	23.8	23.8	23.8	23.8
24	24.8	24.8	24.8	24.8	24.8
30	30.6	30.6	30.6	30.6	30.6
31	31.6	31.6	31.6	31.6	31.6
32	32.6	32.6	32.6	32.6	32.6
33	33.3	33.3	33.3	33.3	33.3
34	34.8	34.8	34.8	34.8	34.8
35	35.5	35.5	35.5	35.5	35.5

Table 3.2. Measured thermal conductivity as a function of the turning angle (degrees) of the top screw for the eicosane specimen associated with the ice-water route and 0 hour vacuum oven time (upper limit of standard deviation is 0.26% as the reported thermal conductivity is the average of three measurements at one temperature).

Turning angle (degrees) of the top screw	Temperature of eicosane specimen (^{o}C)	
	16.2 ^{o}C	22.9 ^{o}C
	Thermal conductivity (W/mK)	Thermal conductivity (W/mK)
0	0.3834	0.3966
90	0.4173	0.4061
180	0.4157	0.4131
270	0.4130	0.41
360	0.4143	0.4128

Table 3.3. Freezing time of octadecane and eicosane specimen with respect to four vacuum oven times (0, 5, 10 and 20 hours) for both ice-water and liquid nitrogen routes determined by visual inspection and a stop watch after the specimen were placed on the cold-stage copper stand.

Materials	Vacuum oven time (hours)	Freezing time associated with the liquid nitrogen route (mean of two specimen) (seconds)	Freezing time associated with the ice-water route (mean of two specimen) (seconds)
Octadecane	0	202.5	905
	5	162	483
	10	163.5	431
	20	186	469
Eicosane	0	162	671
	5	115	225
	10	141.5	312.5
	20	141	373

Table 3.4. Variation of $(H\,h_{sink}\,/\,k_s)$ with t^+ for eicosane specimen associated with both the ice-water and liquid nitrogen routes and all four vacuum oven times (0, 5, 10 and 20 hours) with thermal conductivity evaluated at three (20.9 ^{o}C, 33.3 ^{o}C and 35.5 ^{o}C) temperatures.

Vacuum oven time (hours)		Temperature of the eicosane specimen (20.9 ^{o}C)		Temperature of the eicosane specimen (33.3 ^{o}C)		Temperature of the eicosane specimen (35.5 ^{o}C)	
Ice-water Route		t^+	$(H\,h_{sink}\,/\,k_s)$	t^+	$(H\,h_{sink}\,/\,k_s)$	t^+	$(H\,h_{sink}\,/\,k_s)$
	0	46.5	8.5	40.7	7.9	29	6.63
	5	13.5	4.1	13	4	10	3.6
	10	19.3	5.1	17.2	4.8	12.6	3.98
	20	23.4	5.7	22.2	5.5	18.6	5
Liquid nitrogen Route	0	179.1	17.62	174.2	17.4	131.6	14.9
	5	122	14.37	120.7	14.2	90.5	12.2
	10	153.9	16.2	131.6	14.9	101.57	13
	20	152.2	16.19	139.8	15.4	98.7	12.8

Table 3.5. Variation of $(H\, h_{sink} / k_s)$ with t^+ for octadecane specimen associated with both the ice-water and liquid nitrogen routes and all four vacuum oven times (0, 5, 10 and 20 hours) with thermal conductivity at three (11.5 ^{o}C, 22.9 ^{o}C and 24.8 ^{o}C) temperatures.

Vacuum oven time (hours)		Temperature of the octadecane specimen (11.5 ^{o}C)		Temperature of the octadecane specimen (22.9 ^{o}C)		Temperature of the octadecane specimen (24.8 ^{o}C)	
Ice-water route		t^+	$(H\, h_{sink} / k_s)$	t^+	$(H\, h_{sink} / k_s)$	t^+	$(H\, h_{sink} / k_s)$
	0	44.1	8.2	33.5	7	27	6.25
	5	23.2	5.7	18.3	4.9	15.9	4.5
	10	18.1	4.9	17.9	4.9	16.1	4.6
	20	20.8	5.3	17.5	4.8	14.1	4.2
Liquid nitrogen route	0	210.9	19.2	204.9	18.9	179.5	17.6
	5	176	17.5	136.1	15.2	130.2	14.8
	10	160.8	16.6	139.7	15.4	118.1	14.1
	20	187.6	18.1	152.7	16.2	117.2	14

Table 3.6. Measured thermal conductivity as a function of temperature below the solid-liquid phase transition temperature for eicosane specimen subjected to four vacuum oven times processed by the liquid nitrogen and ice-water routes (upper limit of the standard deviation is 1.07% as each thermal conductivity is the average of three measurements taken at one temperature).

Temperature of the eicosane specimen (^{o}C)	Vacuum oven time (hours)							
	0		5		10		20	
	Ice-water (W/mK)	Liquid N_2 (W/mK)	Ice-water (W/mK)	Liquid N_2 (W/mK)	Ice-water (W/mK)	Liquid N_2 (W/mK)	Ice-water (W/mK)	Liquid N_2 (W/mK)
20.9	0.4135	0.41	0.4748	0.4272	0.4629	0.4168	0.4557	0.42
30.6	0.4183	0.3982	0.4725	0.4177	0.4712	0.4298	0.452	0.4205
32.6	0.4297	0.4051	0.4712	0.4014	0.494	0.4545	0.4686	0.4351
33.3	0.4725	0.4216	0.4961	0.4319	0.5194	0.4875	0.4815	0.4571
34.8	0.5181	0.4694	0.5047	0.5291	0.5495	0.5278	0.5197	0.5704
35.5	0.6438	0.5580	0.5964	0.576	0.7065	0.6317	0.5730	0.6473

Table 3.7 Measured thermal conductivity as a function of temperature below the solid-liquid phase transition temperature for octadecane specimen subjected to four vacuum oven times processed by the liquid nitrogen and ice-water routes (upper limit of the standard deviation is 1.204% as each thermal conductivity is the average of three measurements taken at one temperature).

Temperature of the octadecane specimen (^{o}C)	Vacuum oven time (hours)							
	0		5		10		20	
	Ice-water (W/mK)	Liquid N_2 (W/mK)	Ice-water (W/mK)	Liquid N_2 (W/mK)	Ice-water (W/mK)	Liquid N_2 (W/mK)	Ice-water (W/mK)	Liquid N_2 (W/mK)
11.5	0.4309	0.4254	0.4364	0.4078	0.4983	0.4503	0.4731	0.4392
16.2	0.4271	0.4228	0.4223	0.4129	0.4585	0.4484	0.4756	0.4391
20.9	0.4147	0.4236	0.4603	0.4647	0.4863	0.4893	0.5078	0.4513
21.9	0.4397	0.4278	0.4967	0.486	0.5179	0.499	0.5389	0.4911
22.9	0.567	0.4378	0.5524	0.5273	0.5056	0.5185	0.5608	0.5394
23.8	0.6269	0.4604	0.5429	0.5379	0.5590	0.5722	0.6280	0.6858
24.8	0.704	0.4997	0.6368	0.5512	0.5609	0.6134	0.6989	0.703

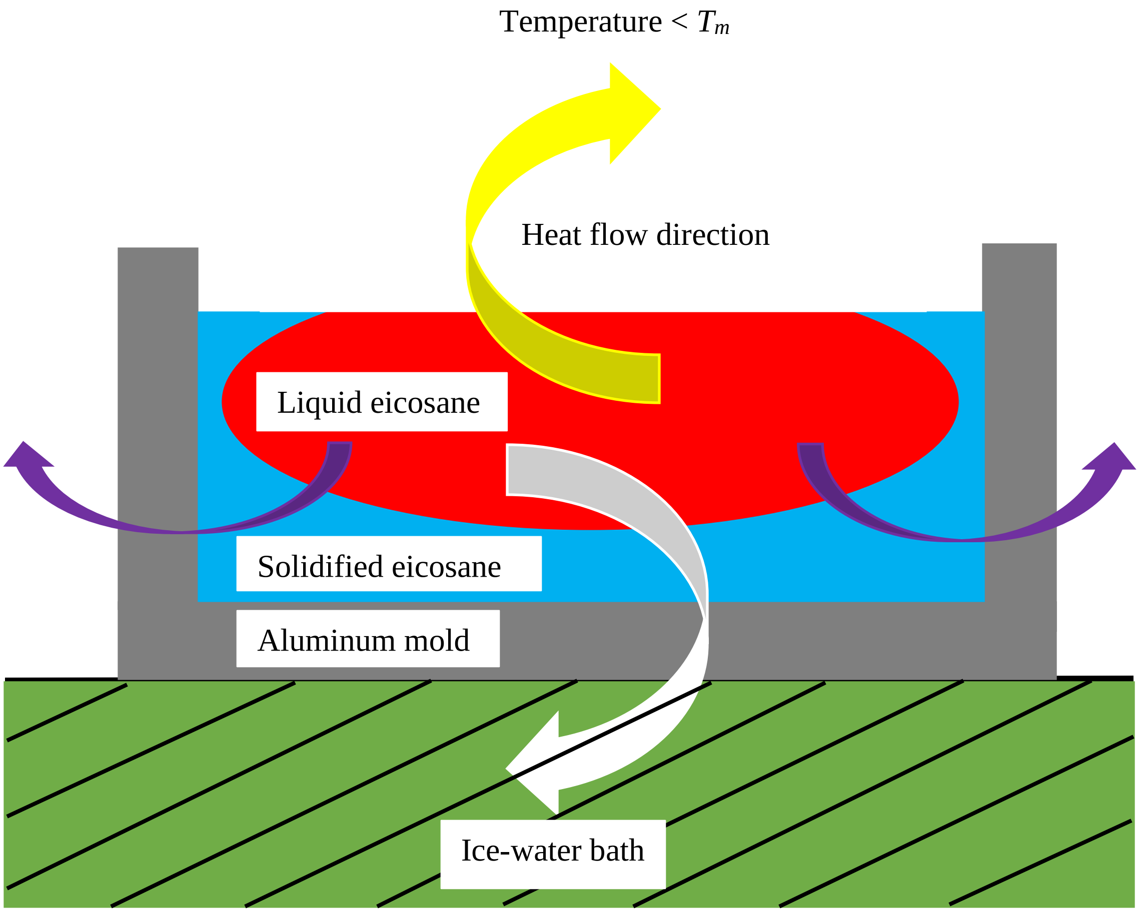

Figure 3.1. Heat flow in three directions (sides, top and bottom) during the preparation of eicosane solid specimen by both Nabil (2013) and Al Ghossein (2015) for the ice-water bath solidification. Within the mold, the solidifying eicosane (blue region) generally encloses the liquid region (red).

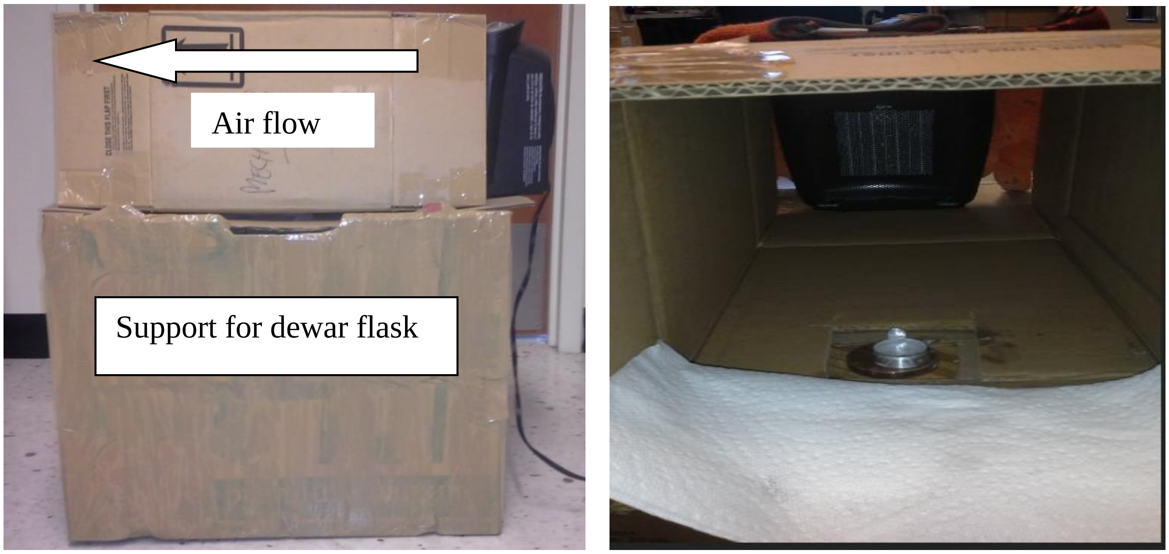

(a) (b)

Figure 3.2. Experimental setup used for sample preparation: (a) side view with heater fan on the right upstream end and (b) front view with mold containing liquid specimen placed downstream of the heater.

Figure 3.3. Heater utilized for maintaining hot air flow over the specimen for both ice-water and liquid nitrogen routes.

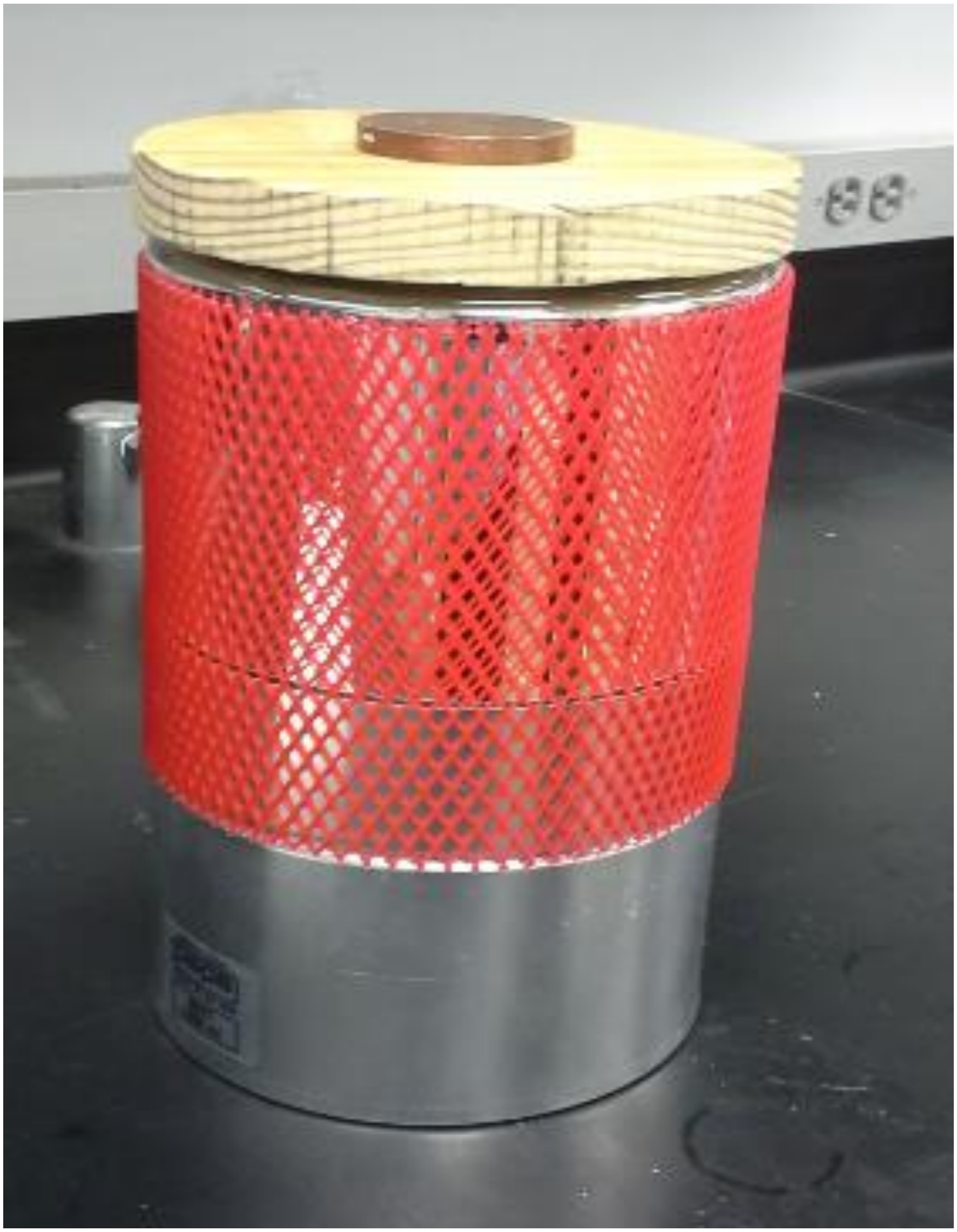

Figure 3.4. The dewar flask along with a vented wooden cap and inserted copper rod utilized to store liquid nitrogen and ice-water.

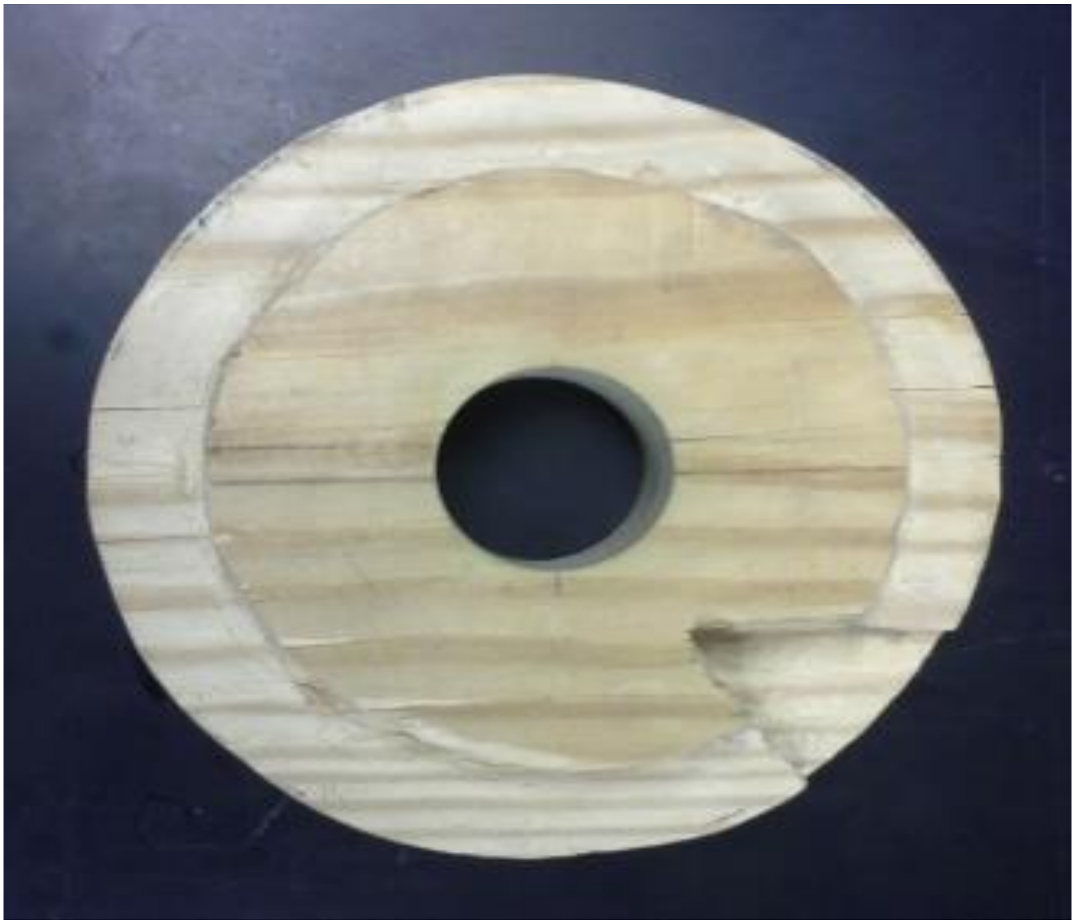

Figure 3.5. The vented wooden cap (diameter of 6 inch, width of 0.75 inch and center hole with diameter of 1.5 inch) utilized to cover the dewar.

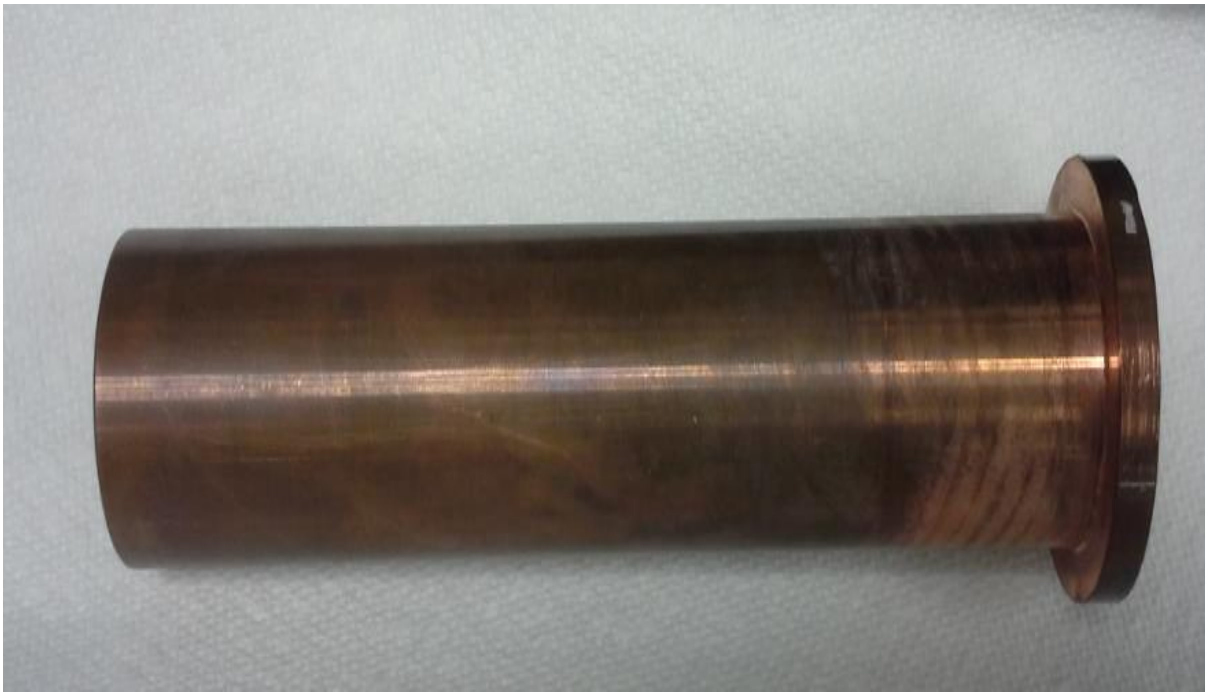

Figure 3.6. Copper rod (diameter of 1.5 inch, stage diameter of 2 inch and length of 7.25 inch) for effective heat transfer to either liquid nitrogen or ice-water routes.

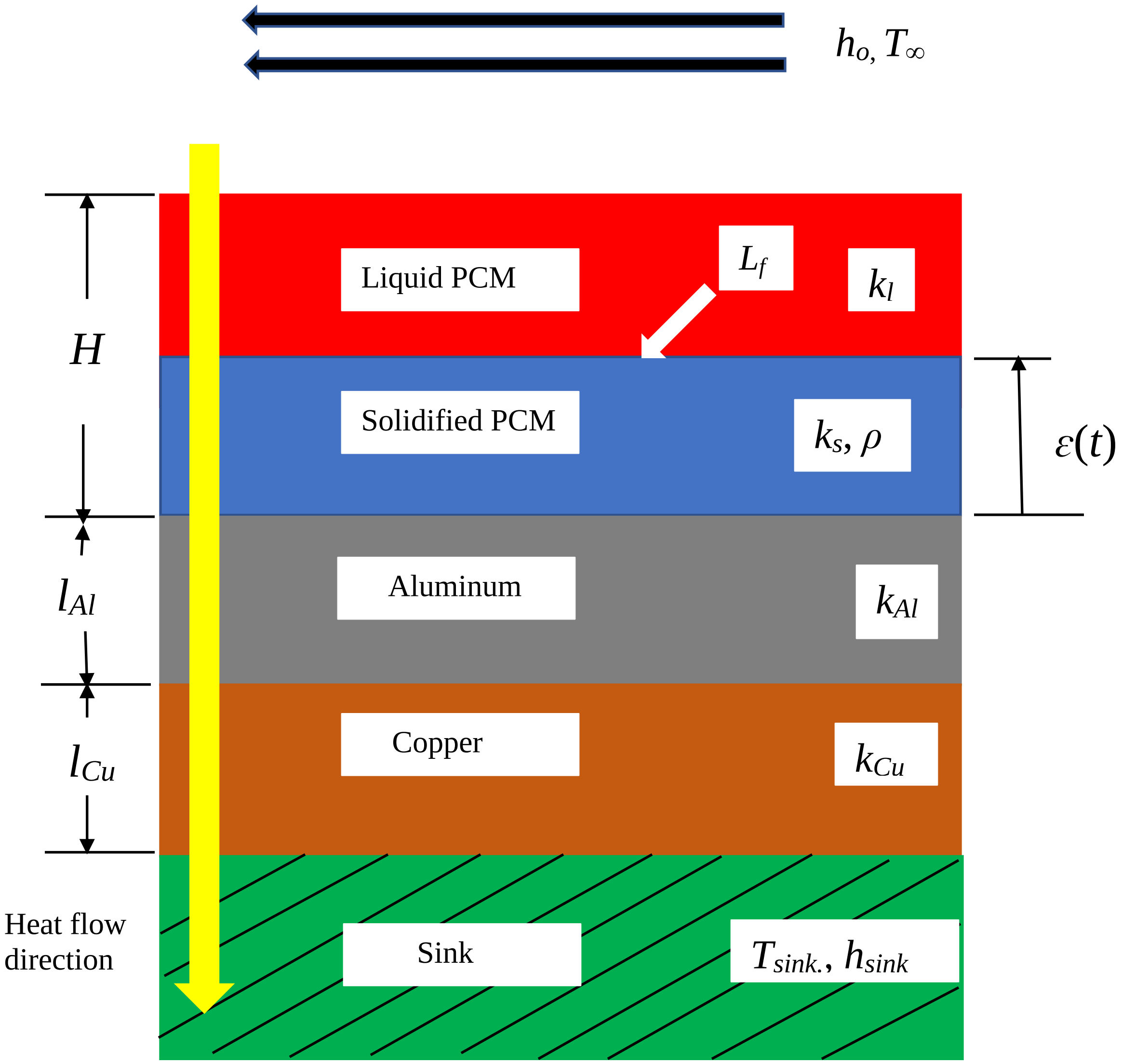

Figure 3.7. Multi-layer model utilized to derive the non-dimensional relations between the dimensionless depth of the solidifying layer and freezing time for heat transfer through six layers from the heat source to the heat sink.

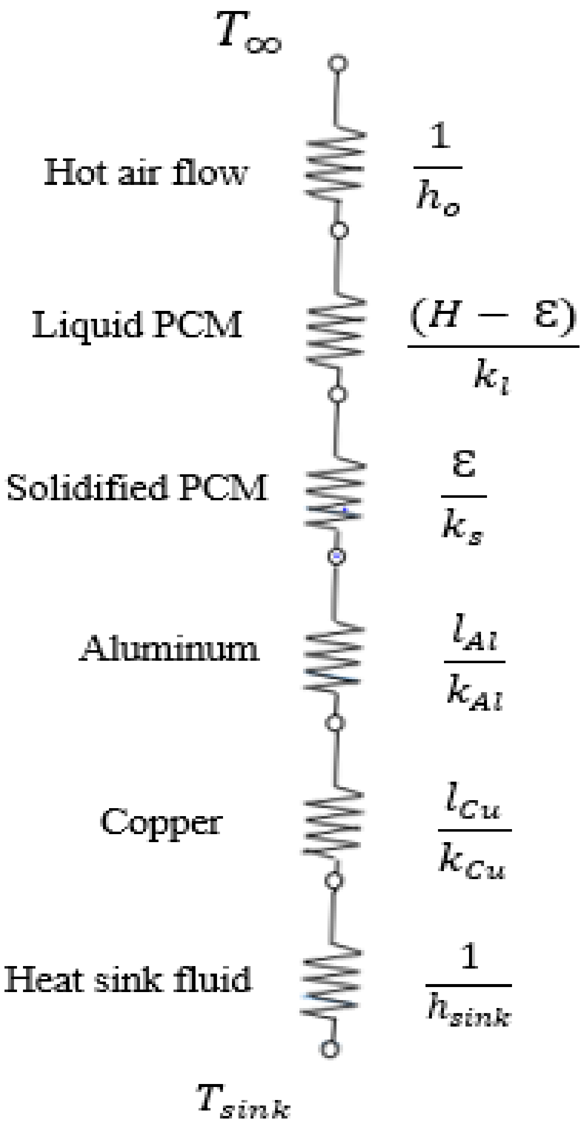

Figure 3.8. Six thermal resistances for heat transfer through hot fluid, liquid PCM, solidified PCM, aluminum, copper and cold fluid from the heat source (T_∞) to the heat sink (T_{sink}) for the model of Figure 3.7.

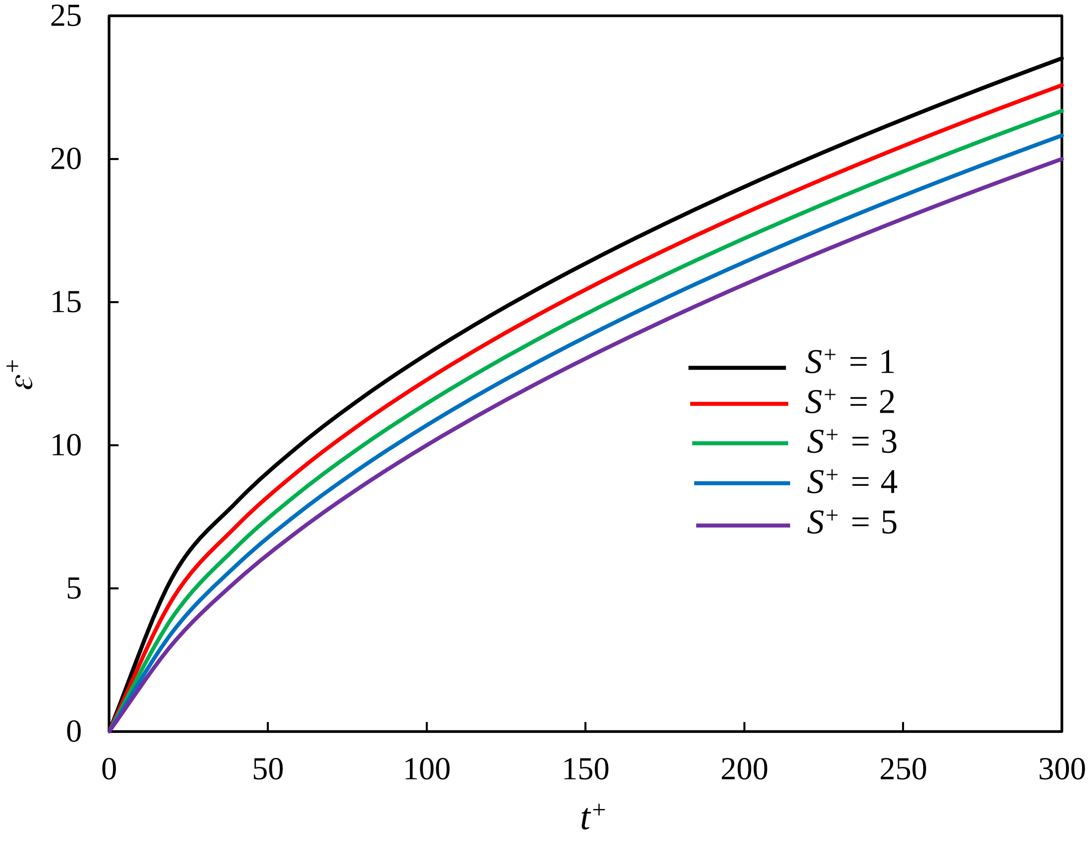

Figure 3.9. Variation of ε^+ with respect to t^+ for theoretical cases of S^+ values of 1, 2, 3, 4 and 5 obtained according to equation (3.4).

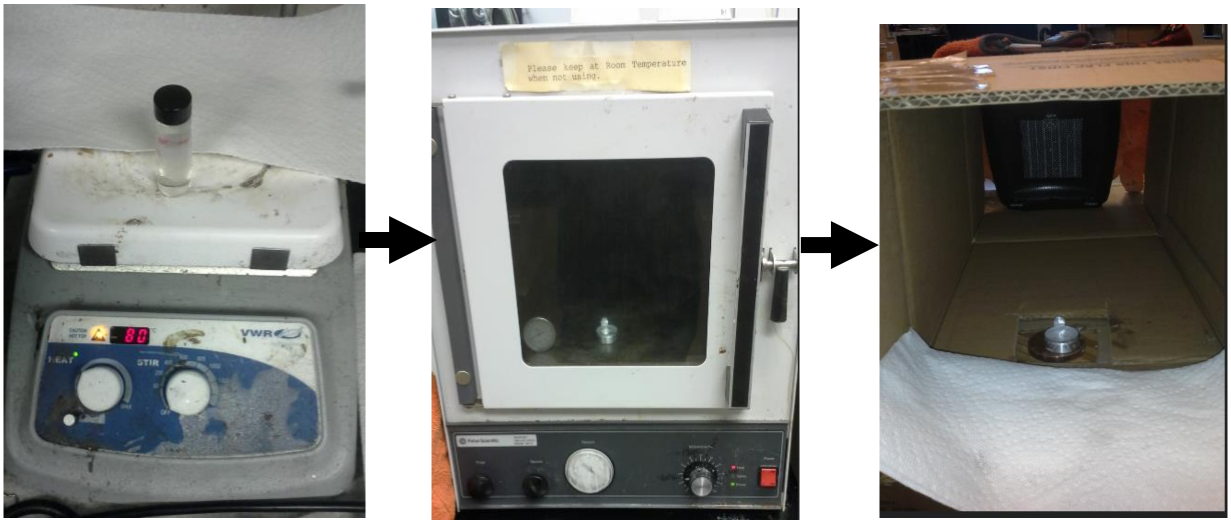

(a) (b) (c)

Figure 3.10. Eicosane and octadecane solid specimen preparation process for both ice-water and liquid nitrogen routes: (a) liquid specimen while maintained at 80 ^{o}C, (b) specimen held at 0 kPa gage pressure in vacuum oven for 0, 5, 10 and 20 hours and (c) specimen during liquid to solid transition while placed on the copper cold stage.


(a) (b) (c)

Figure 3.11. Visually-observed freezing of liquid octadecane specimen associated with the liquid nitrogen route and 20 hours vacuum oven time after (a) 5 seconds, (b) 100 seconds and (c) 193 seconds.

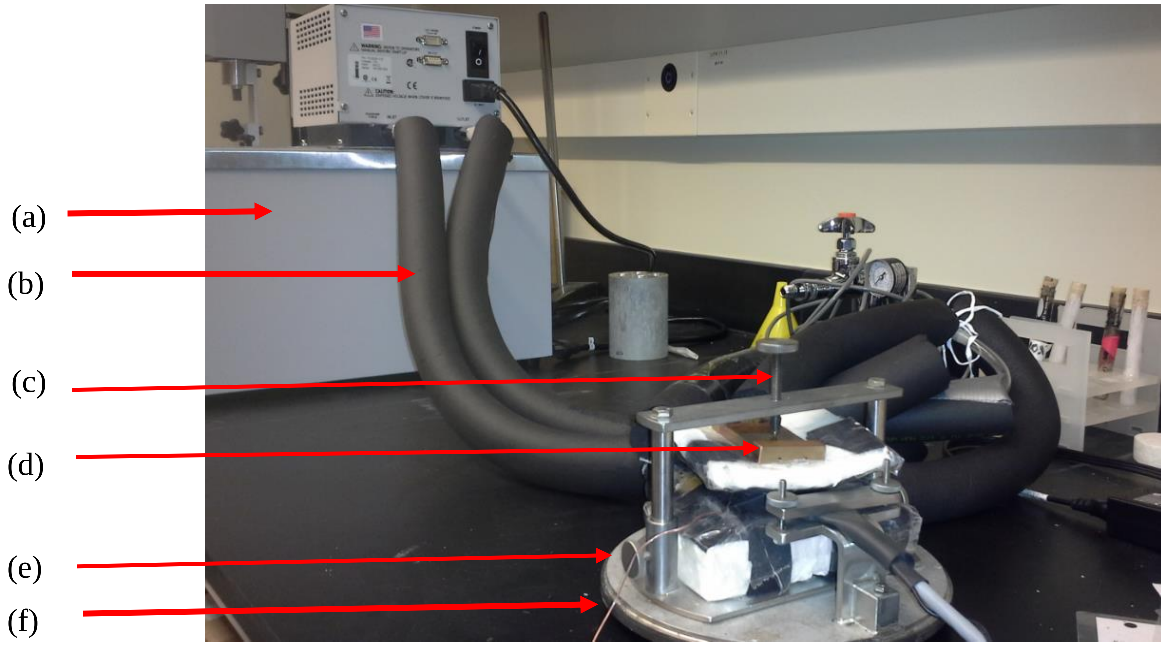

Figure 3.12. Configuration utilized for thermal conductivity determination of octadecane and eicosane specimen featuring (a) circulating bath unit, (b) insulation-covered plastic tubes, (c) top screw crucial to applied pressure, (d) top metal plate,I) side screw and (f) inserted thermocouple to determine specimen measurement temperature.

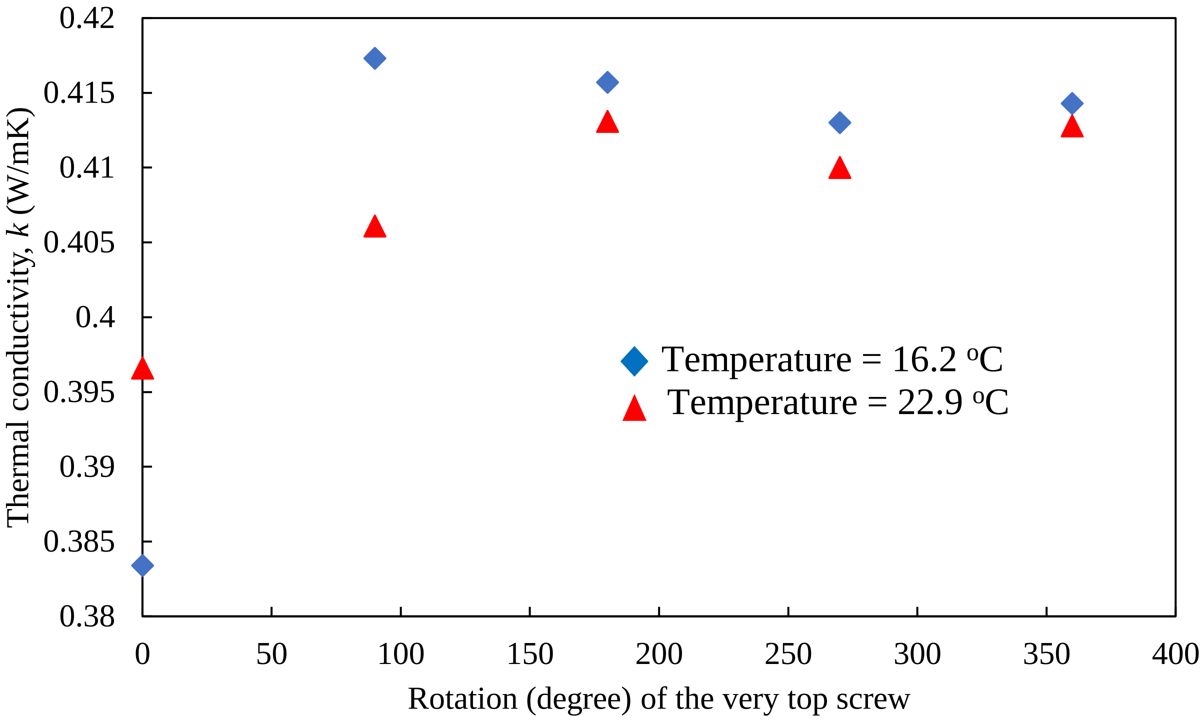

Figure 3.13. Thermal conductivity as a function of turning angle (degree) of the top screw for the eicosane specimen associated with the ice-water route and 0 hour vacuum oven time (upper limit of the standard deviation is 0.26% as each thermal conductivity is the average of three measurements at one temperature).

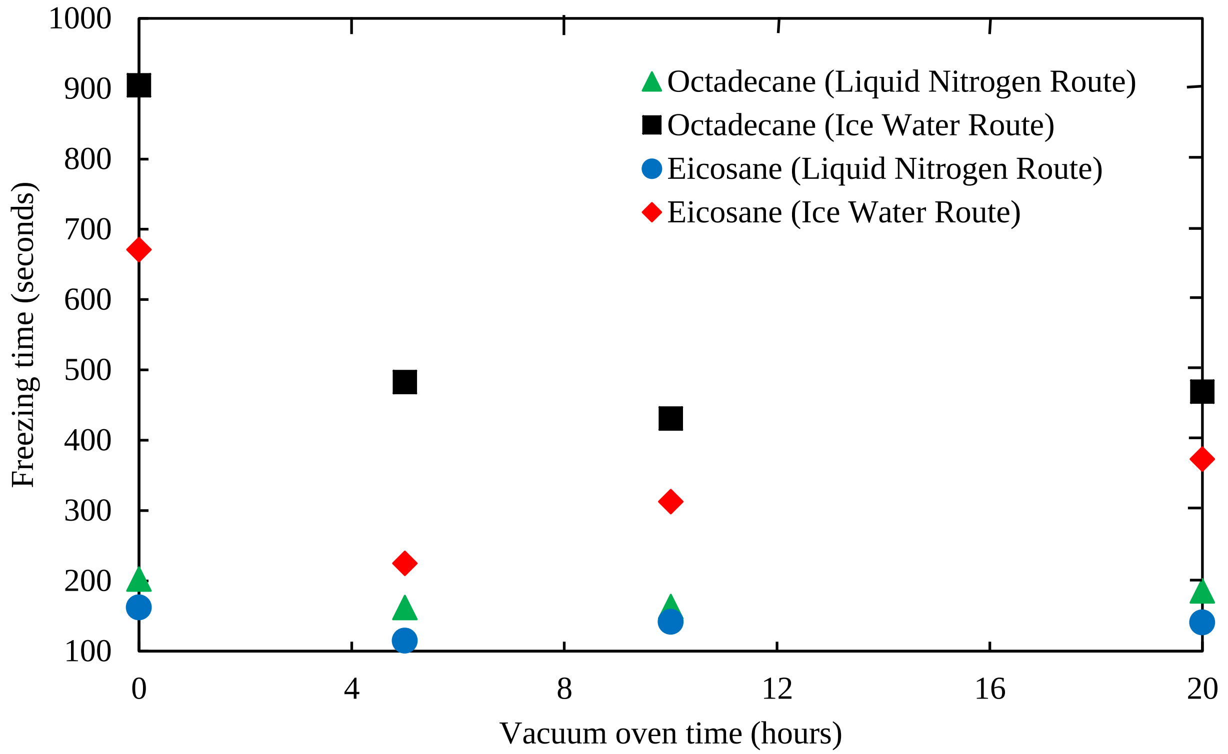

Figure 3.14. Freezing time of the octadecane and eicosane specimen with respect to four vacuum oven times (0, 5, 10 and 20 hours) for both ice-water and liquid nitrogen routes obtained by visual inspection.

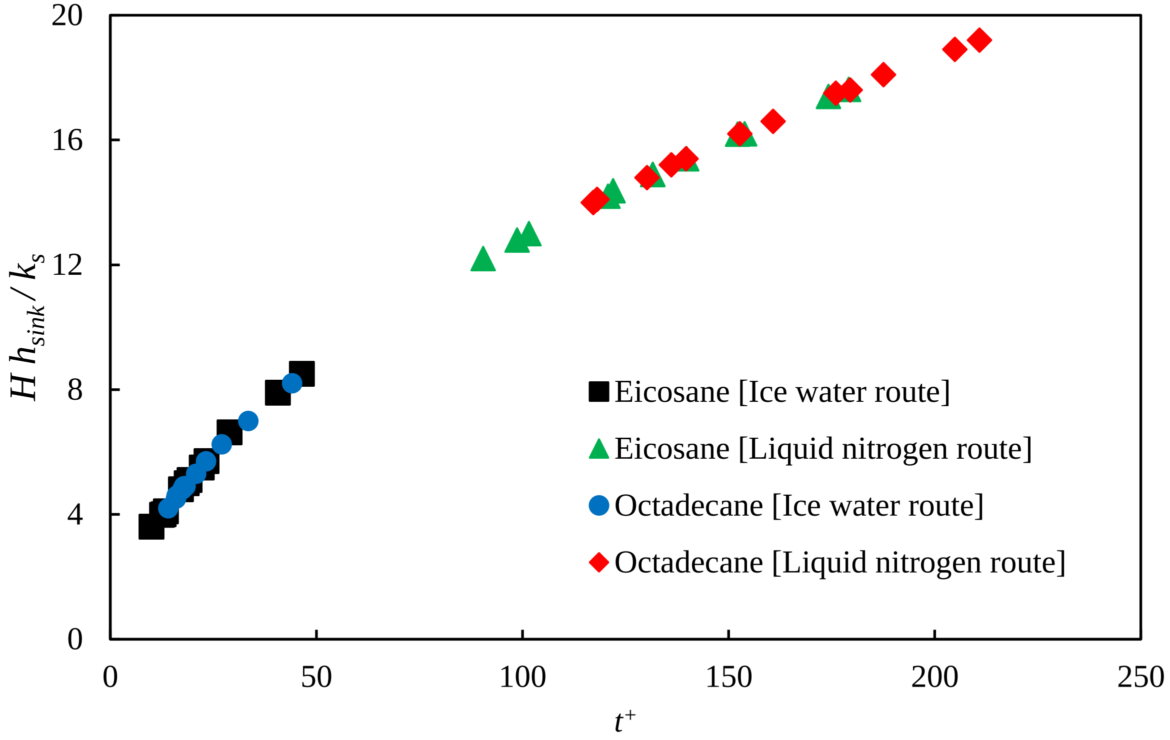

Figure 3.15. Dependence of ($H\ h_{sink} / k_s$) with t^+ for eicosane and octadecane solid specimen associated with both ice-water and liquid nitrogen routes and all four vacuum oven times (0, 5, 10 and 20 hours).

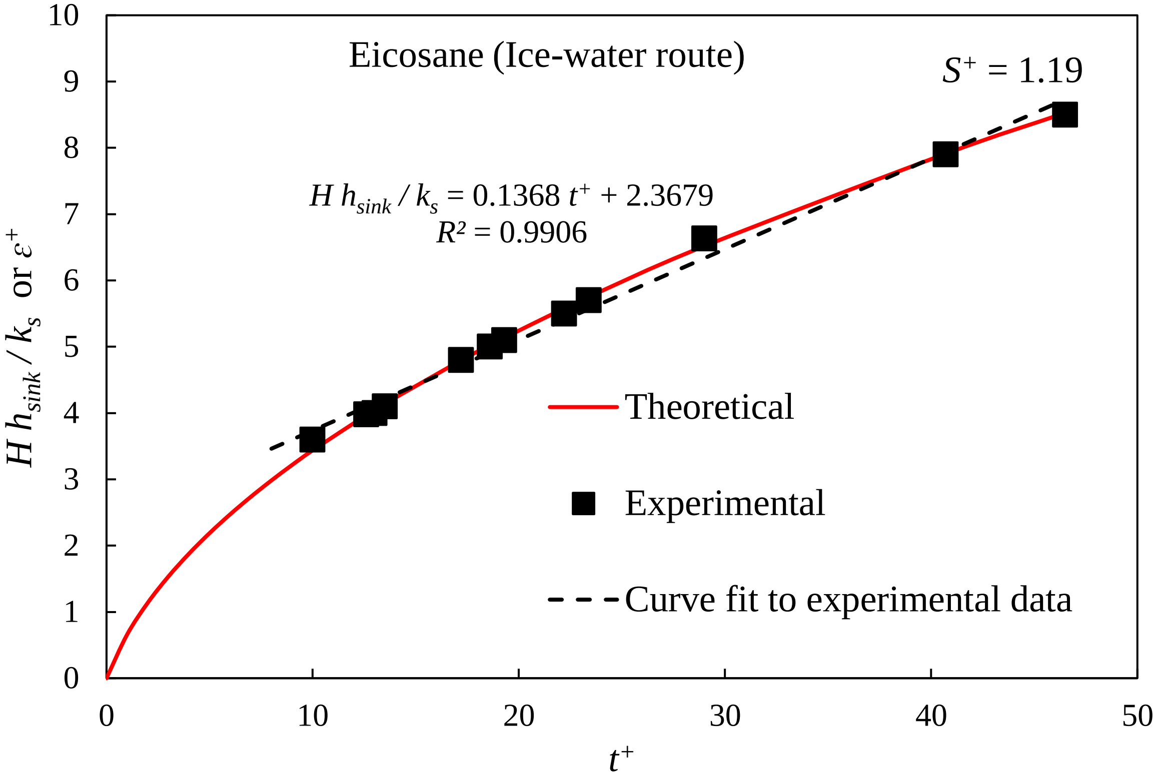

Figure 3.16. Dependence of $H\,h_{sink} / k_s$ or ε^+ with t^+ for solid eicosane specimen associated with the ice-water route for all four vacuum oven times (0, 5, 10 and 20 hours).

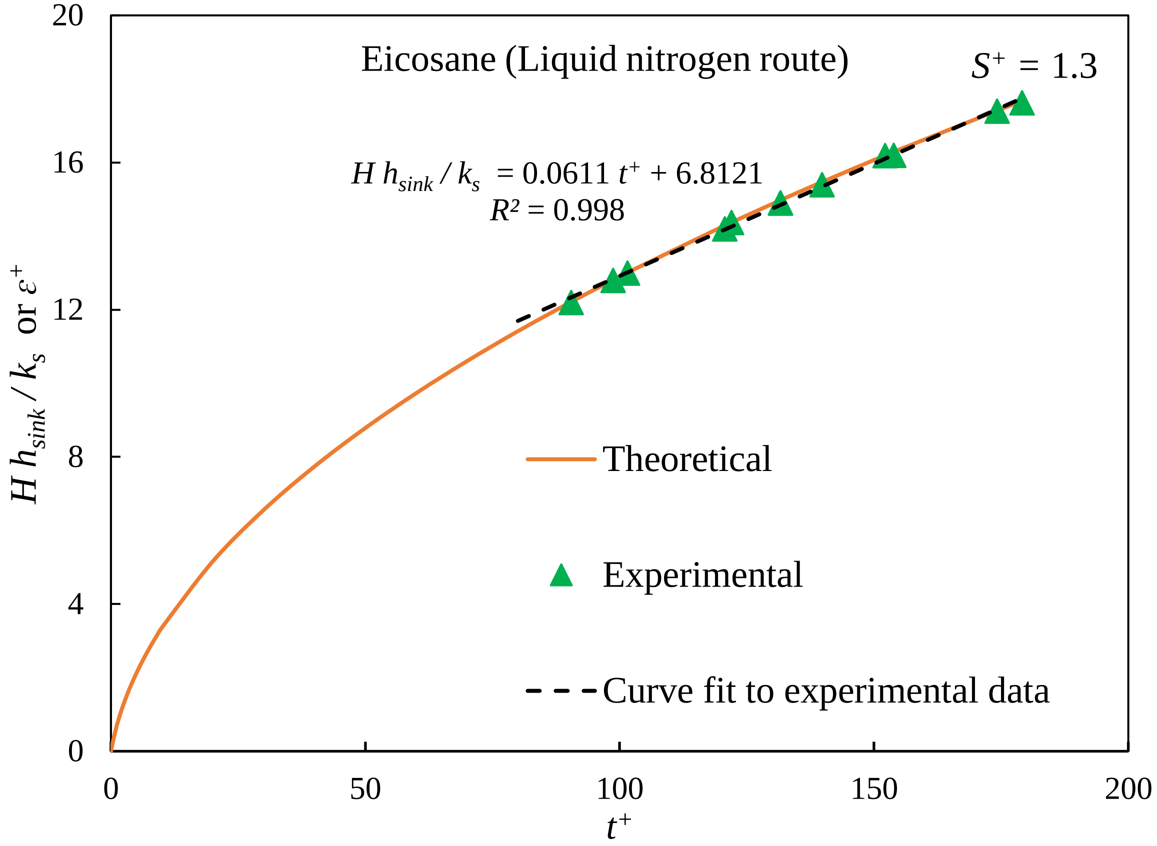

Figure 3.17. Dependence of $H\,h_{sink}/k_s$ or ε^+ with t^+ for solid eicosane specimen associated with the liquid nitrogen route for all four vacuum oven times (0, 5, 10 and 20 hours).

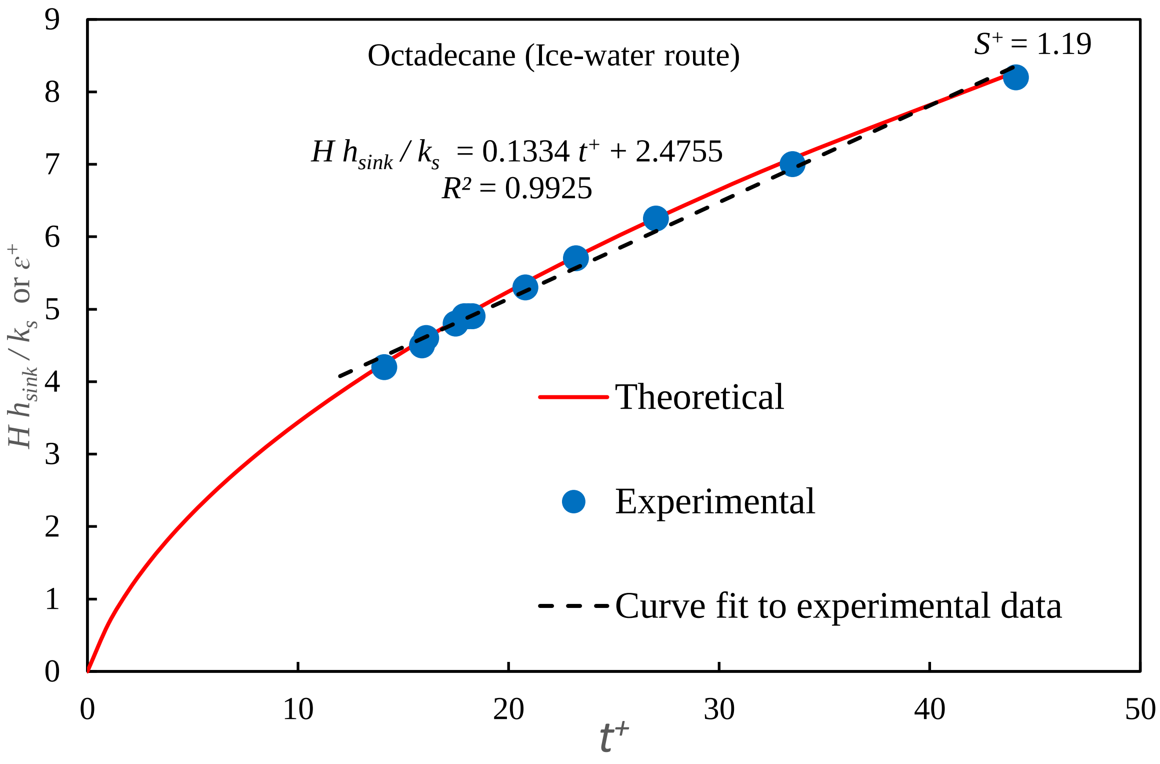

Figure 3.18. Dependence of $H\,h_{sink} / k_s$ or ε^+ with t^+ for solid octadecane specimen associated with the ice-water route for all four vacuum oven times (0, 5, 10 and 20 hours).

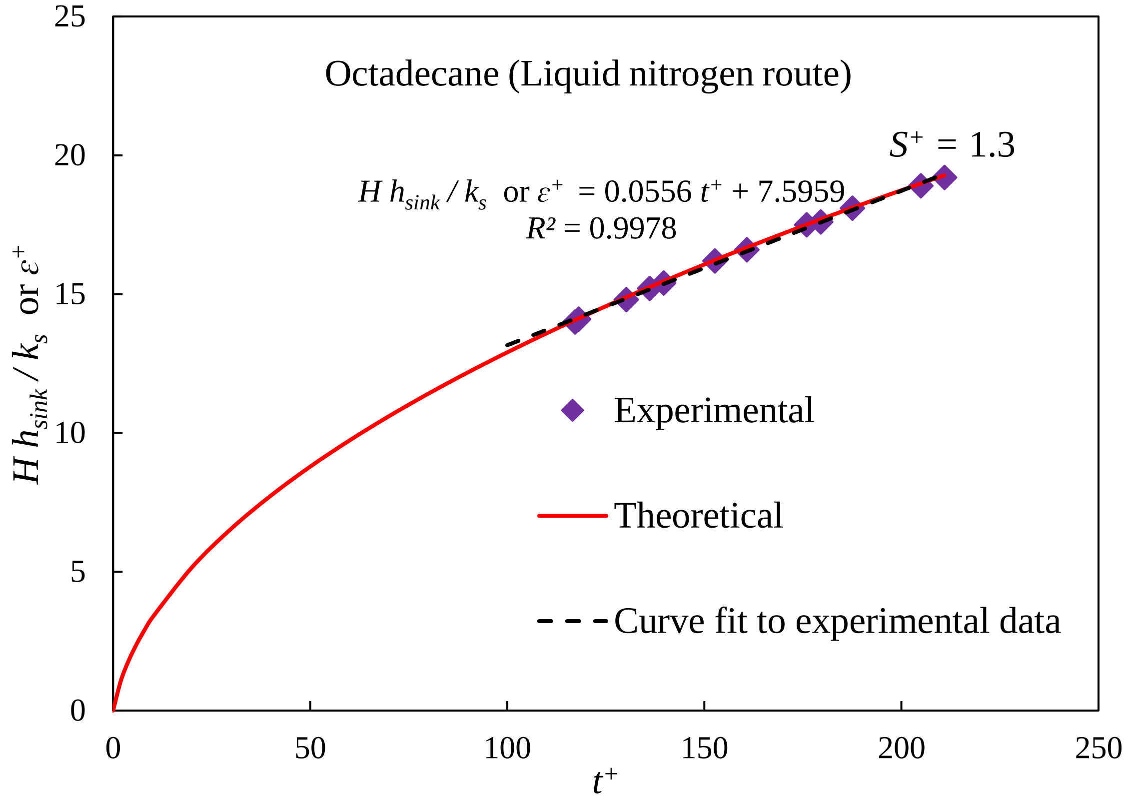

Figure 3.19. Dependence of $H\,h_{sink}\,/\,k_s$ or ε^+ with t^+ for solid octadecane specimen associated with the liquid nitrogen route for all four vacuum oven times (0, 5, 10 and 20 hours).

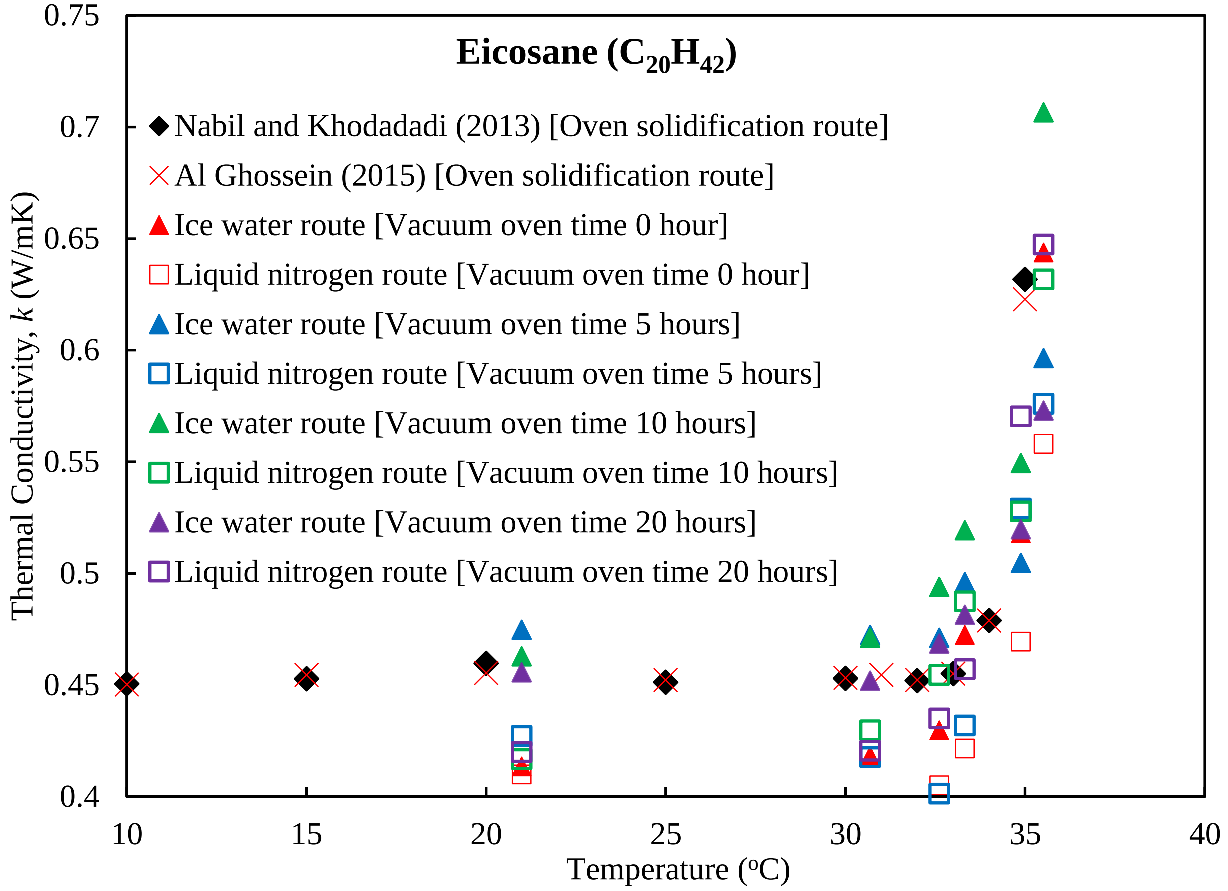

Figure 3.20. Thermal conductivity as a function of temperature below the solid-liquid phase transition temperature (37 °C, Al Ghossein, 2015) for eicosane specimen of four vacuum oven times processed by the liquid nitrogen and ice-water routes in addition to experimental results from Al Ghossein (2015), Nabil and Khodadadi (2013).

)

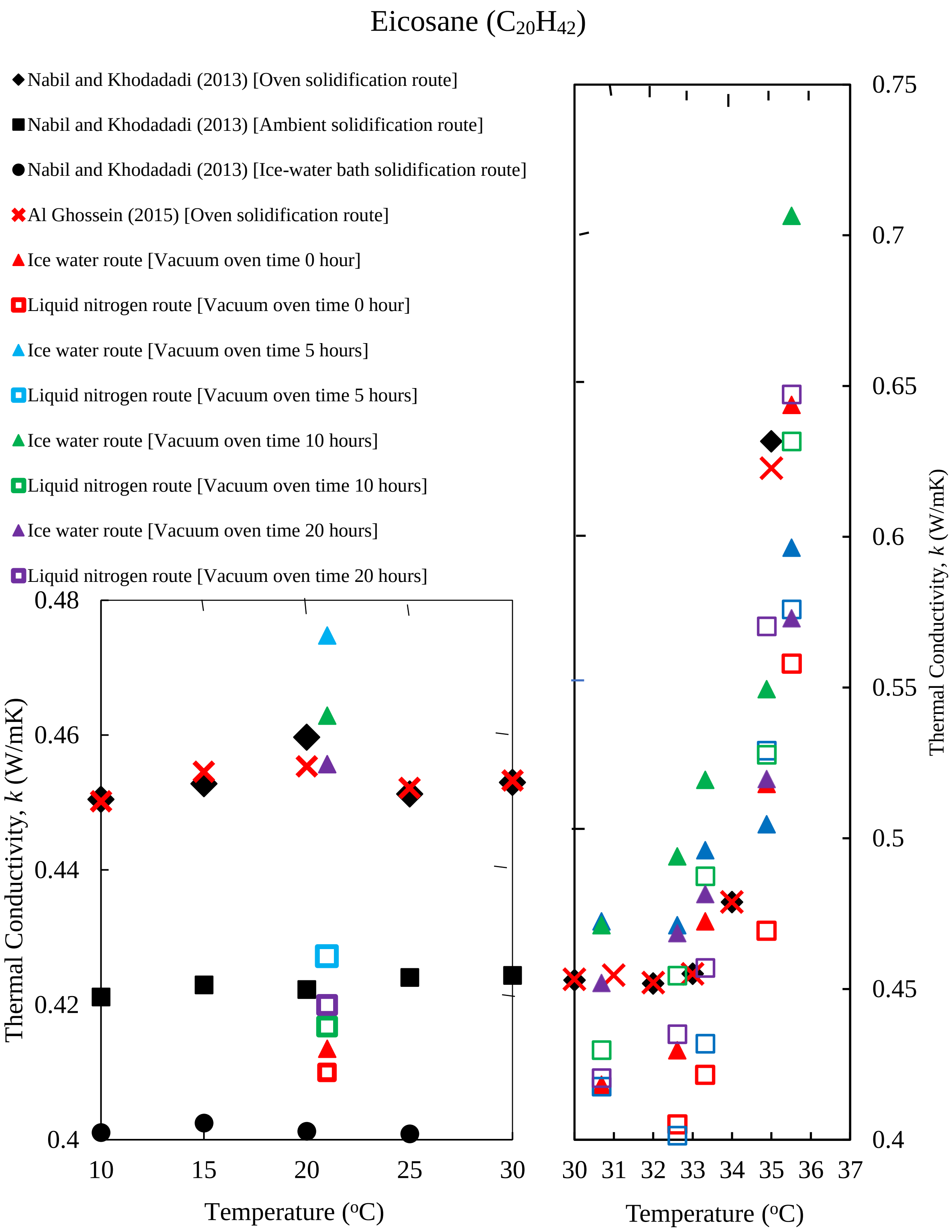

Figure 3.21. Thermal conductivity as a function of temperature below the solid-liquid phase transition temperature (37 °C, Al Ghossein, 2015) for eicosane specimen of four vacuum oven

times associated with the liquid nitrogen and ice-water routes for two different ranges of temperature (10-30 and 30-37 ^{o}C) in addition to experimental results from Al Ghossein (2015), Nabil and Khodadadi (2013).

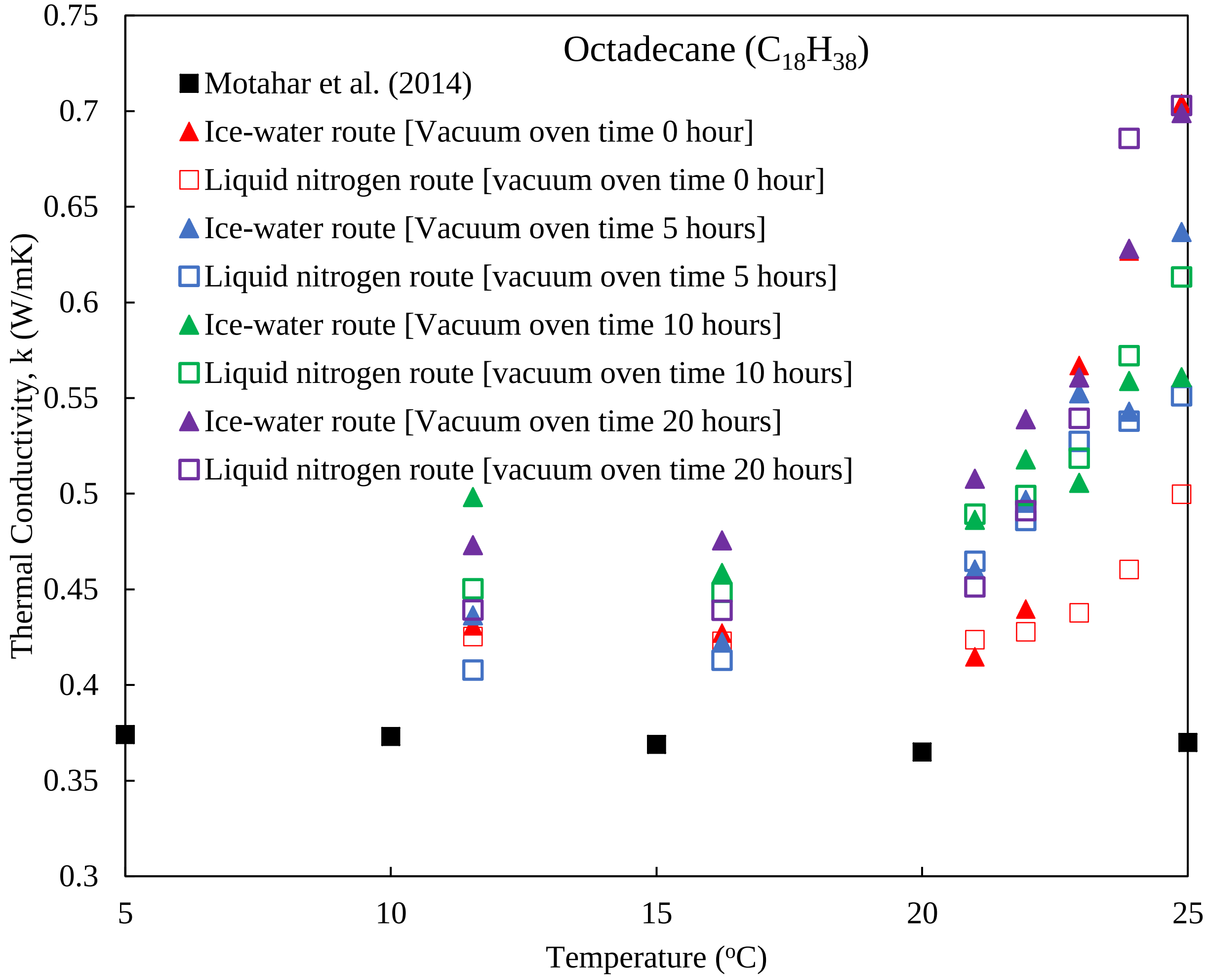

Figure 3.22. Thermal conductivity as a function of temperature below the solid-liquid phase transition temperature (26.5 °C, Ho and Gao, 2009) for octadecane specimen of four vacuum oven times processed by the liquid nitrogen and ice-water routes in addition to results from Motahar et al. (2014).

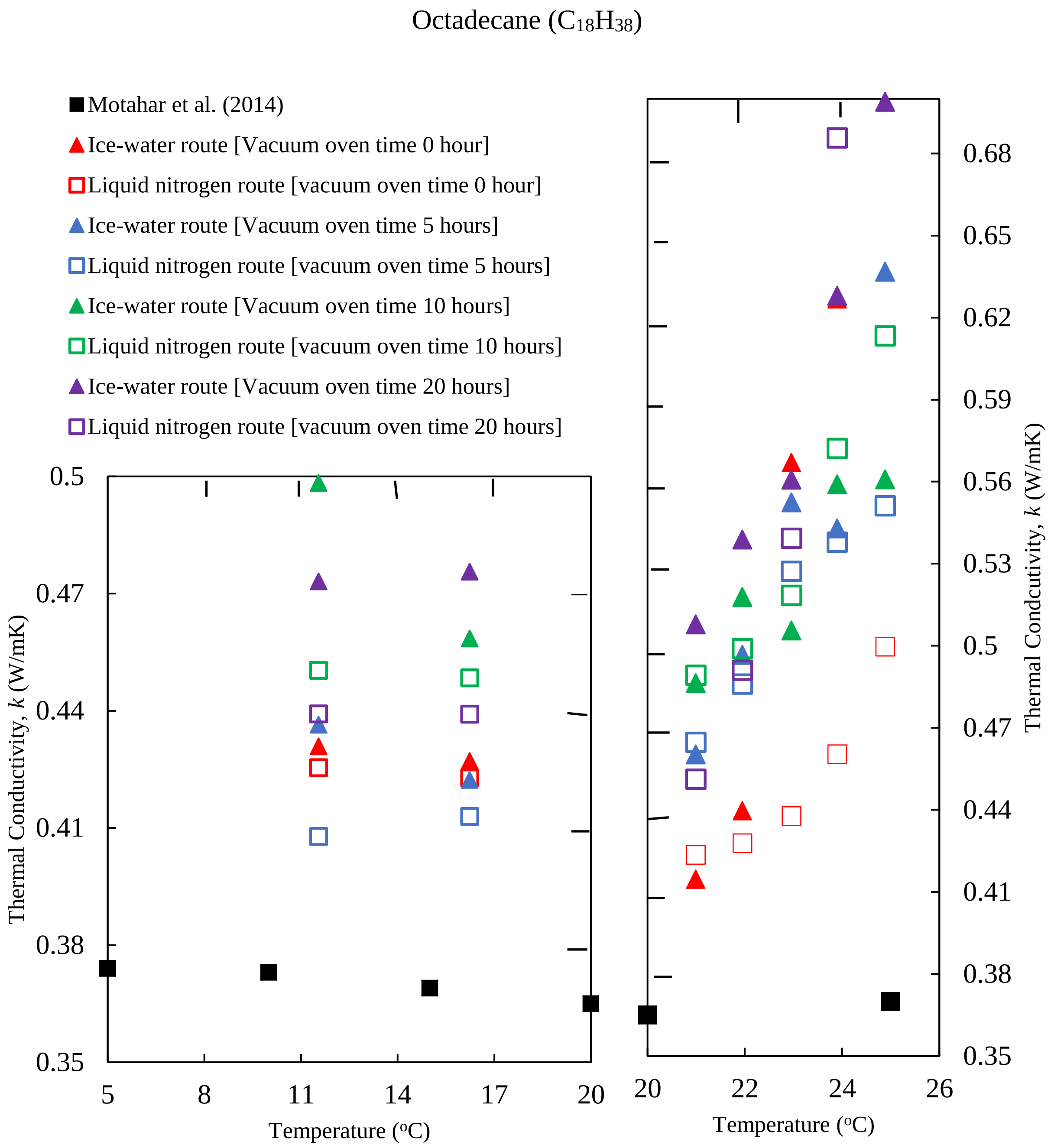

Figure 3.23. Thermal conductivity as a function of temperature below the solid-liquid phase transition temperature (26.5 °C, Ho and Gao, 2009) for octadecane specimen of four vacuum oven times associated with the liquid nitrogen and ice-water routes for two different ranges of temperature (5-20 and 20-26 °C) in addition to results from Motahar et al. (2014).

Chapter 4 Inclusion of the Rotator Phase in a Two-Step Thermal Conductivity Model to Explain the Recorded Enhancements for Eicosane and Octadecane near the Solid-Liquid Phase Transition Point

As discussed in chapter 3, the temperature-dependent thermal conductivity of in-house-prepared eicosane and octadecane samples exhibit enhancements when close to the respective solid-liquid phase transition points. This chapter considers a possible rationale of this behavior by introducing the solid-solid phase transition in a phase change material preceeding solid-liquid phase transition. A computational model of the transient hot-wire technique coded in the ANSYS® FLUENT CFD software is used to determine how the solid-solid phase transition can influence the thermal conductivity behavior of eicosane.

4.1. A brief review of previous publications reporting enhancement in thermal conductivity below the solid-liquid phase transition temperature for different phase change materials

Wang et al. (2008) dispersed chemically-treated multiwalled carbon nanotubes (CNTs) (mean radius 15nm) at 0.5%, 1%, 2% and 5% mass fractions in 98% pure liquid palmitic acid (PA) (Sinopharm Chemical Reagent Co., Ltd, CHINA) by intensive sonication to study the thermal properties such as thermal conductivity, melting temperature and latent heat of the prepared composites. Utilization of the differential scanning calorimetric analysis revealed that the solid-liquid phase change temperature of pure PA was 62.22 ^{o}C and it reduced by 0.07, 1.08, 1.79, 2.4 ^{o}C with 0.5%, 1%, 2% and 5 wt% CNT loadings, respectively. A similar trend was also noticed for latent heat values of the prepared PA/CNT specimen. The authors utilized the transient short-hot-wire method (Xie et al., 2006) to inspect the thermal conductivities of the specimen and it was noticed that the obtained thermal conductivity values remained almost constant below 50 ^{o}C and above 63 ^{o}C. However, as the temperature of the samples approached the solid-liquid phase transition temperature, the thermal conductivity values suddenly rose and then dropped as phase transition occurred (Figure 4.1). The authors stated that this phenomenon related to thermal conductivity was evidence of breakage in the thermal properties of the prepared samples when close to the solid-liquid phase transition. Moreover, based on the findings they suggested the examination of thermal conductivity of pure PA and the PA/CNT composites for three stages: solid phase, liquid phase and from 55 ^{o}C to solid-liquid phase transition. Wang et al. (2009) also carried out a similar study with paraffin wax (PW) (Sinopharm Chemical Reagent Co., Ltd., CHINA) and 95% pure multi-walled carbon nanotubes (MWNTs) (Chendu Organic Chemicals Co. Ltd., CHINA). The authors used ball milling to treat MWNTs before dispersing them at 0.2, 0.5, 1 and 2 wt% loadings in pure liquid PW with a melting point of 53 ^{o}C by intensive sonication to make homogeneous samples. It was observed from differential scanning calorimetry (Diamond DSC, PerkinElmer, USA) that as the MWNTs loading was raised, the latent heat and the solid-liquid phase transition temperatures of the prepared samples decreased. Use of the transient short-hot-wire method (Xie et al., 2006, Sari and Karaipekli, 2007) for measuring the thermal conductivity revealed that the thermal conductivity of the samples did not change significantly below 45 ^{o}C and above 55 ^{o}C, whereas above 45 ^{o}C, as the temperature approached the melting temperatures of pure PW and the composites, the thermal conductivity values increased and then dropped as the orderly solid structure transformed into disorderly liquid structure when the samples changed phase from solid to liquid (Figure 4.2). Wang et al. (2010b) used hydroxide radical functional groups on multi-walled carbon nanotubes before dispersing them at 0.2%, 0.5% and 1%

mass fractions into 98% pure palmitic acid (solid-liquid phase transition temperature 62.4 ^{o}C, Sinopharm Chemical Reagent Co., Ltd., CHINA) to improve its thermal properties. The composites were characterized by scanning electron microscope, differential scanning calorimetry and Fourier transformation infrared spectroscopy. Utilization of the transient-short-hot wire method (Xie et al., 2006) for evaluating the thermal conductivity of the samples required a platinum wire (radius 35 µm) which had the dual function of a heating unit and an electrical resistance thermometer. The results revealed that the prepared composite samples possessed improved thermal conductivities and the determined values continued rising with nanotubes loadings as exhibited in Figure 4.3. Similar to the above discussed studies, as the temperatures of the solid samples became close to the solid-liquid phase transition temperatures, a sudden jump in values of the thermal conductivity was observed and the authors attributed this to the accelerated molecular vibration in solid samples due to temperature rise. Similar to the above-mentioned studies, Nabil and Khodadadi (2013), Fang et al. (2013), Angayarkanni and Philip (2014), and Al Ghossein et al. (2017) reported this "anomalous" behavior of thermal conductivity below the solid-liquid phase transition. These researchers utilized various forms of the transient class of methods (transient plane source method and transient hot-wire method) for investigating the thermal conductivity behavior of different phase change materials such as eicosane and hexadecane with respect to temperature. Figure 4.4 exhibits a collection of enhanced temperature-dependent thermal conductivity data as a function of temperature deviation from respective melting temperatures for four phase change materials when various types of transient methods were applied by different researchers (Wang et al., 2008, Wang et al., 2009, Angayarkanni and Philip, 2014, Nabil and Khodadadi, 2013). No conclusive evidence as to the reason of the observed enhancements in the thermal conductivity of different PCM in the literature has been found. In this chapter, we theorize that the presence of the rotator phase in PCM before solid-liquid phase transition point is responsible for this observed enhancement in thermal conductivity.

4.2. A detailed outline of the problem addressed in the current investigation

In several publications, dependence of the thermal conductivity of solid phase change materials with respect to temperature have been discussed with a specific focus given to when the PCM is about to change phase from solid to liquid. Utilization of the transient techniques in these publications revealed a sudden rise in thermal conductivity when close to melting temperatures as discussed in previous section. As the liquid phase having disorganized molecular motion possess a smaller value of thermal conductivity than the well-structured solid phase of a PCM, the idealized one-step model (relates thermal conductivity and temperature) presented in Figure 4.5 incorporates two different constant values of thermal conductivity (k_s for the solid phase and k_l for the liquid phase with $k_s > k_l$) before and after the solid-liquid phase transition temperatI(T_m) with an instantaneous decrease from k_s to k_l at T_m. The theory of Carslaw and Jaeger (1959) for using the transient hot wire method to obtain a thermal conductivity value requires equilibrium condition and homogeneous medium, so when a portion of PCM remains solid and another portion starts to change phase from solid to liquid, this theory cannot be justifiably used, and any value obtained according to this theory will be erroneous. Nabil and Khodadadi (2017) discussed this problem of using the transient methods specifically the transient hot-wire technique for determination of thermal conductivity in the solid state near the solid-liquid phase transition temperature by developing both analytical and numerical models, Their numerical procedure has been used and extended in the current investigation.

The theory of Carslaw and Jaeger (1959) requires a heating wire of zero-thickness located precisely at the symmetry axis of a solid cylinder-shaped bar of infinite radius (Figure 4.6, replicated from

Nabil and Khodadadi, 2017). Since this is physically not possible, the model geometry includes a cylindrical bar of *2b* diameter and a wire of *2a* diameter. The upper and lower sides of the cylindrical bar are insulated to prevent any heat transfer along the axial direction and as the thermal conductivity near the solid-liquid phase transition temperature is of interest, the outer surface of the cylindrical bar stays at the initial temperature (which is very close to melting point differing only by $-_T = T_m - T_i$) resulting in all thermal conductivity values determined by the transient hot-wire technique in the present study to be taken at this initial temperature. Heat generation inside the wire for a fixed period of time ($0 < t < \tau_p$) as required by the transient methods results in steady increase in the temperature of the wire and because the initial temperature is very close to solid-liquid phase transition point, at time delay τ_m, the solid in contact with the wire may start turning to liquid after which the created solid-liquid interface (shown in Figure 4.6 at position s (t)) will advance toward the remaining solid materials with time producing more liquid content around the heat source.

4.3 Mathematical equations used in the present computation model

We have considered the density of the PCM to remain unchanged before and after solid-liquid phase transition (to avoid any effect of shrinkage). Modeling the case of axisymmetric time-dependent solid-liquid phase transition caused by heat conduction in the radial direction, any heat convection in the formed liquid PCM is neglected. Adopting the simplification of homogeneity and isotropy in the solid wire and the PCM before and after phase transition, the following heat conduction equations were used to determine the temperature variation in the considered geometry:

$$(\rho C_p)_x \frac{\partial T_x}{\partial t} = \frac{1}{r}\frac{\partial}{\partial r}\left(k_x r \frac{\partial T_x}{\partial r}\right) + G_x,\ x = l,\ s,\ w \ \ldots\ldots\ldots\ldots\ldots\ldots\ldots\ldots\ldots\ldots (4.1)$$

with subscripts *l*, s and *w* designating liquid PCM (liquid eicosane), solid PCM (solid eicosane) and wire (platinum), respectively in equation (4.1). The stated heat conduction equation has been applied in this model for the following conditions:

At the solid phase: $a< r < b; t > 0$ and $G_s = 0$, i.e. no heat generation inside solid PCM.

At the liquid phase: $a \leq r < s(t), t \geq \tau_m$ and $G_l = 0$, i.e. no heat generation inside liquid PCM.

For wire: $0 < r \leq a, t > 0$ and $G_w = \frac{q}{\pi a^2}$, heat is generated inside the wire of diameter $2a$ for a fixed time period.

At the wire-solid PCM interface before melting starts:

When $0 < t < \tau_m$, and $r = a$, $k_w \left(\frac{\partial T_w}{\partial r}\right)_{r=a} = k_s \left(\frac{\partial T_s}{\partial r}\right)_{r=a}$ and $T_w(a,t) = T_s(a,t)$.

At the wire-liquid PCM interface after melting starts:

When $t \geq \tau_m$, and $r = a$, $k_w \left(\frac{\partial T_w}{\partial r}\right)_{r=a} = k_l \left(\frac{\partial T_l}{\partial r}\right)_{r=a}$ and $T_w(a,t) = T_l(a,t)$.

At the interface of two different phases of the PCM after melting starts:

When $t \geq \tau_m$, and $r = s(t)$, $T_s(r,t) = T_l(r,t) = T_m$ and $k_s \frac{\partial T_s}{\partial r} - k_l \frac{\partial T_l}{\partial r} = \rho L \frac{ds(t)}{dt}$.

At $t = 0$ and $r > 0$, $T_w = T_s = T_i$

At $t > 0$ and $r = 0$, $\frac{\partial T_w}{\partial r} = 0$

At $t > 0$ and $r = b$, $T_s = T_i$.

In the current investigation, ρ, r, T, t, C_p, k, q, a, $s(t)$, L and G used in above equations designate density, radius, temperature, time, specific heat, thermal conductivity, heat source with a fixed value, radius of the wire, time-dependent position of the solid-liquid interface, latent heat and heat generation inside the wire, respectively. When equation (4.1) is applied under the conditions of liquid phase and solid wire, they become similar to the equations used by Assael et al. (1998). In this formulation, the non-dimensional parameters $Ste = \frac{(C_p)_l(T_m - T_i)}{L}, \frac{a}{b}, \frac{k_s}{k_l}, \frac{\alpha_w}{\alpha_l}, , \frac{q}{k_l(T_m - T_i)}, \frac{\alpha_l}{\alpha_s}$, and $\frac{k_w}{k_l}$ become relevant.

4.4. A detailed description of the FLUENT model utilized to simulate the transient hot-wire method for determining the thermal conductivity of eicosane with respect to temperature

Like Nabil and Khodadadi (2017), in the current investigation, to solve the phase change (utilizing the enthalpy model) and the heat conduction equations, the ANSYS® FLUENT 17.1 CFD package was used. The physical system was modeled as a cylindrical bar of 5.992 mm radius and 1 mm height along with a wire (radius 8 μm and 1 mm height) placed along the symmetry axis. With the wire acting as the heat source, the bar and the wire consist of solid eicosane and platinum, respectively and properties of these materials have been taken from Nabil and Khodadadi (2017) as presented in Table 4.1. At initial time instant t = 0, the wire begins to discharge heat at constant 1 W/m and stops discharging after 1 sec, similar to a pulse function. The values 1 W/m and 1 sec had been used by Nabil and Khodadadi (2017) and Assael et al. (1998). We have used the following equation reported by Carslaw and Jaeger (1959) to calculate the thermal conductivity of eicosane from the slope of the wire surface temperature increase ($\Delta T(a, t)$) vs. time period curve represented on a semi-logarithmic scale:

$$\Delta T(a,t) = \frac{q}{4\pi k} \ln\left(\frac{4\alpha t}{a^2 C}\right), \tag{4.2}$$

This equation applies for the idealized transient hot wire technique, and α and k stand for the two properties of the phase change material. As discussed in great detail by de Groot et al. (1974), Healy et al. (1976) and Roder (1981), we can calculate the thermal conductivity of eicosane by equating $\frac{q}{4\pi k}$ to the numerical value of the slope of the $\Delta T(a,\ t)$ versus the heating time period curve. We allocated 20 elements to the platinum wire and 230 elements to the solid eicosane using variable spacings. As heat conduction occurs only in radial direction, the height of the cylindrical bar and wire can be any arbitrary value. The geometric shrinkage ratios utilized to produce variable grids for the platinum wire and solid eicosane were 0.9 and 0.98, respectively to generate dense mesh near the platinum wire and solid eicosane interface. Along the radial direction, the height of both components was separated into three identical portions generating a total of 750 mesh elements. To run the model of current investigation, time step size of 10 μs and 100,000 time steps were selected. The under-relaxation factors were as follows: pressure 0.3, momentum 0.7, liquid fraction update 0.9, and energy 1. In the current investigation, the selected convergence criterion (10^{-9}) was fulfilled at 20 iterations or less at each time step.

4.5. A short description of the presence of solid-solid phase transition or the rotator phase before the solid-liquid phase transition in eicosane

One intriguing attribute detected in several long-chain n-alkanes is the existence of the solid-solid phase transition (commonly referred as the rotator phase) which is characterized by the rotation of each molecule up to a limit, usually a few degrees at high temperatures (Müller, 1927, Vélez et al., 2015, Briard et al., 2003, Xie et al., 2008). We have theorized that this structural transformation before the solid-liquid phase transition point (de Zárate et al., 2010, Vélez et al., 2015) leads to quite high thermal conductivity values and is possibly responsible for the widely-recorded enhancement of thermal conductivity of phase change materials.

4.6. Thermal conductivity behavior with respect to the initial temperature ($<T_m$) for eicosane through solid-liquid phase transition corresponding to the one-step model

In order to validate their numerical model, Nabil and Khodadadi (2017) used two special cases where the initial temperatures were precisely 306 K and 313 K. They chose these initial temperatures to guarantee that no phase transition occurs at the upper limit of the adopted heating period. The thermal conductivity values acquired from the model by Nabil and Khodadadi (2017) for these two special cases were 0.4242 W/mK and 0.1468 W/mK, yielding an error of 1% for solid state and 0.81% for liquid state, respectively. We made several modifications in the settings of our model when compared to Nabil and Khodadadi (2017) as mentioned in Table 4.2 to reduce the errors in the acquired thermal conductivity values. This modified model used in the current investigation gave a value of 0.4186 W/mK for T_i = 306 K and 0.1475 W/mK for T_i =313 K, reducing the errors to 0.33% for solid state and 0.28% for liquid state, respectively. Figure 4.5 and Table 4.2 show the comparison between the thermal conductivity values acquired by Nabil and Khodadadi (2017) and present superior numerically-modified model with respect to numerous initial temperatures. In the current upgraded investigation, we used five initial temperatures of 308.4, 308.6, 308.8, 309 and 309.1 K (ε_T = 1.6, 1.4, 1.2, 1.0 and 0.9 ^{o}C, respectively) as opposed to six initial temperatures (308.3, 308.4, 308.5, 308.6, 308.7 and 308.9 K) used by Nabil and Khodadadi (2017). It is evident that, the thermal conductivity values acquired by the present upgraded model are greater than the values obtained by Nabil and Khodadadi (2017). For the initial temperature of 308.4 K, the thermal conductivity value acquired in the present upgraded study was 5.76% larger than the value acquired by Nabil and Khodadadi (2017). For T_i = 308.6 K, the present upgraded study gave 4.30% larger value than Nabil and Khodadadi (2017). Like the findings of Nabil and Khodadadi (2017), as the initial temperature gradually ascended, two things became conspicuously apparent (Figure 4.7). First, with the gradual ascension of initial temperature, the melting point was reached relatively swiftly (310 K) on the surface of the wire. So, the time period for gradual temperature ascension was basically cut short and eicosane adjoining the wire started to melt relatively sooner. Secondly, as the thermal conductivity of liquid eicosane is nearly one-third of solid eicosane and thermal diffusivity of solid and liquid eicosane have a 3.64:1 ratio, it required a relatively longer period of time for heat from the energy source to pierce through the liquid eicosane encircling the wire. When T_i =308.4 K, the melting temperature was attained near the upper limit of the heating period and the difference between the assigned value and acquired thermal conductivity value was 2.38%. For initial temperatures of 308.6, 308.8, 309 and 309.1 K, these differences were 32.4%, 57.3%, 62.4%, and 62.4%, respectively, ascending with the initial temperature. As clearly observed from Table 4.2, the acquired R^2 values non-monotonically varied from 0.9212-0.9999 in the present study (Figure 4.8-4.10). In the numerical upgraded model, 200 temperature ascension output points were generated at identical time gaps and among the 200 output points, the first 10 and last 10 output points were not considered (de Groot et al., 1974). Not considering the first 10 and last 10 data points did not have any obvious influence on the slope of the generated curves and the acquired thermal conductivity values. For five initial temperatures carefully studied with the present upgraded model, nearly all acquired thermal conductivity values were between the assigned values of solid eicosane and liquid eicosane, and approached the assigned value of liquid eicosane with ascension of the initial temperature.

4.7 Theory of the two-step model for eicosane relating thermal conductivity and temperature near the solid-liquid phase transition

To show that the declared rotator phase can be responsible for the sudden climb of thermal conductivity near the melting temperature, we have proposed a variation of thermal conductivity of eicosane as a two-step model as exhibited in Figure 4.11. We have assumed that the rotator phase commences forming at T_R =309 K and at T_R, the thermal conductivity suddenly ascends like a step function to k_R = 0.84 W/mK. In effect, we have added two new parameters, i.e. $\frac{k_R}{k_l}$ and $\frac{T_R-T_m}{T_i-T_m}$ to the theoretical model. It is important to mention that, the allotted values of T_R and k_R are chosen arbitrarily to show how the thermal conductivity of eicosane changes with temperature when the rotator phase commences forming. We have considered that before $T_{R,}$ thermal conductivity of eicosane is 0.42 W/mK and at the designated melting point (310 K), thermal conductivity swiftly falls from 0.84 W/mK to 0.148 W/mK, as 0.42 W/mK and 0.148 W/mK are the thermal conductivity values used by Nabil and Khodadadi (2017) for solid and liquid eicosane, respectively.

4.8 Thermal conductivity behavior with respect to the initial temperature (<T_m) for eicosane through solid-solid and solid-liquid phase transition corresponding to the two-step model

As exhibited in Figure 4.11 and Table 4.3, when the solid-solid phase transition or rotator phase is included in the two-step model, thermal conductivity of eicosane obviously displays three specific trends: 1) for temperature difference ε'_{-} = (T_R - T_i) =1.6 to 1 °C, and T_i = 307.4 to 308 K, thermal conductivity increases similar to the anomalous climb recorded in experimental results, 2) for ε'_T = 0.8 to -0.14 °C, and T_i = 308.2 to 309.14 K, thermal conductivity becomes virtually stable with respect to the initial temperature (< T_m) and 3) for ε'_T = -0.18 to -0.8 °C, and T_i = 309.18 to 309.8 K, thermal conductivity descends swiftly to k_l much like the behavior of the one-step model, and the corresponding R^2 coefficients of determination varied non-monotonically from 0.987-0.9991, 0.9833-0.9898 and 0.8019-0.9985, respectively (Figure 4.12-4.20). As the positive-sign ε'_T values decreased towards zero, T_R was attained relatively sooner and the ascension of wire surface temperature became more time-consuming (Figure 4.21). Because the solid phase and rotator phase have a thermal conductivity ratio of 1:2 and a thermal diffusivity ratio of 1:2, the bulk share of the energy from the heated wire was conducted easily through the rotator phase leaving only a small share at the wire surface. It was clearly noticed that for all positive or zero values of ε'_T, wire surface temperature remained less than T_m after the heating period was over.

Opposite to the above phenomenon, as the negative-sign ε'_T values decreased towards -0.8 ^oC, the eicosane encircling the wire started to melt relatively sooner and the ascension of wire surface temperature significantly accelerated (Figure 4.22). Because the rotator phase and liquid phase have a thermal conductivity ratio of 5.675:1 and a thermal diffusivity ratio of 7.28:1 (= α_R/α_l), only a minor share of energy from the heated wire was able to pierce through the reduced conductive liquid phase leaving the major share at the wire surface.

4.9 Analysis and interpretation of the numerical results in relation to the experimental findings and suggestions for subsequent similar studies

Combining data from Figure 4.11 acquired from the present numerical study (also found in Hoque et al., 2018) with the experimental data of Figure 4.4, a striking similarity is clearly exhibited in the trend of climb of thermal conductivity before T_m (Figure 4.23). Therefore, it can be stated that the current two-step model of the solid-solid phase transition is capable of resolving the observed enhancements of temperature-dependent thermal conductivity when close to T_m. However, it is important to mention that if we want to compare the results given by the computational study to any experimental results, values of k_R and T_R are necessary. In the literature, we did not find any value of k_R for eicosane. In the experimental portion of this work, an effort was made to find the highest attainable value of thermal conductivity of eicosane before T_m in order to establish an estimated value of k_R. However, above 35.5 ^oC, for even the lowest heating power and time duration, eicosane sample temperature reached above T_m and damaged the specimen. At 35.5 ^{o}C, the highest value of thermal conductivity of eicosane was 0.7065 W/mK obtained by the ice-water route corresponding to 10 hour vacuum oven time. As it is apparent from Figure 4.11, after thermal conductivity reaches the highest value, it does not exhibit any significant change within a certain temperature range. Since the experimental thermal conductivity values for the two routes continued ascending, 0.7065 W/mK is not the highest possible value for eicosane and higher values can be achieved. Thus, there is a future scope of extending this work by finding a definite value of k_R and then observing the error percentage between the numerical and experimental values. In conclusion, the presence of rotator phase can successfully explain the sudden anomalous ascend in thermal conductivity before solid-liquid phase transition temperature is reached.

Table 4.1. Properties of Platinum (heating wire) in solid phase and eicosane (surrounding cylindrical medium) in liquid and solid phases taken from Nabil and Khodadadi (2017)

Platinum (Pt)	
ρ (kg/m^3)	21,450
C_p (J/kgK)	130
k (W/mK)	71.7
Eicosane	
ρ (kg/m^3)	840
$(C_p)_s$ & $(C_p)_l$ (J/kgK)	1,920 & 2,460
k_s & k_l (W/mK)	0.42 & 0.148
L (J/kg)	247,000
T_m (K)	310

Table 4.2. Distinctions in the settings of present upgraded model when compared to Nabil and Khodadadi (2017) along with evaluated thermal conductivity of eicosane with respect to the initial temperature (< T_m) and the R^2 coefficients of determination for the case of the one-step model without considering the rotator phase.

	Nabil and Khodadadi (2017)	Present Study
Details of the Computational Methodology		
- Spatial Discretization of Pressure Eq.	Standard	Second Order
- Spatial Discretization of Momentum Eq.	First Order Upwind	Second Order Upwind
- Spatial Discretization of Energy Eq.	First Order Upwind	Second Order Upwind
Transient Term Formulation	First Order Implicit	First Order Implicit
Convergence Criterion for Energy Eq. Residuals	10^{-9}	10^{-9}
Initial (Measurement) Temperature T_i (K)	k (W/mK) / R^2	k (W/mK) / R^2
308.3	0.4250 / 1	
308.4	0.4066 / 0.9675	0.43 / 0.9939
308.5	0.3239 / 0.9243	
308.6	0.2723 / 0.9312	0.284 / 0.9212
308.7	0.1861 / 0.9215	
308.8		0.1793 / 0.9815
308.9	0.1486 / 0.9523	
309		0.1579 / 0.9998
309.1		0.1578 / 0.9999

Table 4.3. Thermal conductivity values of eicosane with respect to twenty-two initial temperatures (<T_m) and temperature differences, ε'_T (defined as: $T_R - T_i$), along with the R^2 coefficients of determination for the two-step model (including the rotator phase).

Initial (Measurement) Temperature T_i (K)	Temperature Difference ε'_T (°C)	k (W/mK)	R^2
307.4	1.6	0.43	0.9939
307.5	1.5	0.4537	0.998
307.6	1.4	0.4858	0.9991
307.7	1.3	0.5443	0.9927
307.8	1.2	0.6149	0.9873
307.9	1.1	0.68	0.987
308	1	0.7307	0.9889
308.2	0.8	0.784	0.9898
308.4	0.6	0.7973	0.986
308.6	0.4	0.7902	0.9861
308.8	0.2	0.7878	0.9857
309	0	0.7871	0.9855
309.1	-0.1	0.7871	0.9855
309.14	-0.14	0.7817	0.9833
309.18	-0.18	0.6848	0.9166
309.22	-0.22	0.5147	0.8193
309.26	-0.26	0.376	0.8019
309.3	-0.3	0.2906	0.837
309.4	-0.4	0.1956	0.9318
309.5	-0.5	0.164	0.9791
309.7	-0.7	0.1496	0.9985
309.8	-0.8	0.15	0.998

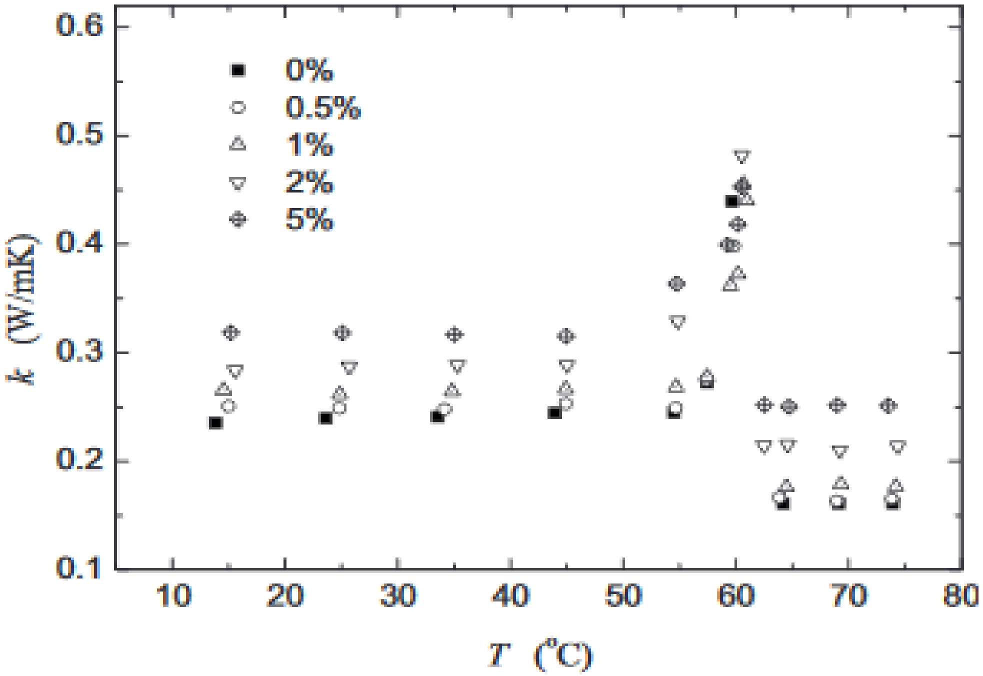

Figure 4.1 Thermal conductivity of Palmitic acid/CNT specimen with respect to temperature for 0, 0.5, 1, 2 and 5 wt% concentrations of CNTs before and after solid-liquid phase transition point inspected by a transient method (Wang et al., 2008)

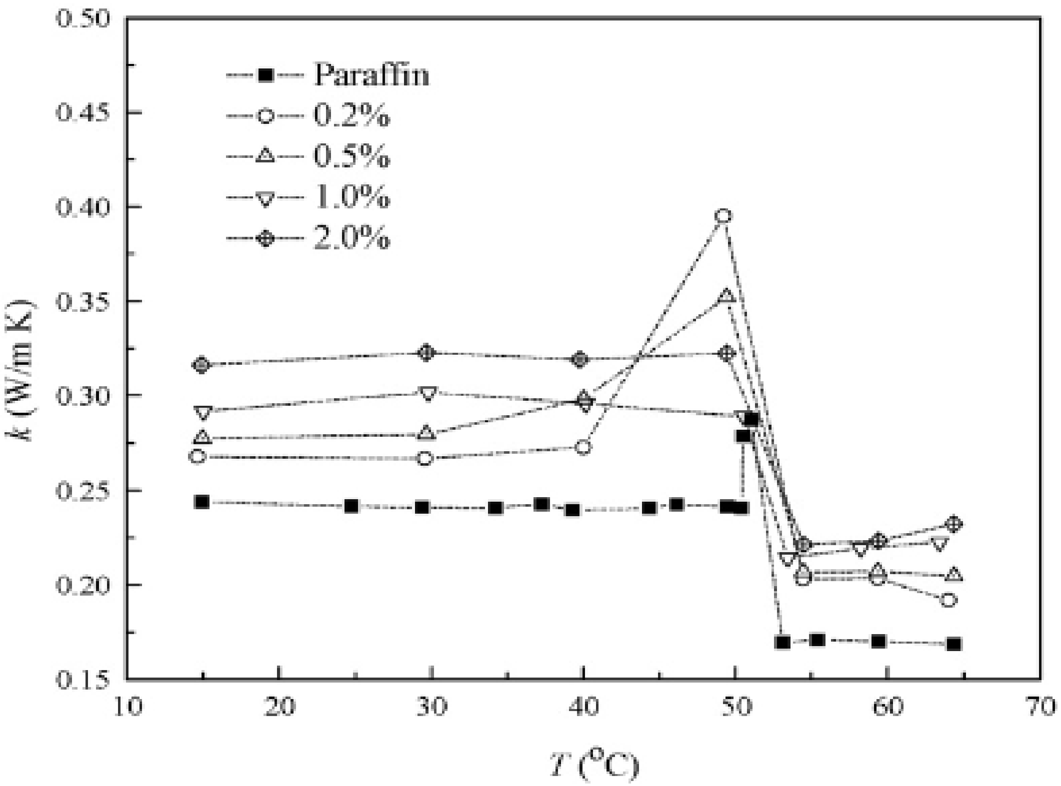

Figure 4.2. Thermal conductivity of paraffin wax/MWNT specimen with respect to temperature for 0, 0.2, 0.5, 1 and 2 wt% concentrations of MWNTs before and after solid-liquid phase transition point inspected by a transient method (Wang et al., 2009)

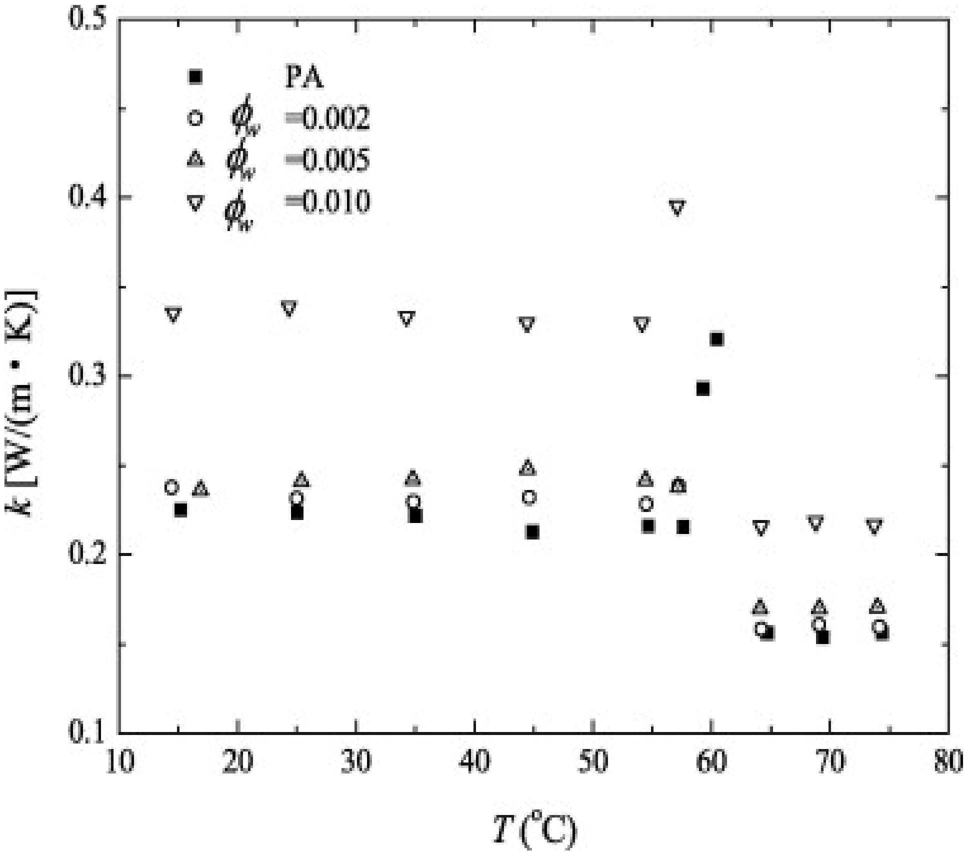

Figure 4.3. Thermal conductivity of palmitic acid/TCNT specimen with respect to temperature for 0, 0.2, 0.5 and 1 wt% concentrations of TCNTs before and after solid-liquid phase transition point inspected by a transient method (Wang et al., 2010b)

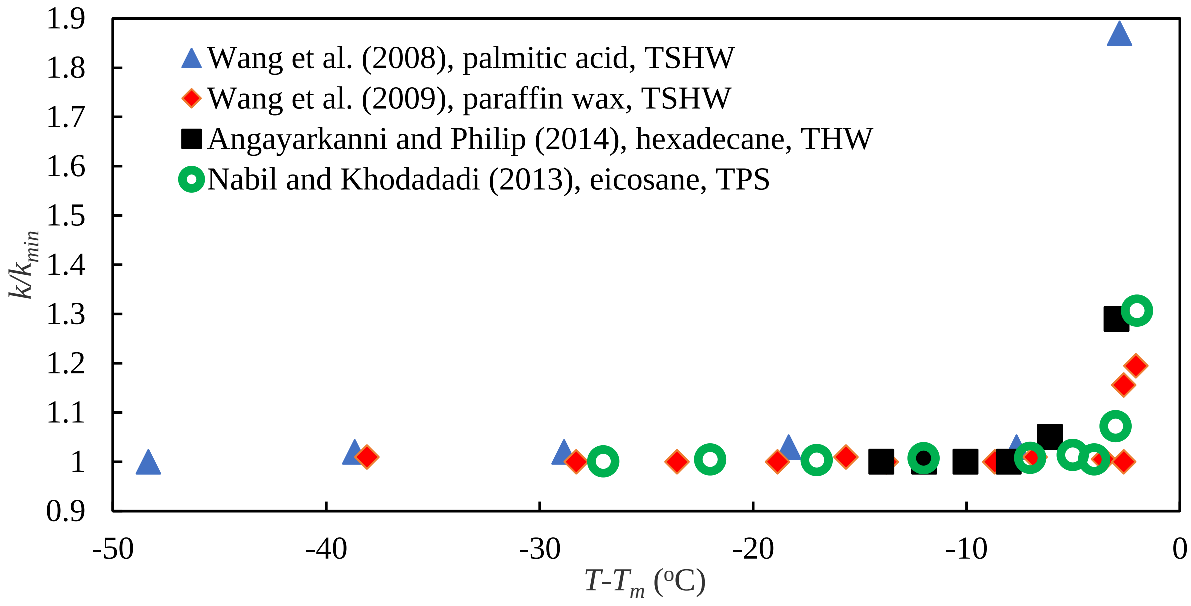

Figure 4.4. Collection of temperature-dependent thermal conductivity dataas a function of temperature deviation from the respective melting temperatures for four phase change materials when various types of transient methods were applied by different researchers (Wang et al., 2008, Wang et al., 2009, Angayarkanni and Philip, 2014, Nabil and Khodadadi, 2013)

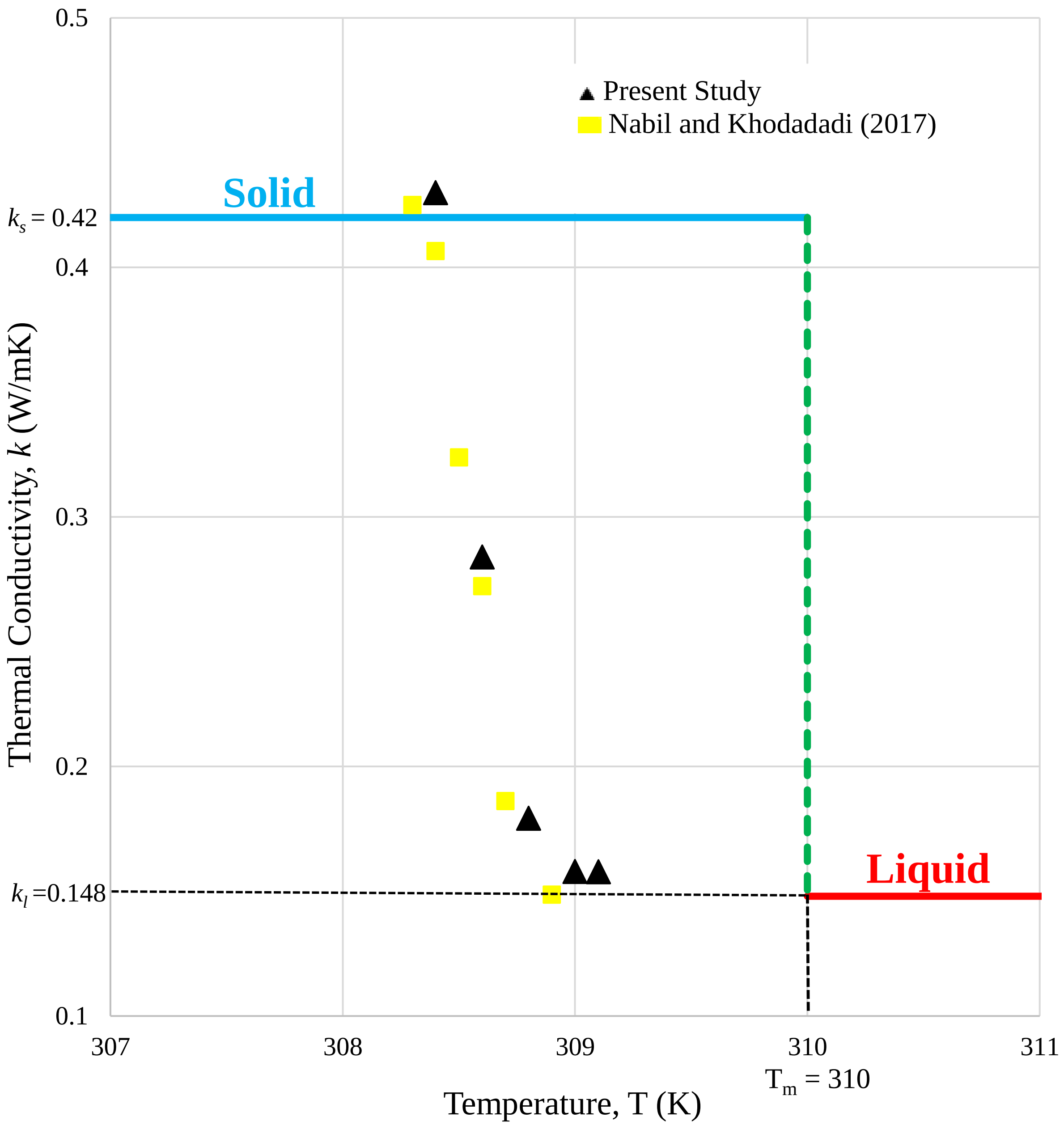

Figure 4.5. Idealized variation of thermal conductivity with respect to temperature for the case of the one-step model when solid-liquid phase transition is very close and comparison between the results acquired by the present upgraded model and the one used by Nabil and Khodadadi (2017) for the transient hot-wire method.

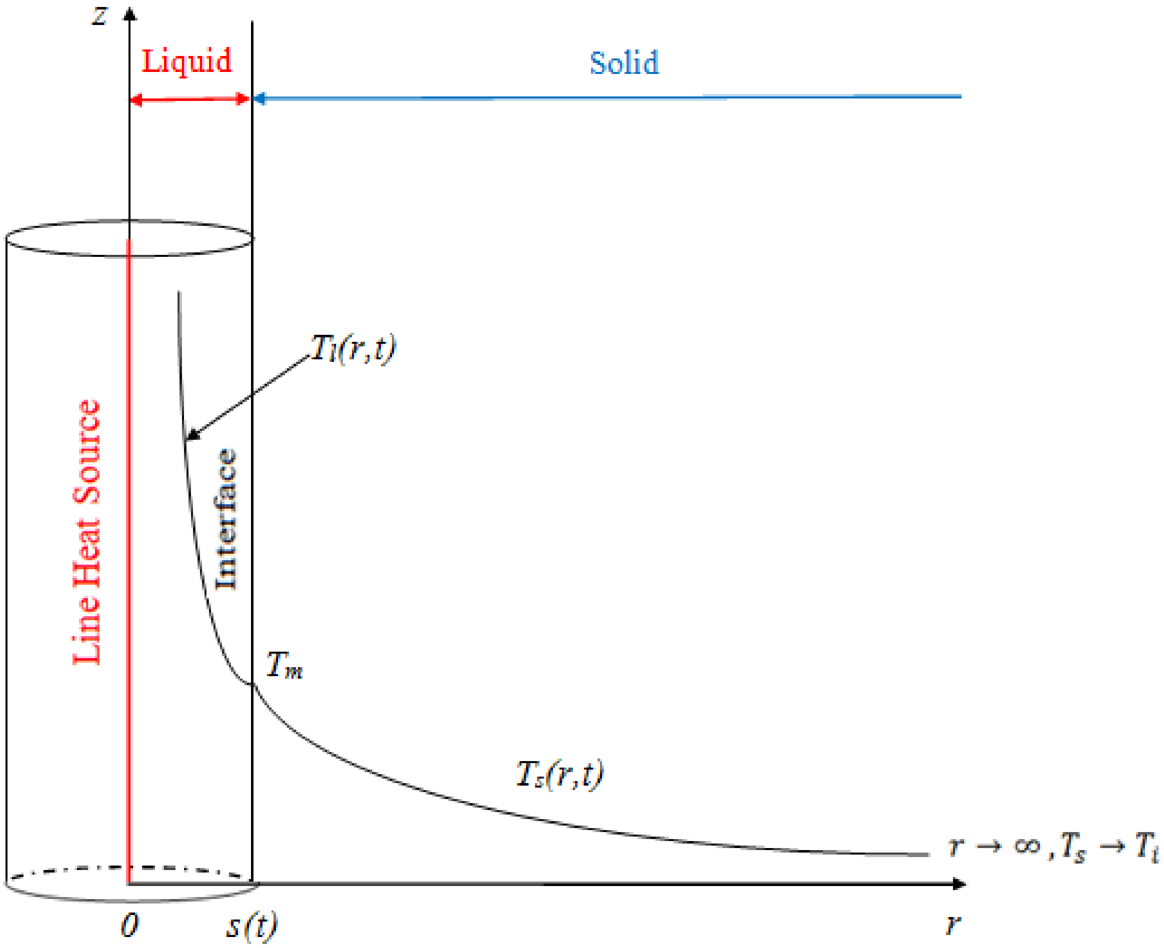

Figure 4.6. Current model of solid-liquid phase transition in the transient hot wire method where a heating wire of zero-thickness is located precisely along the symmetry axis of a solid cylinder-shaped bar of infinite radius (Nabil and Khodadadi, 2017)

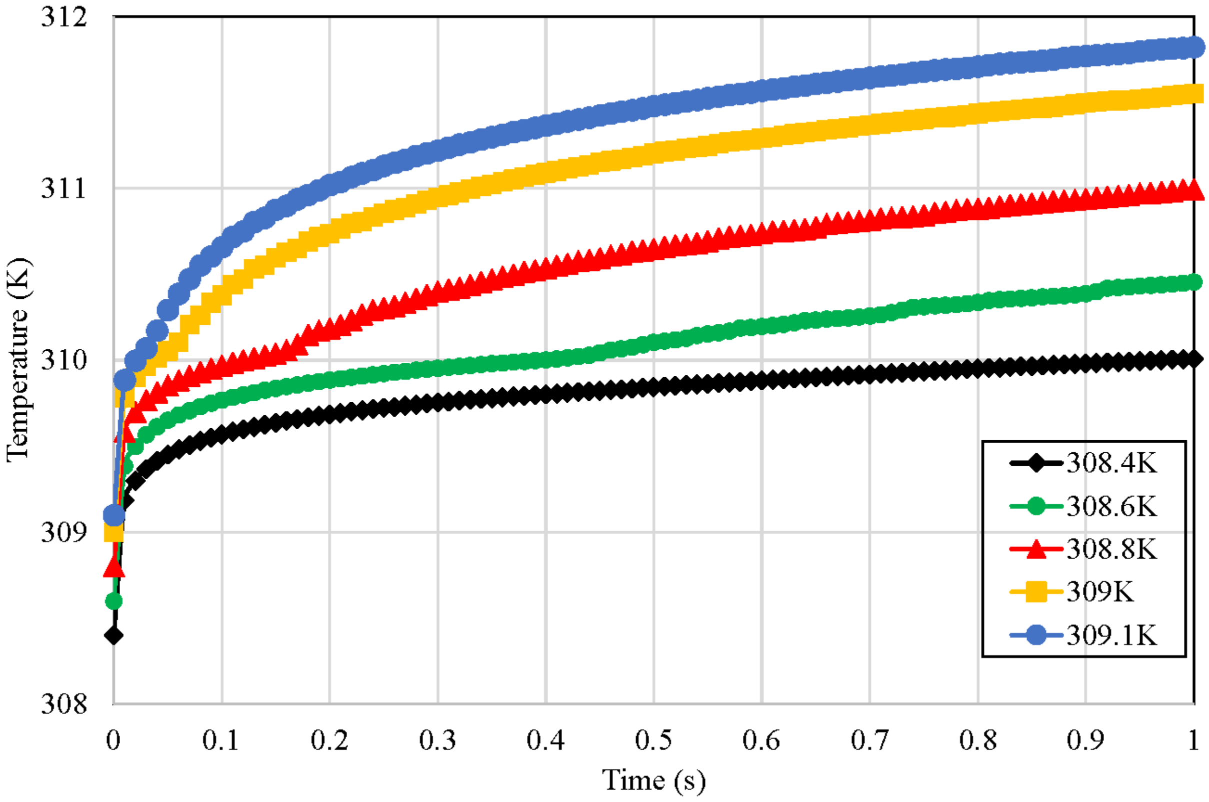

Figure 4.7. Dependence of the wire surface temperature with the heating time for the one-step model (excludes the rotator phase) in transient hot-wire method

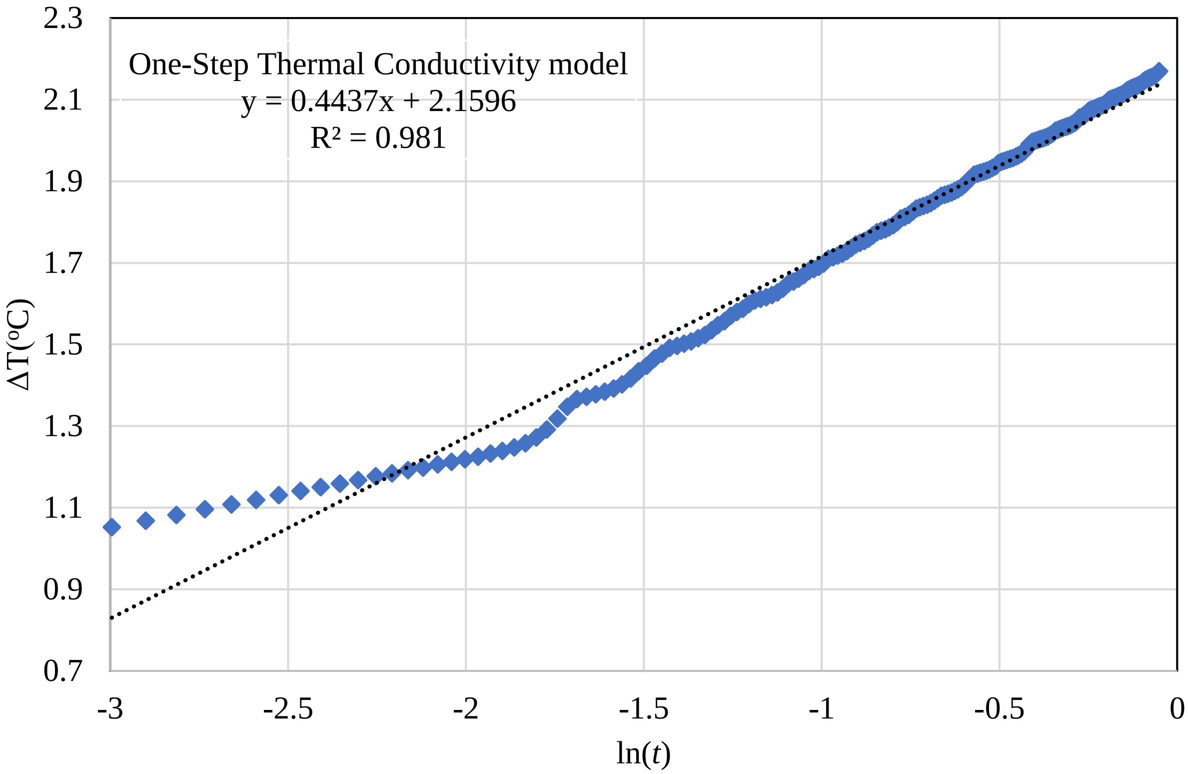

Figure 4.8. Ascension of wire surface temperature with the heating time for the one-step model (excluding the rotator phase) in transient hot-wire method with T_i = 308.8 K

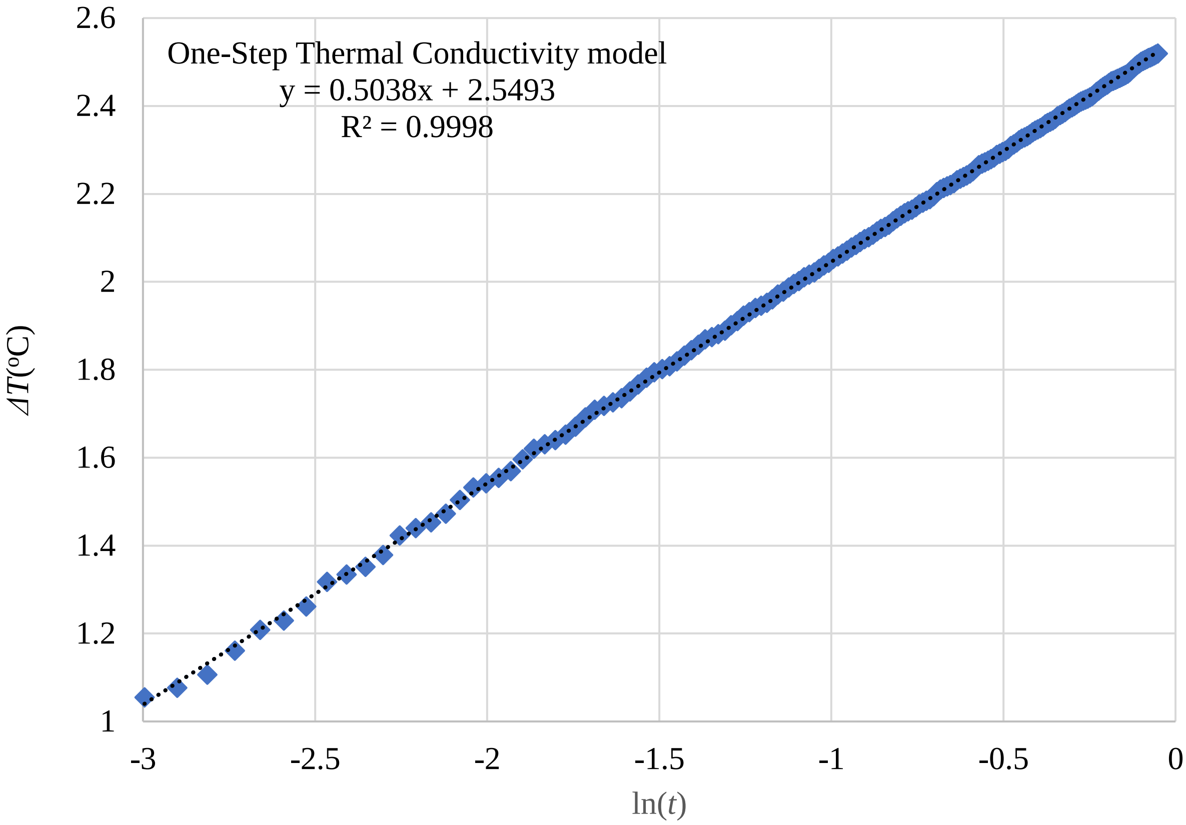

Figure 4.9. Ascension of wire surface temperature with the heating time for the one-step model (excluding the rotator phase) in transient hot-wire method with T_i = 309 K.

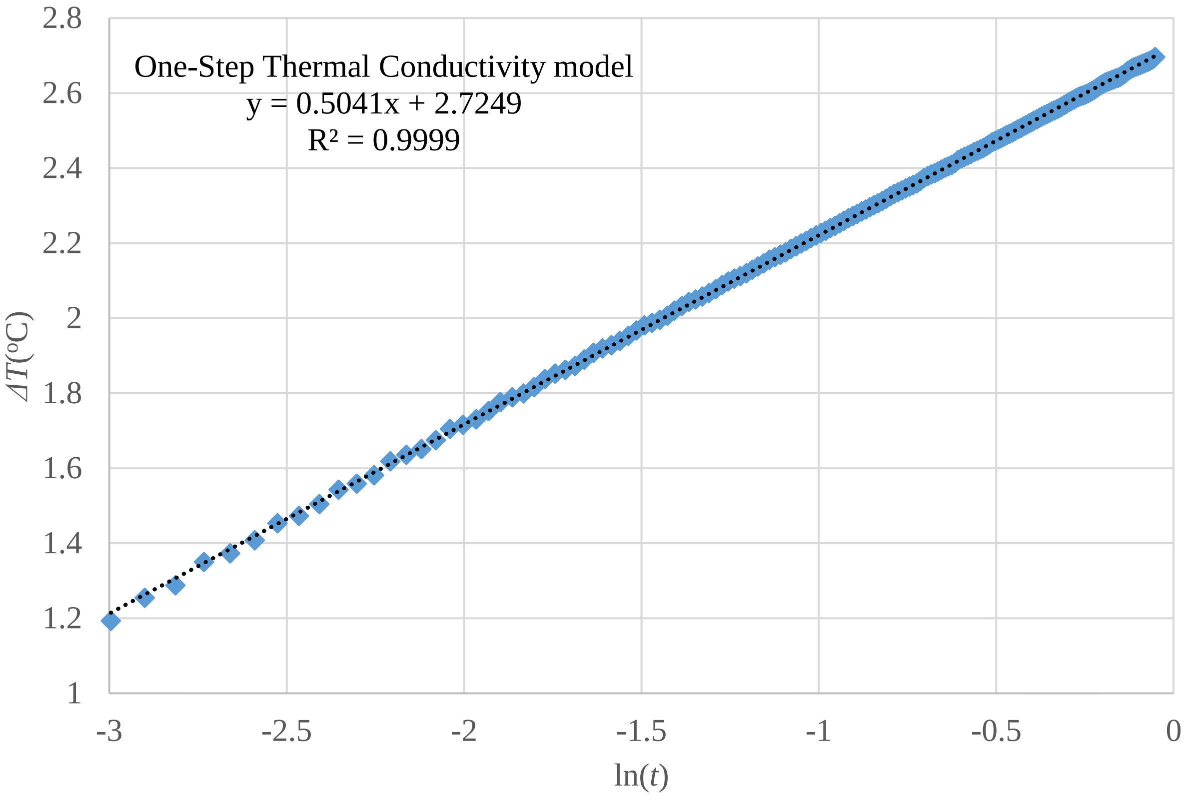

Figure 4.10. Ascension of wire surface temperature with the heating time for the one-step model (excluding the rotator phase) in transient hot-wire method with T_i = 309.1 K.

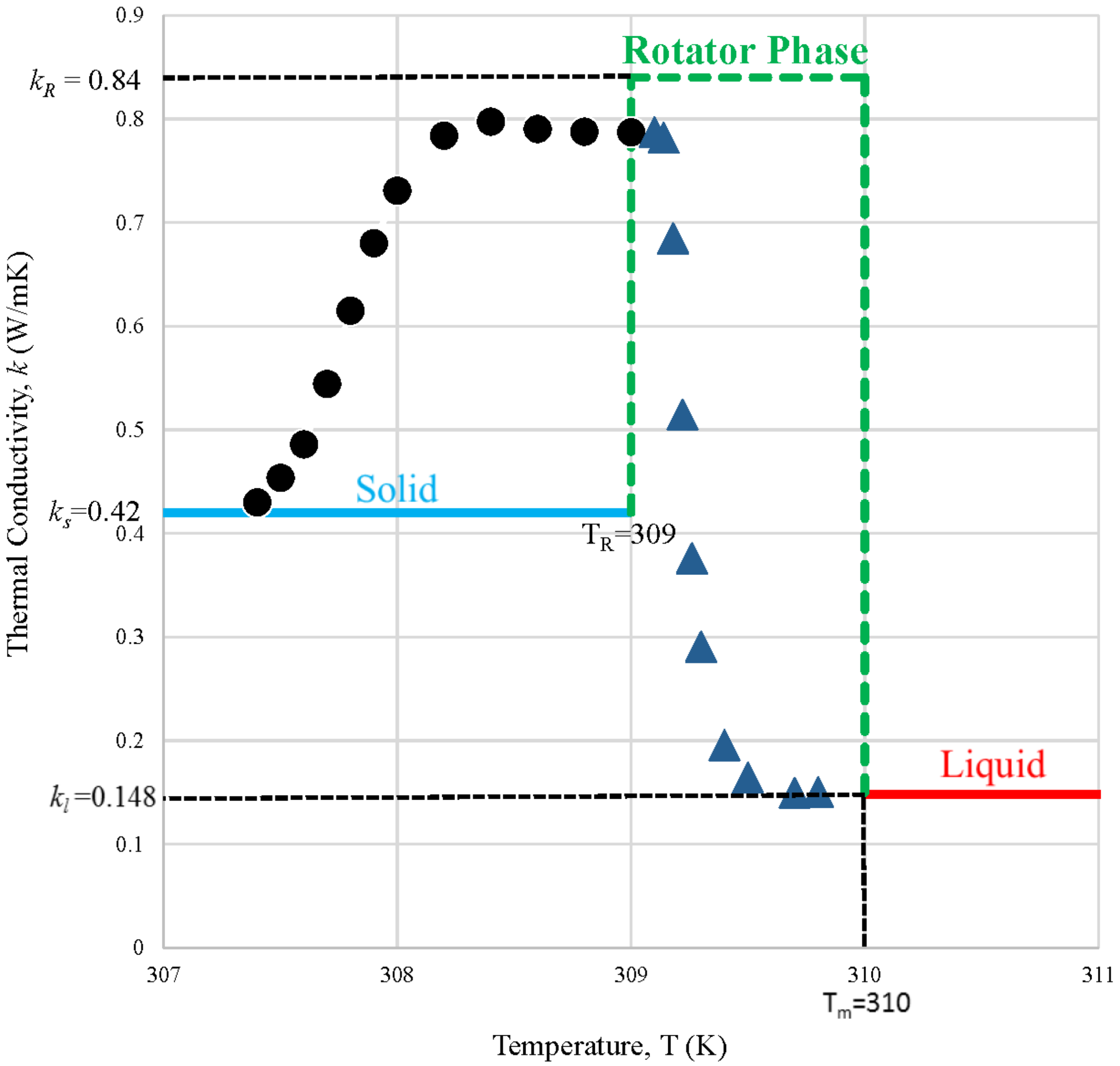

Figure 4.11. Thermal conductivity variation as a function of temperature for the case of the two-step model (including the rotator phase) .

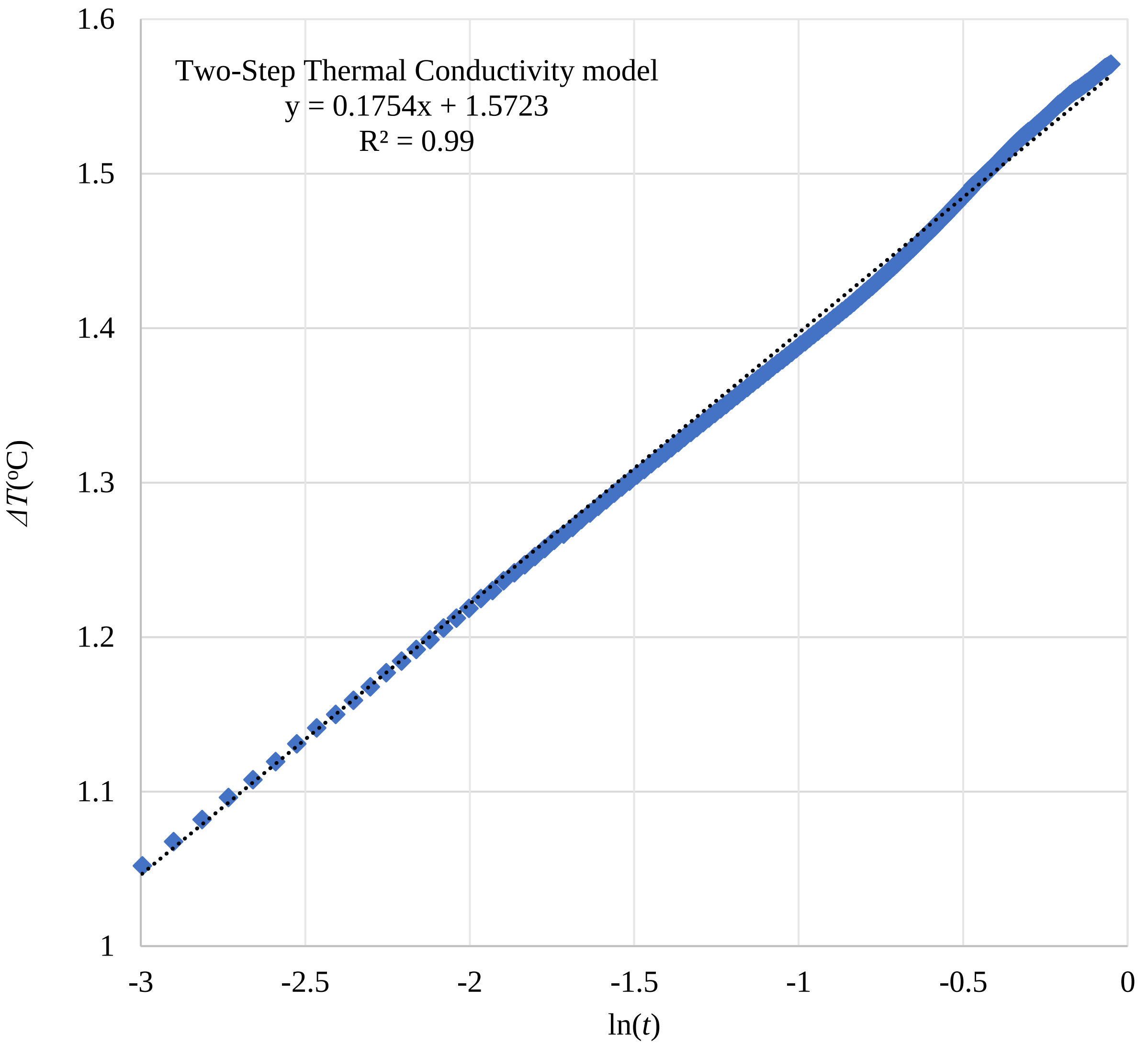

Figure 4.12. Ascension of wire surface temperature with respect to heating time especially through phase transition for the two-step model (includes rotator phase) in the transient hot-wire method with T_i =307.5 K is exhibited here.

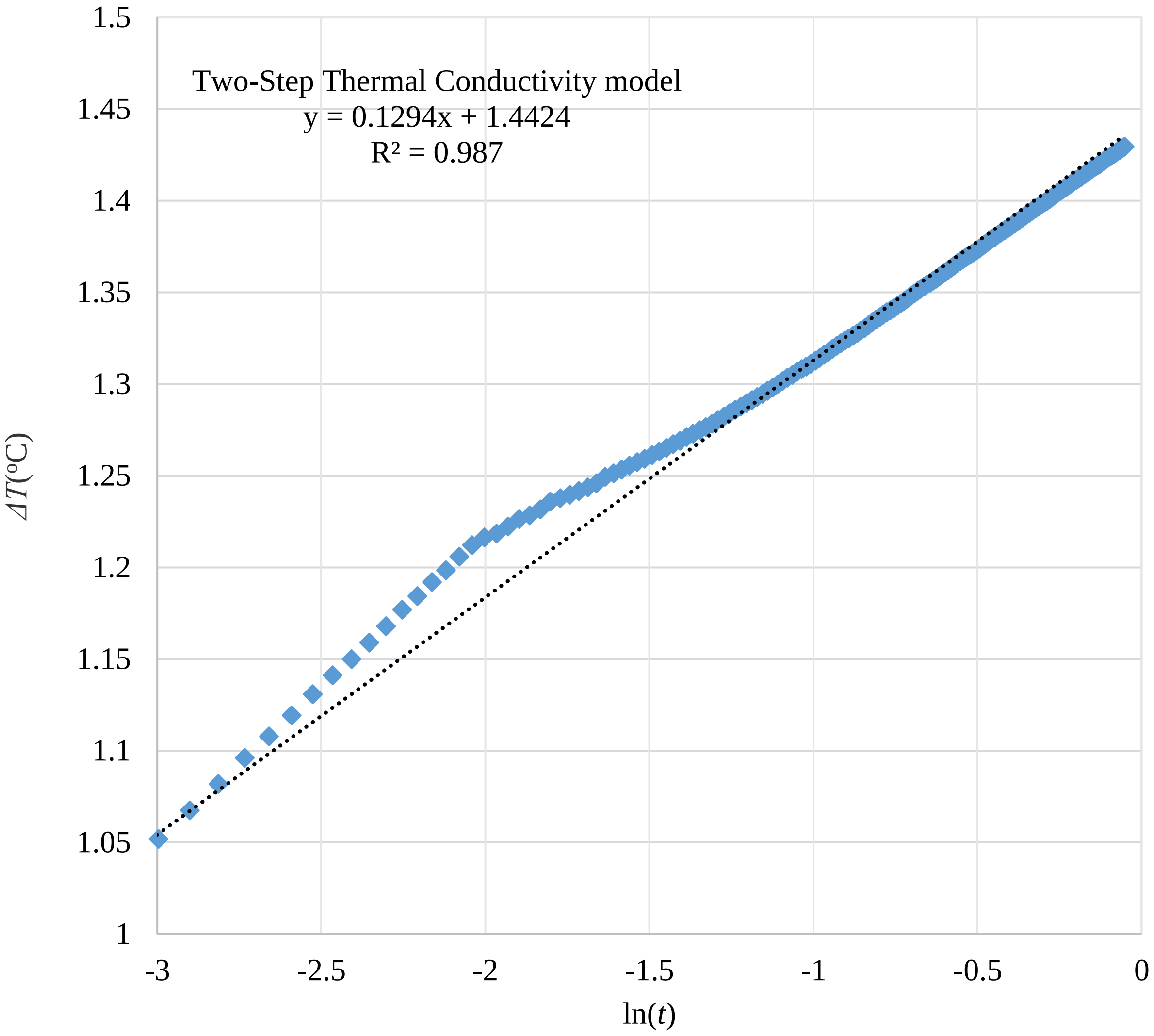

Figure 4.13. Ascension of wire surface temperature with respect to heating time especially through phase transition for the two-step model (includes rotator phase) in the transient hot-wire method with T_i =307.8 K is exhibited here.

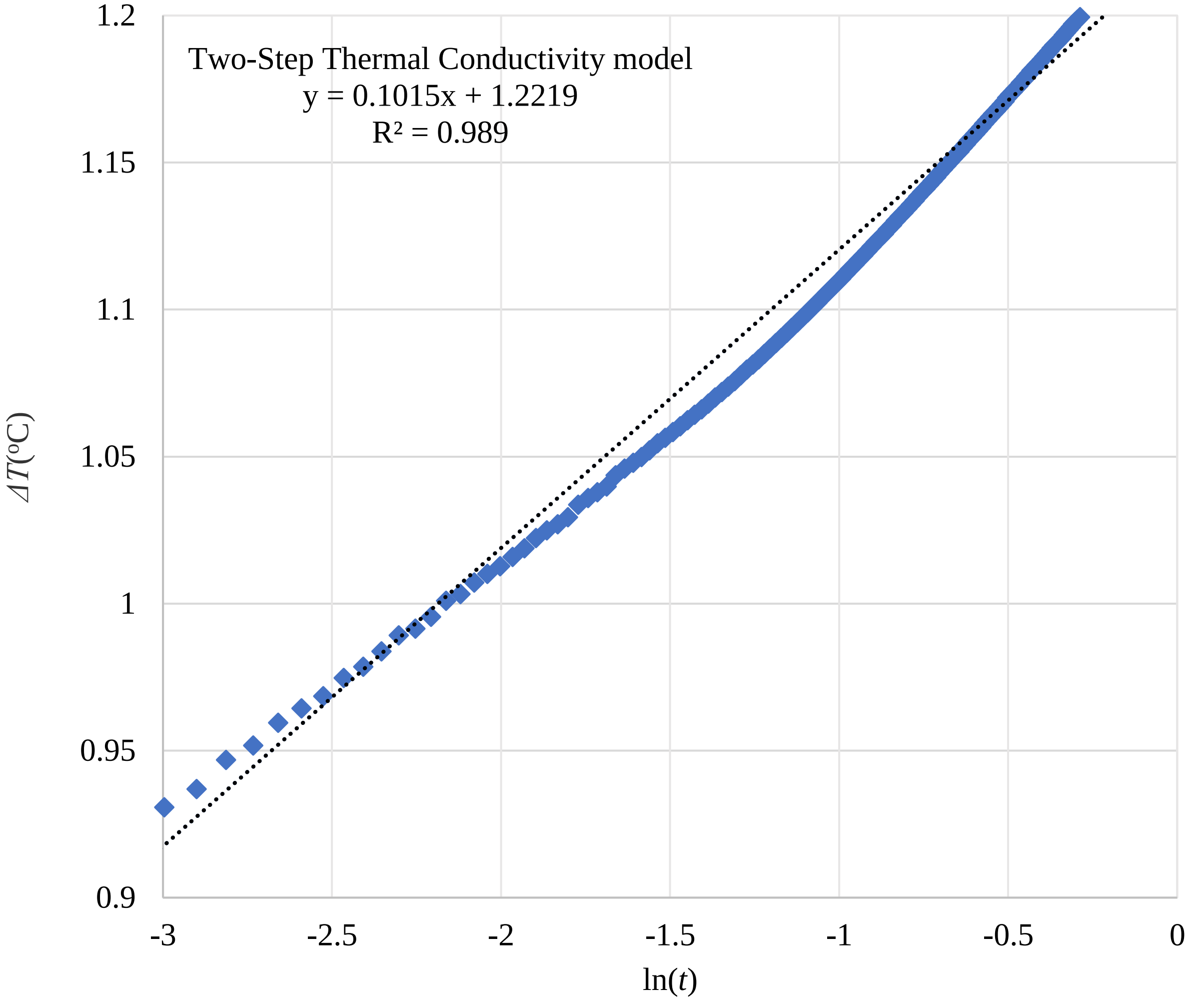

Figure 4.14. Ascension of wire surface temperature with respect to heating time especially through phase transition for the two-step model (includes rotator phase) in the transient hot-wire method with T_i =308.2 K is exhibited here.

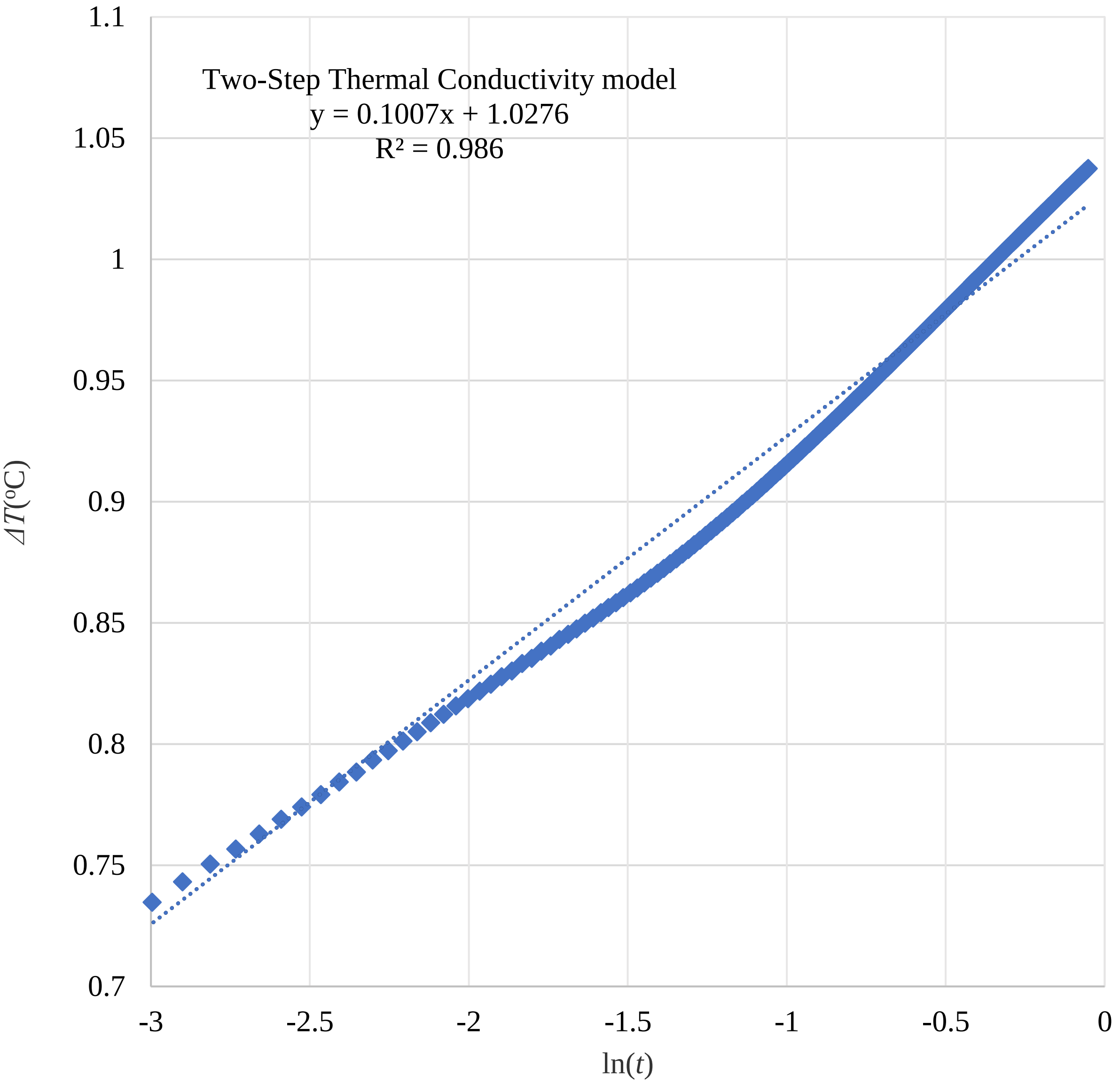

Figure 4.15. Ascension of wire surface temperature with respect to heating time especially through phase transition for the two-step model (includes rotator phase) in the transient hot-wire method with T_i =308.6 K is exhibited here.

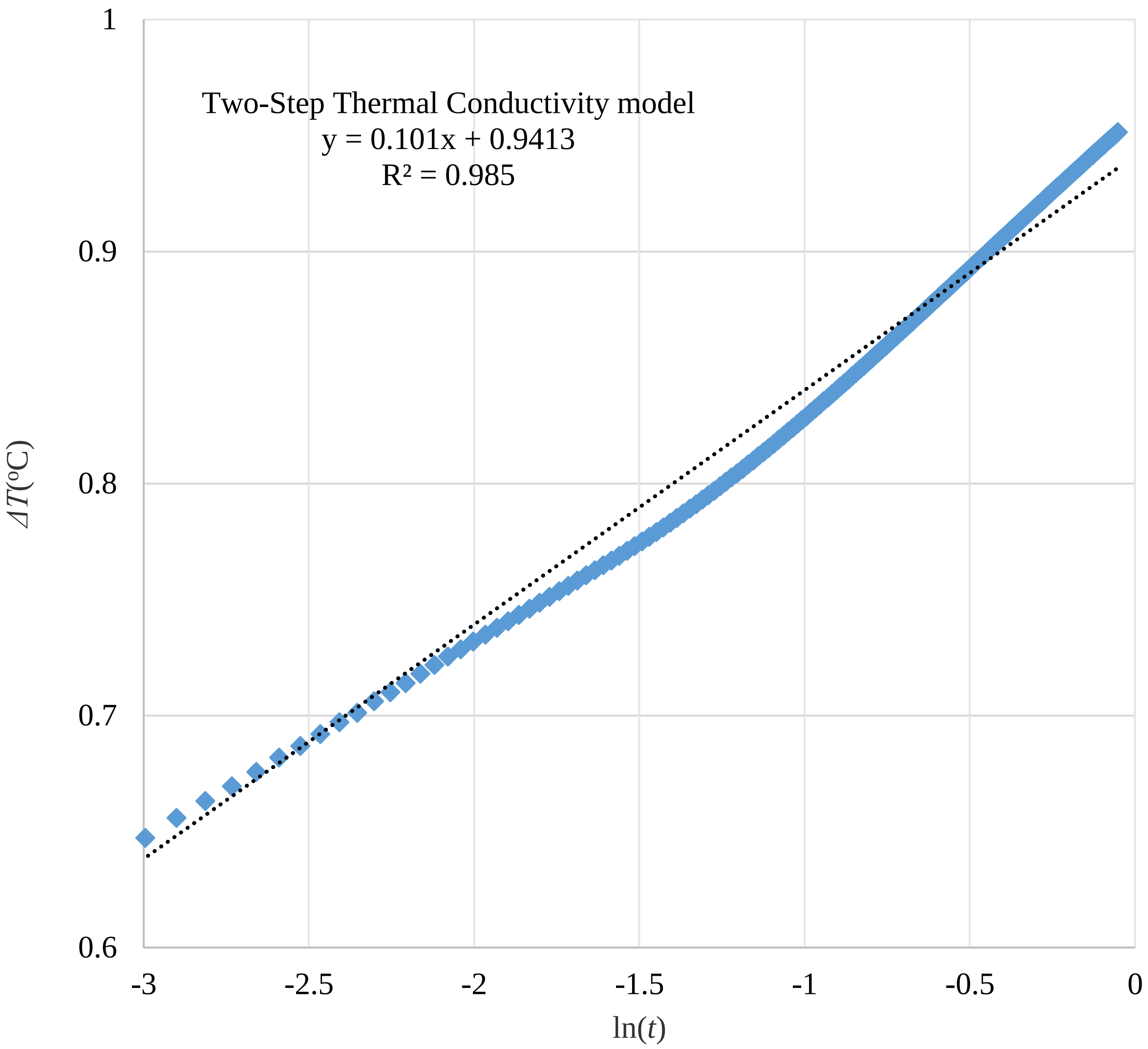

Figure 4.16. Ascension of wire surface temperature with respect to heating time especially through phase transition for the two-step model (includes rotator phase) in the transient hot-wire method with T_i =308.8 K is exhibited here.

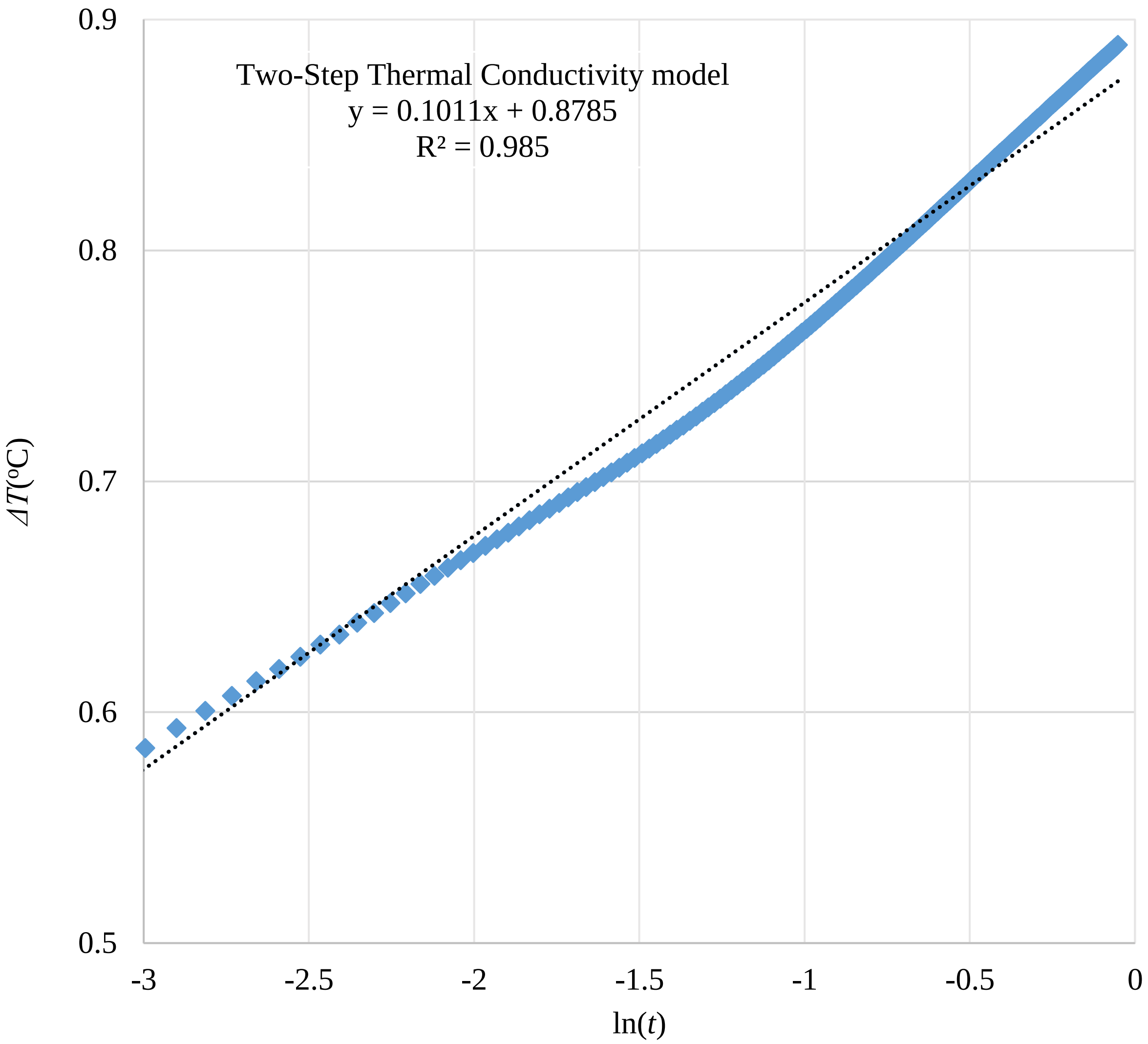

Figure 4.17. Ascension of wire surface temperature with respect to heating time especially through phase transition for the two-step model (includes rotator phase) in the transient hot-wire method with T_i =309 K is exhibited here.

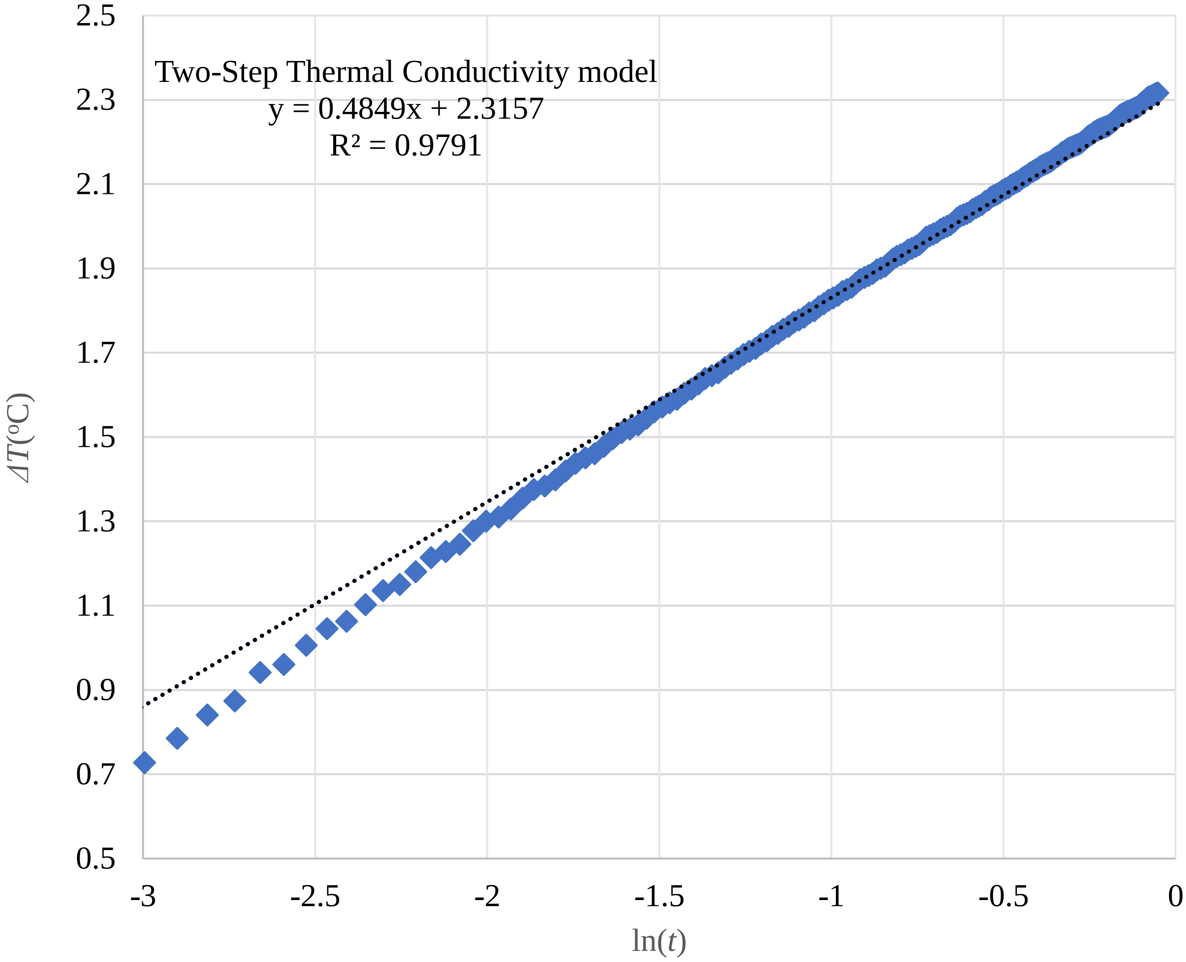

Figure 4.18. Ascension of wire surface temperature with respect to heating time especially through phase transition for the two-step model (includes rotator phase) in the transient hot-wire method with T_i =309.5 K is exhibited here.

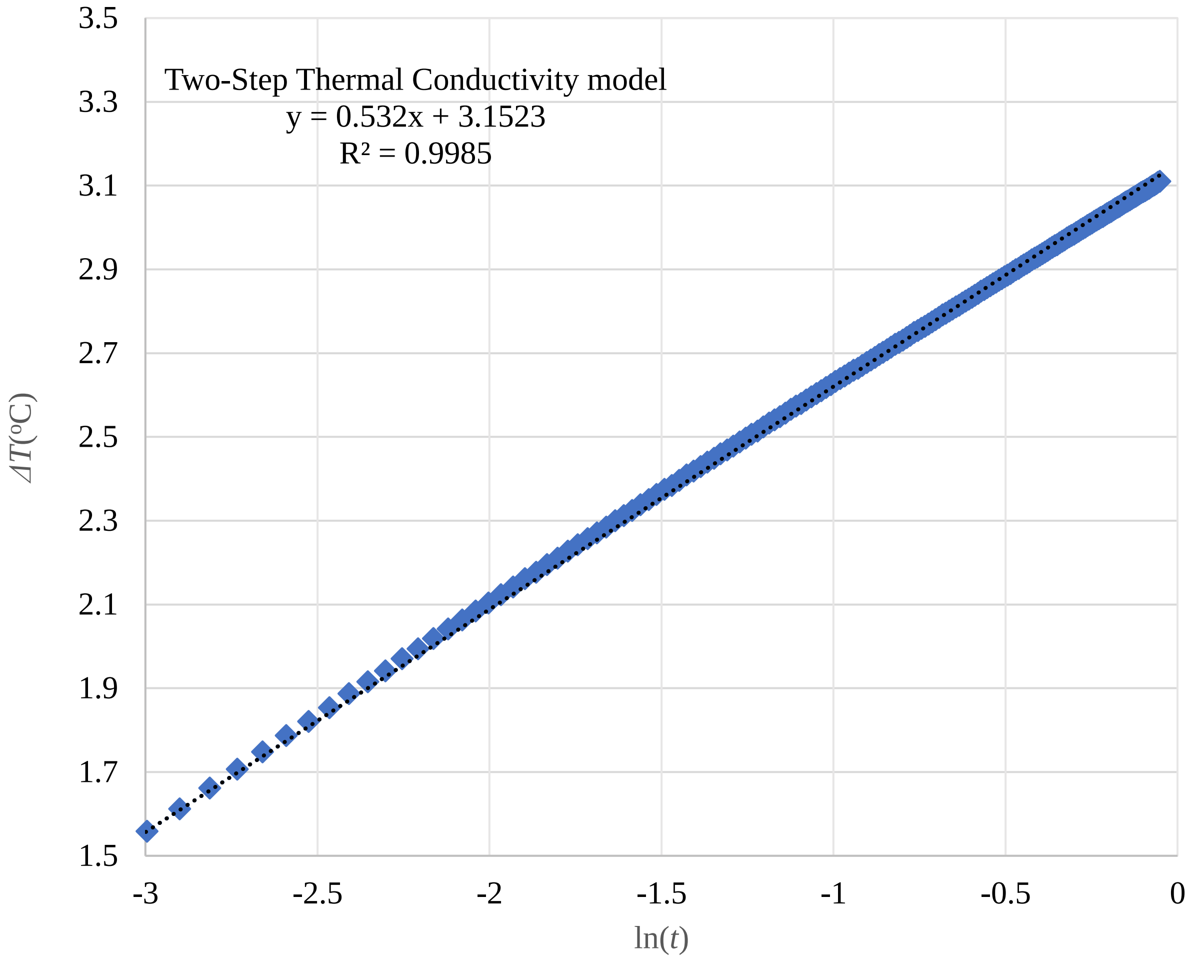

Figure 4.19. Ascension of wire surface temperature with respect to heating time especially through phase transition for the two-step model (includes rotator phase) in the transient hot-wire method with T_i =309.7 K is exhibited here.

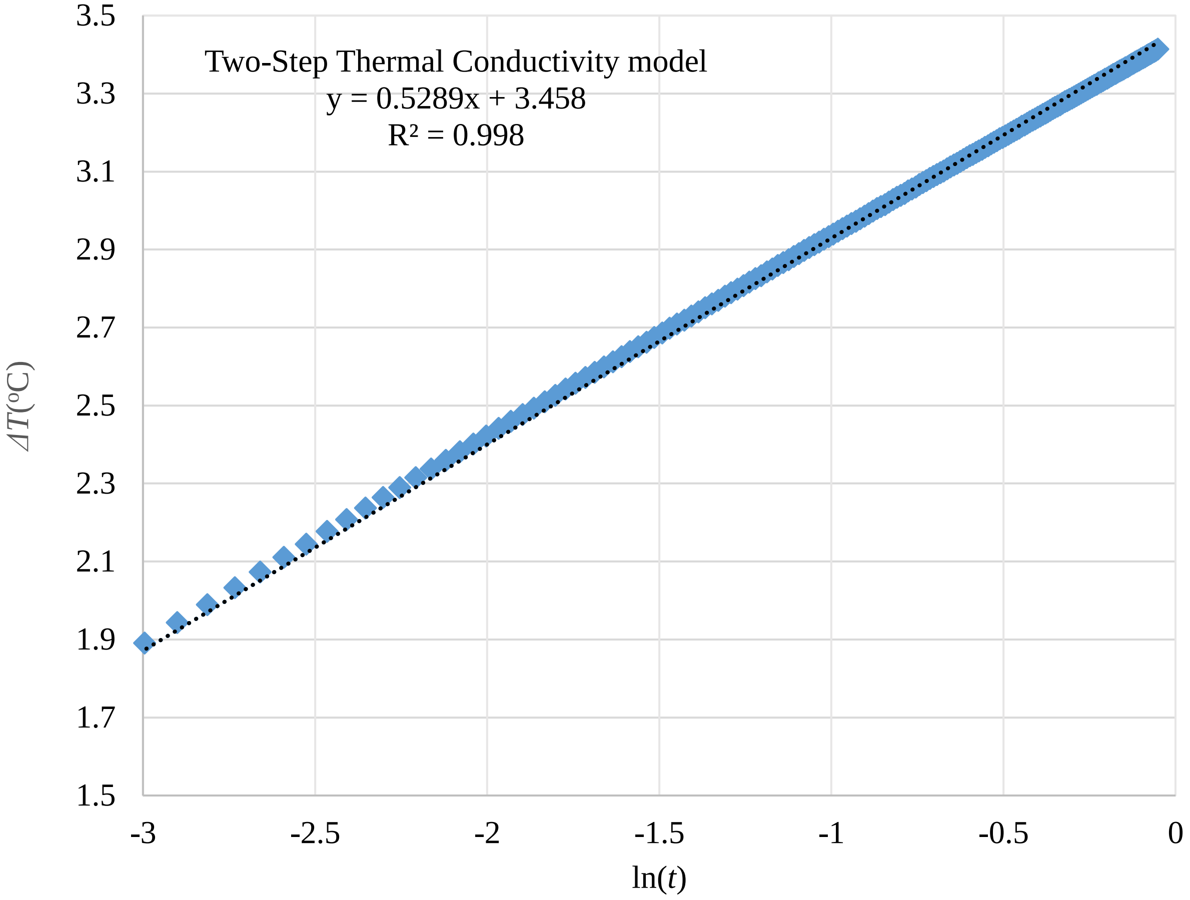

Figure 4.20. Ascension of wire surface temperature with respect to heating time especially through phase transition for the two-step model (includes rotator phase) in the transient hot-wire method with T_i =309.8 K is exhibited here.

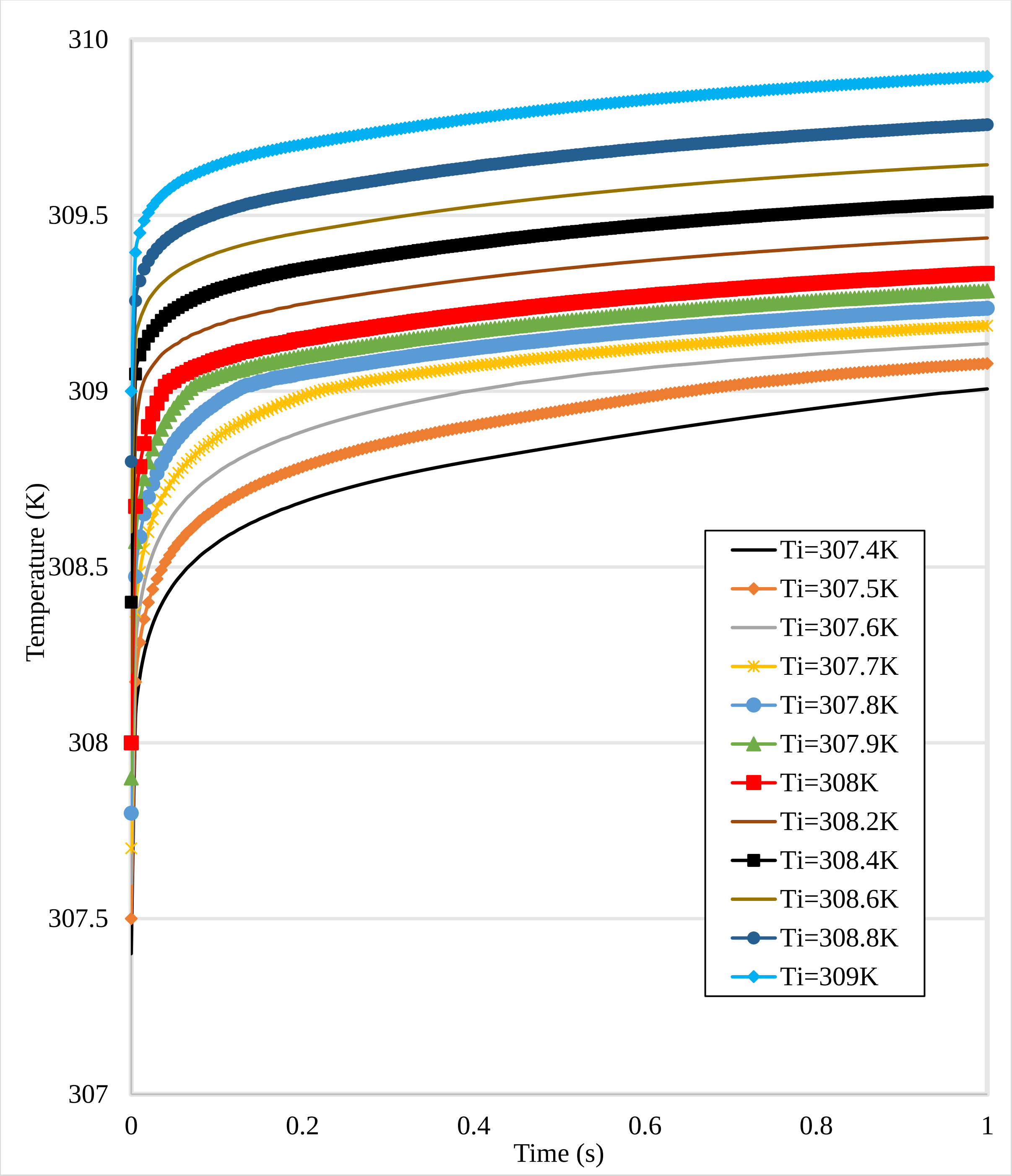

Figure 4.21. Wire surface temperature as a function of the heating time for the two-step model (including the rotator phase) for zero/positive-sign ε'_T values.

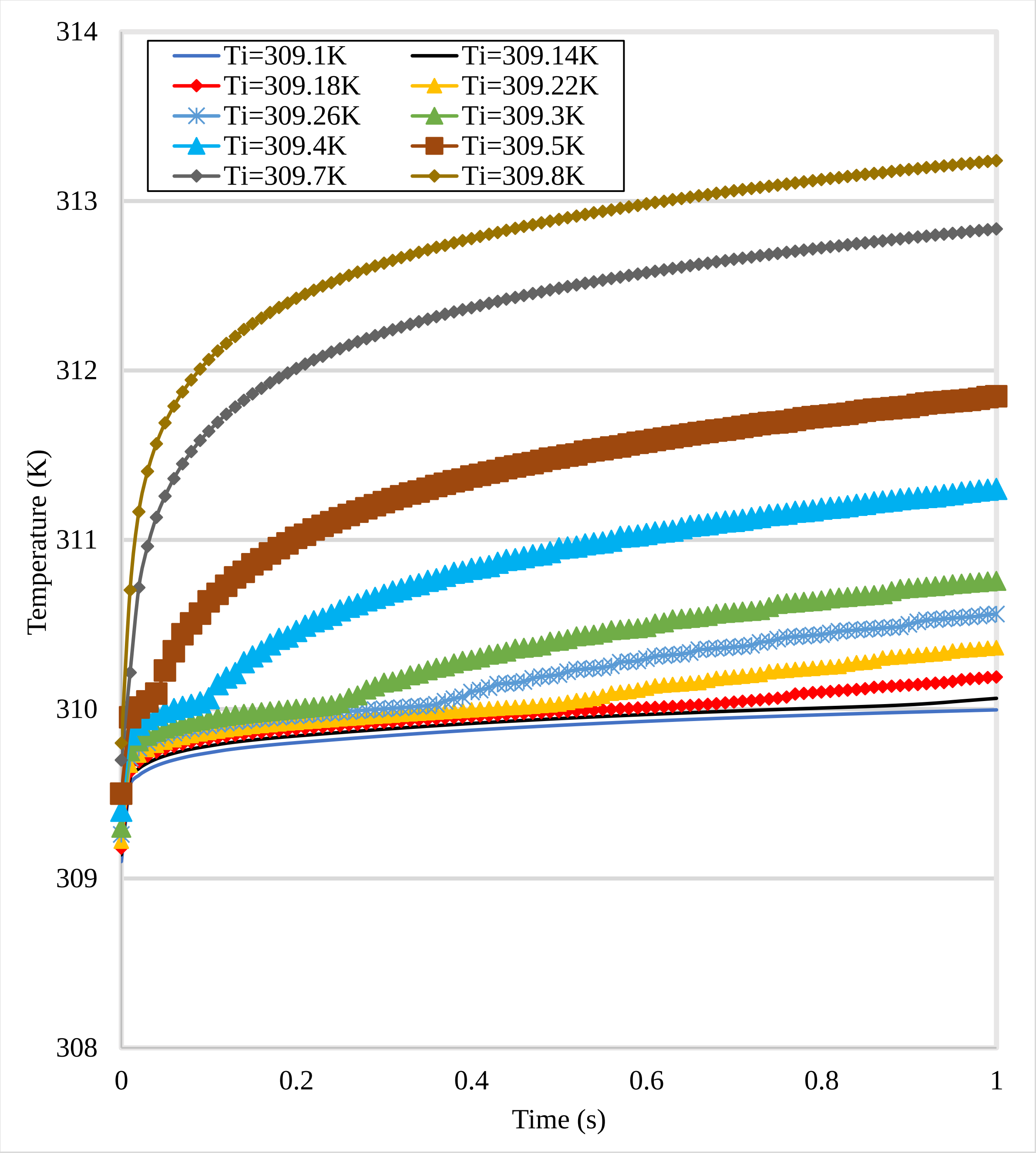

Figure 4.22. Wire surface temperature as a function of the heating time for the two-step model (including the rotator phase) for negative-sign ε'_T values.

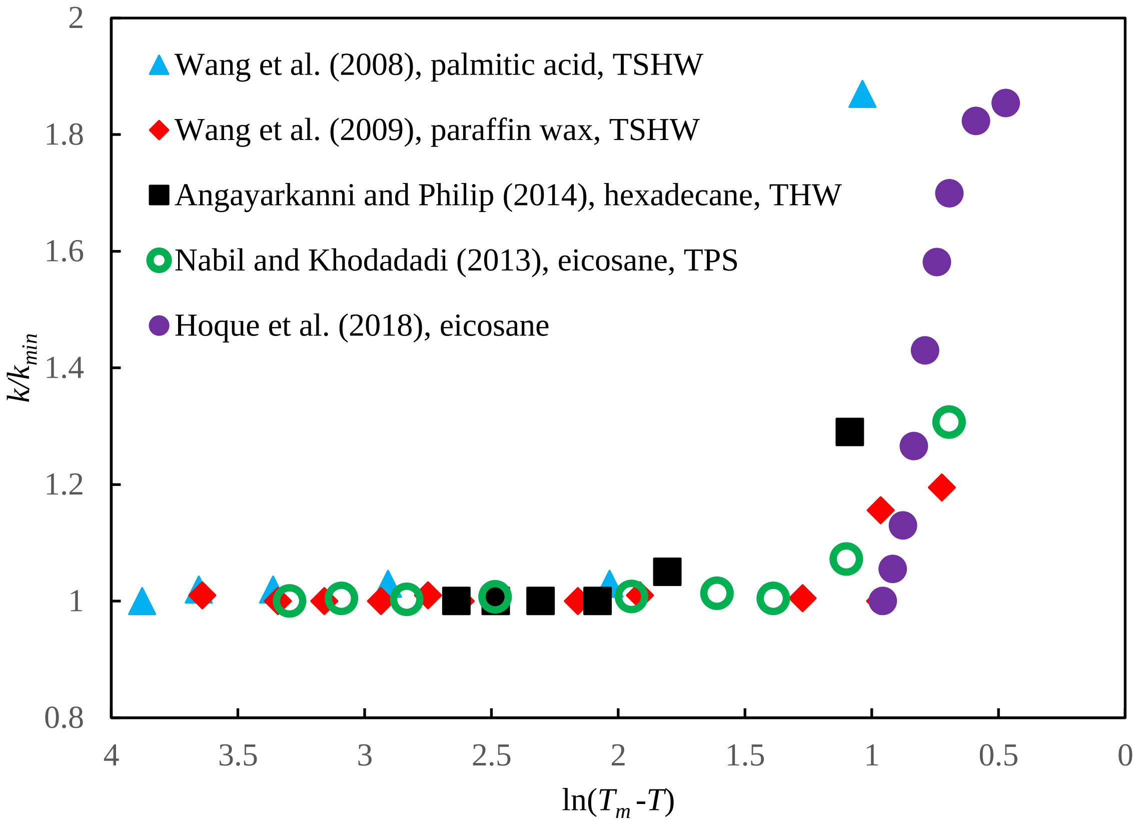

Figure 4.23. Collection of the experimental temperature-dependent thermal conductivity behavior of four phase change materials when various types of transient methods were applied (Wang et al., 2008, Wang et al., 2009, Angayarkanni and Philip, 2014, Nabil and Khodadadi, 2013) in comparison to numerical results of current investigation for eicosane (Hoque et al., 2018).

Chapter 5: Conclusions

The influences of temperature, freezing time and vacuum oven time on the thermal conductivity of two solid samples of pure eicosane and octadecande have been studied. The ice-water and liquid nitrogen routes were used to freeze pure liquid eicosane and octadecane samples degassed at four different vacuum oven times (0, 5, 10, 20 hours). A simplified one-dimensional heat transfer analytical model was proposed to derive a relationship between the dimensionless thickness of the solid specimen and the freezing time. Specific focus was given to the thermal conductivity values when the eicosane and octadecane sample temperatures were close to the solid-liquid phase transition points. A computational model was used to provide a rationale for the recorded enhancements in the thermal conductivity of both materials close to the solid-liquid phase change temperatures. Specific conclusions of this study are:

1. Vacuum oven times have significant influence on the thermal conductivity and the freezing time of the samples of both materials. For eicosane, the minimum freezing time corresponded to the vacuum oven time of 5 hours for both routes. The freezing times of both eicosane and octadecane first decreased with the vacuum oven time followed by an increasing trend.
2. The thermal conductivity of the samples prepared by the liquid nitrogen route for both eicosane and octadecane were almost always lower than the samples associated with the ice-water route with some deviations observed near the solid-liquid phase transition points.

No clear relationship between the freezing time and thermal conductivity for a particular freezing route could be established.

3. Theoretical relations between the dimensionless thickness of the prepared solidifying specimen (ε^+) and t^+ were generally in great agreement with the visually-observed quantities. The determined thermal conductivity of both eicosane and octadecane samples exhibited enhancements close to solid-liquid phase transition. The anomalous behavior recorded in this study can be explained by the presence of solid-solid phase transition (rotator phase) before the melting temperature. The higher thermal conductivity values associated with the rotator phase can cause this sudden enhancement near the solid-liquid phase transition points of the paraffins.

References

Águila, B., Vasco, D. A., Galvez, P., and Zapata, P. A., 2018, "Effect of temperature and CuO-nanoparticle concentration on the thermal conductivity and viscosity of an organic phase-change material," *International Journal of Heat and Mass Transfer*, 120, pp. 1009-1019.

Air Products Industry Co., Ltd., Technical data, http://www.apithailand.com/nitrogen.html, Bangkok, THAILAND.

Al Ghossein, R., 2015, "Thermal Conductivity Enhancement of Solid Eicosane-Based Silver Nanostructure-Enhanced Phase Change Materials for Thermal Energy Storage," M.Sc. Thesis, Mechanical Engineering Department, Auburn University, Alabama, USA, https://etd.auburn.edu/handle/10415/4825. https://etd.auburn.edu/bitstream/handle/10415/4825/Masters_Thesis_Rabih_AlGhossein.pdf?sequence=2&isAllowed=y.

Al Ghossein, R. M., Hossain, M. S., and Khodadadi, J. M., 2017, "Experimental determination of temperature-dependent thermal conductivity of solid eicosane-based silver nanostructure-enhanced phase change materials for thermal energy storage," *International Journal of Heat and Mass Transfer*, 107, pp. 697-711.

Angayarkanni, S. A., and Philip, J., 2014, "Tunable Thermal Transport in Phase Change Materials using Inverse Micellar Templating and Nanofillers," *The Journal of Physical Chemistry C*, 118(25), pp. 13972-13980.

Angayarkanni, S. A., and Philip, J., 2015, “Thermal Conductivity Measurements in Phase Change Materials under Freezing in Presence of Nanoinclusions,” *Journal of Applied Physics*, 118(9), p.094306.

Assael, M. J., Antoniadis, K. D., and Wakeham, W. A., 2010, “Historical evolution of the transient hot-wire technique,” *International journal of thermophysics*, *31*(6), pp. 1051-1072.

Assael, M. J., Charitidou, E., and Karagiannidis, L., 1991, “The thermal conductivity of n-hexadecane+ ethanol and n-decane+ butanol mixtures,” *International journal of thermophysics*, 12(3), pp. 491-500.

Assael, M. J., Karagiannidis, L., Malamataris, N., and Wakeham, W. A., 1998, “The Transient Hot-Wire Technique: A Numerical Approach,” *International Journal of Thermophysics,* 19(2), pp. 379-389.

Bashirnezhad, K., Rashidi, M. M., Yang, Z., Bazri, S., and Yan, W. M., 2015, “A comprehensive review of last experimental studies on thermal conductivity of nanofluids,” *Journal of Thermal Analysis And Calorimetry*, *122*(2), pp. 863-884.

Briard, A. J., Bouroukba, M., Petitjean, D., Hubert, N., and Dirand, M., 2003, “Experimental enthalpy increments from the solid phases to the liquid phase of homologous n-alkane series (C_{18} to C_{38} and C_{41}, C_{44}, C_{46}, C_{50}, C_{54}, and C_{60},” *Journal of Chemical & Engineering Data*, *48*(3), pp. 497-513.

Bejan, A., 2003, *Convection Heat Transfer* (third ed.), Wiley, New York, pp. 222–223.

Bergman, T. L., Incropera, F. P., DeWitt, D. P., and Lavine, A. S., 2011, *Fundamentals of Heat and Mass Transfer*, John Wiley & Sons.

Bran-Anleu, G., Lavine, A. S., Wirz, R. E., and Kavehpour, H. P., 2014, "Algorithm to Optimize Transient Hot-Wire Thermal Property Measurement," *Review of Scientific Instruments*, 85(4), p.045105.

Brookfield, Circulating Baths with Programmable Controller, Operators manual, Brookfield Engineering Labs. Inc., Middleboro, MA, 2009.

Carslaw, H. S., and Jaeger, J. C., 1959, *Conduction of Heat in Solids*, 2nd edition, Oxford University Press, London, UK.

Clary, D. R., and Mills, G., 2011, "Preparation and thermal properties of CuO particles," *The Journal of Physical Chemistry C*, *115*(5), pp. 1767-1775.

Darvin, J. R., Nabil, M., Uertz, J. and Mills, G., 2016, "Concentrated Ag colloids in dodecane relevant to nanostructure-enhanced PCM," Private communication.

De Groot, J. J., Kestin, J., and Sookiazian, H., 1974, "Instrument to Measure the Thermal Conductivity of Gases," *Physica*, 75(3), pp. 454-482.

de Zárate, J. M. O., Hita, J. L., Khayet, M., and Legido, J. L., 2010, "Measurement of the thermal conductivity of clays used in pelotherapy by the multi-current hot-wire technique," *Applied Clay Science, 50*(3), pp. 423-426.

Duluc, M. C., Xin, S., and Le Quere, P., 2003, "Transient Natural Convection and Conjugate Transients around a Line Heat Source," *International Journal of Heat and Mass Transfer*, 46(2), pp. 341-354.

Dyer, J. D., 1975, *Study of the solidification and melting of nonadecane and hexadecane including solid phase thermal conductivity measurements: a thesis presented to the faculty of the Graduate*

School, Tennessee Technological University (Doctoral dissertation, Tennessee Technological University).

Dyer, J. D., and Griggs, E. I., June 1975, "*Study of the solidification and melting of nonadecane and hexadecane including solid phase thermal conductivity measurements,*" Report ME-49, Tennessee Technological University, College of Engineering.

Elsebay, M., Elbadawy, I., Shedid, M. H., and Fatouh, M., 2016, "Numerical resizing study of Al_2O_3 and CuO nanofluids in the flat tubes of a radiator," *Applied Mathematical Modelling*, *40*(13-14), pp. 6437-6450.

Fan, L., 2011, "Enhanced thermal conductivity and expedited freezing of nanoparticle suspensions utilized as novel phase change materials," PhD Thesis, Mechanical Engineering Department, Auburn University, Auburn, Alabama, USA, https://etd.auburn.edu/bitstream/handle/10415/2707/Dissertation_Fan_0717.pdf?sequence=2

Fan, L. W., Fang, X., Wang, X., Zeng, Y., Xiao, Y. Q., Yu, Z. T., Xu, X., Hu, Y. C., and Cen, K. F., 2013, "Effects of various carbon nanofillers on the thermal conductivity and energy storage properties of paraffin-based nanocomposite phase change materials," *Applied Energy*, 110, pp. 163-172.

Fang, X., Ding, Q., Li, L. Y., Moon, K. S., Wong, C. P., and Yu, Z. T., 2015, "Tunable thermal conduction character of graphite-nanosheets-enhanced composite phase change materials via cooling rate control," *Energy Conversion and Management*, 103, pp. 251-258.

Fang, X., Fan, L. W., Ding, Q., Wang, X., Yao, X. L., Hou, J. F., Yu, Z. T., Cheng, G. H., Hu, Y. C., and Cen, K. F., 2013, "Increased thermal conductivity of eicosane-based composite phase change materials in the presence of graphene nanoplatelets," *Energy & Fuels*, 27(7), pp. 4041-4047.

Förster, S., 1963, "Viscosity measurements in liquid neon, argon, and nitrogen," *Cryogenics*, *3*, pp. 176-177.

Freund, M., Csikos, R., Keszthelyi, S. and Mozes, G. Y., 1982, *Paraffin Products: Properties, technologies, applications*, ed. G. Y. Mozes, Elsevier Scientific Publishing Company, Amsterdam–Oxford - New York, Chapters 1 and 3.

GetData Graph Digitizer, http://getdata-graph-digitizer.com/.

Gilmore, D. G., and Donabedian, M., eds., 2003, *Spacecraft thermal control handbook: cryogenics* (Vol. 2). AIAA.

Griggs, E. I., and Yarbrough, D. W., 1978, "Thermal conductivity of solid unbranched alkanes from n-hexadecane to n-eicosane," in *Proceedings of the Southeastern Seminar on Thermal Sciences*, North Carolina State University, Raleigh, pp. 256-267.

Hale, D. V., Hoover, M. J., and O'Neill, M. J., 1971, *Phase Change Materials Handbook*, National Aeronautics and Space Administration (NASA), Huntsville, AL, USA.

Hawken, P., 2010, The ecology of commerce, revised edition, New York, Harper Business.

Healy, J. J., De Groot, J. J., and Kestin, J., 1976, "The Theory of the Transient Hot-Wire Method for Measuring Thermal Conductivity," *Physica B+C*, 82(2), pp. 392-408.

Ho, C. J., and Gao, J. Y., 2009, "Preparation and thermophysical properties of nanoparticle-in-paraffin emulsion as phase change material," *International Communications in Heat and Mass Transfer*, 36(5), pp. 467-470.

Holmen, R., Lamvik, M., and Melhus, O., 2002, "Measurements of the thermal conductivities of solid and liquid unbranched alkanes in the C_{16}-to-C_{19} range during phase transition," *International journal of thermophysics*, *23*(1), pp. 27-39.

Holmes® Heater, Owner's Guide, Jarden Consumer Solutions, Boca Raton, FL, 2013.

Hoque, M. S. B., Ansari, N., and Khodadadi, J. M., 2018, "Explaining the "anomalous" transient hot wire-based thermal conductivity measurements near solid-liquid phase change in terms of solid-solid transition," *International Journal of Heat and Mass Transfer*, *125*, pp. 210-217.

Hossain, M. S., 2017, "Stable Colloidal Dispersions of Highly Concentrated Thermo-efficient Nanomaterials," PhD thesis, Auburn University, Auburn, Alabama, USA, https://etd.auburn.edu/bitstream/handle/10415/5577/Dissertation%20Sharif%20Hossain.pdf?sequence=2.

Hot Disk, Inc., 2009, 2014 "Instruction Manual, Hot Disk Thermal Constants Analyser," *ThermTest Inc.*, Fredericton, New Brunswick, CANADA.

Humphries, W. R., and Griggs, E. I., 1977, *A Design Handbook for Phase Change Thermal Control and Energy Storage Devices*, National Aeronautics and Space Administration (NASA), Huntsville, AL, USA.

Huxtable, S. T., Cahill, D. G., Shenogin, S., Xue, L., Ozisik, R., Barone, P., Usrey, M., Strano, M. S., Siddons, G., Shim, M., and Keblinski, P., 2003, "Interfacial Heat Flow in Carbon Nanotube Suspensions," *Nature Materials*, 2(11), p. 731.

Jensen, J. E., Stewart, R. G., Tuttle, W. A., Brechna, H., and Prodell, A. G., 1980, *Brookhaven National Laboratory Selected Cryogenic Data Notebook: Sections I-IX* (Vol. 1), Brookhaven National Laboratory.

Kadoya, K., Matsunaga, N., and Nagashima, A., 1985, “Viscosity and thermal conductivity of dry air in the gaseous phase,” *Journal of physical and chemical reference data*, *14*(4), pp. 947-970.

Kang, G. U., Chung, B. J., and Kim, H. J., 2014, “Natural convection heat transfer on a vertical cylinder submerged in fluids having high Prandtl number,” *International Journal of Heat and Mass Transfer*, *79*, pp. 4-11.

Keesom, W. H., and Bijl, A., 1937, “Determination of the vapour pressures of liquid nitrogen below one atmosphere, and of solid nitrogeN β: The boiling point and triple point of nitrogen,” *Physica*, *4*(4), pp. 305-310.

Kell, G. S., 1967, “Precise representation of volume properties of water at one atmosphere,” *Journal of Chemical and Engineering data*, 12(1), pp. 66-69.

Kolesnikov, S. I. and Syunyaev, Z. I., 1985, “Phase transitions in the melting and crystallization of n-$C_{18}H_{38}$ and n-$C_{20}H_{42}$,” *Journal of Applied Chemistry of the USSR*, 58, 10, pp. 2097-2101.

Kreith, F., 1967, *Principles of Heat Transfer*, International Textbook Company, Scranton, PA.

Lazaro, A., Peñalosa, C., Solé, A., Diarce, G., Haussmann, T., Fois, M., Zalba, B., Gshwander, S. and Cabeza, L.F., 2013, “Intercomparative tests on phase change materials characterisation with differential scanning calorimeter,” *Applied Energy*, *109*, pp.415-420.

Li, C. C., and Chang, M. H., 2004, “Colloidal stability of CuO nanoparticles in alkanes via oleate modifications,” *Materials Letters*, 58(30), pp. 3903-3907.

Mehling, H. and Cabeza, L. F., 2008, *Heat and Cold Storage with PCM: An up to date introduction into basics and applications (Heat and Mass Transfer)*, Springer, Berlin, Chapters 1, 2 & 3.

Mehlon, R. J., 1977, “Thermal conductivity of heavy hydrocarbons,” unpublished thesis, Tennessee Technological University.

Mehlon, R.J., August 1979a, The Thermal Conductivity of Heavy Hydrocarbons. *Master of Science Thesis, Tennessee Technological University, Cookeville, Tennessee*.

Mehlon, R. J., 1979b, *The thermal condutivity of heavy hydrocarbons: a thesis presented to the faculty of the Graduate School, Tennessee Technological University* (Doctoral dissertation, Tennessee Technological University).

Motahar, S., Nikkam, N., Alemrajabi, A. A., Khodabandeh, R., Toprak, M. S., and Muhammed, M., 2014, “A novel phase change material containing mesoporous silica nanoparticles for thermal storage: A study on thermal conductivity and viscosity,” *International Communications in Heat and Mass Transfer,* 56, pp. 114-120.

Moussa, M. R., Muijlwijk, R., and Van Dijk, H., 1966, “The vapour pressure of liquid nitrogen,” *Physica*, *32*(5), pp. 900-912.

Müller, A., 1927, “An X-ray investigation of certain long-chain compounds,” *Proceedings of the Royal Society of London. Series A,* 114 (768), pp. 542-561.

Nabil, M., 2013, “Thermal conductivity of nanostructure-enhanced phase change materials: measurements for solid eicosane-based copper oxide and carbon nanotube colloids and numerical modeling of anomalous measurements near phase transition,” M.Sc. Thesis, Mechanical Engineering Department, Auburn University, Alabama, USA, https://etd.auburn.edu/handle/10415/3672.

https://etd.auburn.edu/bitstream/handle/10415/3672/M.Sc.%20Thesis%20Mahdi%20Nabil.pdf?sequence=2&isAllowed=y.

Nabil, M. and Khodadadi, J. M., 2013, “Experimental determination of temperature-dependent thermal conductivity of solid eicosane-based nanostructure-enhanced phase change materials,” *International Journal of Heat and Mass Transfer*, 67, pp. 301-310.

Nabil, M., and Khodadadi, J. M., 2017, “Computational/analytical study of the transient hot wire-based thermal conductivity measurements near phase transition,” *International Journal of Heat and Mass Transfer*, 111, pp. 895-907.

Papanikolaou, N., 2008, “Nonequilibrium Radiation Dosimetry,” *J Phys Condens Matter*, 20(135201), pp.1-6.

Papapetrou, M., Kosmadakis, G., Cipollina, A., La Commare, U. and Micale, G., 2018, “Industrial waste heat: Estimation of the technically available resource in the EU per industrial sector, temperature level and country,” *Applied Thermal Engineering*, *138*, pp. 207-216.

Parker, W. J., Jenkins, R. J., Butler, C. P., and Abbott, G. L., 1961, “Flash method of determining thermal diffusivity, heat capacity, and thermal conductivity,” *Journal of applied physics*, *32*(9), pp. 1679-1684.

Paterson, S., 1952, “Propagation of a Boundary of Fusion,” *Proceedings of the Glasgow Mathematical Association*, 1, pp. 42-47.

Peñas, J. R. V., Ortiz de Zarate, J. M., and Khayet, M., 2008, “Measurement of the thermal conductivity of nanofluids by the multicurrent hot-wire method,” *Journal of Applied Physics*, *104*(4), p. 044314.

Powell, R. W., Challoner, A. R., and Seyer, W. F., 1961, “Correspondence. Measurement of Thermal Conductivity of n-Octadecane,” *Industrial & Engineering Chemistry, 53*(7), pp. 581-582.

Powers, R. W., Mattox, R. W., and Johnston, H. L., 1954, “Thermal Conductivities of Condensed Gases. I. The Thermal Conductivity of Liquid Nitrogen between 65 and 90° K,” *Journal of the American Chemical Society, 76*(23), pp. 5968-5971.

Rathod, M. K. and Banerjee, J., 2013, “Thermal stability of phase change materials used in latent heat energy storage systems: a review,” *Renewable and Sustainable Energy Reviews*, 18, pp. 246-258.

Roder, H. M., 1981, “A Transient Hot Wire Thermal Conductivity Apparatus for Fluids,” *Journal of Research of the National Bureau of Standards*, 86(5), pp. 457-493.

Rusconi, R., Williams, W. C., Buongiorno, J., Piazza, R., and Hu, L. W., 2007, “Numerical Analysis of Convective Instabilities in A Transient Short-Hot-Wire Setup for Measurement of Liquid Thermal Conductivity,” *International Journal of Thermophysics*, 28(4), pp. 1131-1146.

Sari, A., and Karaipekli, A., 2007, “Thermal Conductivity and Latent Heat Thermal Energy Storage Characteristics of Paraffin/Expanded Graphite Composite as Phase Change Material,” *Applied Thermal Engineering*, 27(8-9), pp. 1271-1277.

Schiffres, S. N., Harish, S., Maruyama, S., Shiomi, J., and Malen, J. A., 2013, “Tunable electrical and thermal transport in ice-templated multilayer graphene nanocomposites through freezing rate control,” *ACS nano, 7*(12), pp. 11183-11189.

Siegel, R., 1977, “Solidification of low conductivity material containing dispersed high conductivity particles,” *International Journal of heat and mass transfer, 20*(10), pp.1087-1089.

Sharma, A., Tyagi, V. V., Chen, C. R., and Buddhi, D., 2009, “Review on thermal energy storage with phase change materials and applications,” *Renewable and Sustainable Energy Reviews*, 13 (2), pp. 318-345.

Shen, F., and Khodadadi, J. M., 1999, “Combined thermocapillary and buoyancy-driven convection within short-duration pulse-heated liquid droplets,” *Numerical Heat Transfer: Part A: Applications*, 36(8), pp. 839-857.

Shima, P. D., Philip, J., and Raj, B., 2010, “Synthesis of Aqueous and Nonaqueous Iron Oxide Nanofluids and Study of Temperature Dependence on Thermal Conductivity and Viscosity,” *The Journal of Physical Chemistry C*, 114 (44), pp. 18825-18833.

Stryker, P. C., and Sparrow, E. M., 1990, “Application of a spherical thermal conductivity cell to solid n-eicosane paraffin,” *International journal of heat and mass transfer*, *33*(9), pp. 1781-1793.

Tan, F. L., and Tso, C. P., 2004, “Cooling of mobile electronic devices using phase change materials,” *Applied thermal engineering*, *24*(2-3), pp. 159-169.

Testo, Inc., 480, Climate measuring instrument, Instruction manual, 0970 4800 en 05 V01.05 en-GB, testo, Testo, Inc., Sparta, N.J.

Testo, Inc., Wheel measuring head 100 mm, Application information, 0970 0473 en 01, Testo Inc., Sparta, NJ.

Vargaftik, N. B., 1975, *Tables on the thermophysical properties of liquids and gases*, 2nd ed., New York: Halsted Press, Division of John Wiley & Sons, Inc.

Vélez, C., Khayet, M., and De Zárate, J. O., 2015, “Temperature-dependent thermal properties of solid/liquid phase change even-numbered n-alkanes: n-Hexadecane, n-octadecane and n-eicosane,” *Applied Energy*, *143*, pp. 383-394.

Wakeham, W. A., and Assael, M. J., 1999, “Thermal Conductivity Measurement,” in *Mechanical Variables Measurement - Solid, Fluid, and Thermal*, edited by Webster, J. G., CRC Press.

Wakeham, W. A., Nagashima, A., and Sengers, J. V., (eds.), 1991, *Experimental Thermodynamics. Vol. III, Measurement of the Transport Properties of Fluids* (Blackwell Scientific Publications, London).

Wang, J., Xie, H., Li, Y., and Xin, Z., 2010a, “PW Based Phase Change Nanocomposites Containing γ −Al_2O_3,” *Journal of Thermal Analysis and Calorimetry*, 102(2), pp. 709-713.

Wang, J., Xie, H., and Xin, Z., 2008, “Thermal properties of heat storage composites containing multiwalled carbon nanotubes,” *Journal of applied physics*, *104*(11), p.113537.

Wang, J., Xie, H., and Xin, Z., 2009, “Thermal properties of paraffin based composites containing multi-walled carbon nanotubes,” *Thermochimica Acta*, 488(1-2), pp. 39-42.

Wang, J., Xie, H., Xin, Z., Li, Y., and Chen, L., 2010b, “Enhancing Thermal Conductivity of Palmitic Acid Based Phase Change Materials with Carbon Nanotubes as Fillers,” *Solar Energy*, 84(2), pp. 339-344.

Wiebe, R., and Brevoort, M. J., 1930, “The heat capacity of saturated liquid nitrogen and methane from the boiling point to the critical temperature,” *Journal of the American Chemical Society*, *52*(2), pp. 622-633.

Xie, H., Gu, H., Fujii, M., and Zhang, X., 2006, "Short Hot Wire Technique for Measuring Thermal Conductivity and Thermal Diffusivity of Various Materials," *Measurement Science and Technology*, 17, pp. 208-214.

Xie, B., Liu, G., Jiang, S., Zhao, Y., and Wang, D., 2008, "Crystallization behaviors of n-octadecane in confined space: crossover of rotator phase from transient to metastable induced by surface freezing," *The Journal of Physical Chemistry B*, 112(42), pp. 13310-13315.

Yarbrough, D. W., and Kuan, C. N., 1981, "The thermal conductivity of solid n-eicosane, n-octadecane, n-heptadecane, n-pentadecane, and n-tetradecane," in *Proceeding of the 17th International Thermal Conductivity Conference*, pp. 15-19.

Yarbrough, D. W., and Kuan, C. N., 1983, "The Thermal Conductivity of Solid N-Eicosane, N-Octadecane, N-Heptadecane, N-Pentadecane, and N-Tetradecane," in *Thermal Conductivity*, Edited by Hust, J. G., Plenum Press, New York & London, pp. 265-274. DOI: 10.1007/978-1-4899-5436-7_25.

Yaws, C. L., 1995, *Handbook of Thermal Conductivity, Volume 3: Organic Compounds* C_8 *to* C_{28}, Gulf Professional Publishing, Houston, TX, USA.

Zalba, B., Marín, J. M., Cabeza, L. F., and Mehling, H., 2003, "Review on thermal energy storage with phase change: materials, heat transfer analysis and applications," *Applied Thermal Engineering*, 23(3), pp. 251-283.

Zhang, S., Wu, J. Y., Tse, C. T., and Niu, J., 2012, "Effective dispersion of multi-wall carbon nano-tubes in hexadecane through physiochemical modification and decrease of supercooling," *Solar Energy Materials and Solar Cells*, 96, pp. 124-130.

Zheng, R., Gao, J., Wang, J., and Chen, G., 2011, “Reversible Temperature Regulation of Electrical and Thermal Conductivity using Liquid-Solid Phase Transitions,” *Nature Communications, 2,* p. 289.

Zhong, H., and Lukes, J. R., 2006, “Interfacial Thermal Resistance Between Carbon Nanotubes: Molecular Dynamics Simulations and Analytical Thermal Modeling,” *Physical Review B,* 74(12), p. 125403.

Appendix A: Calculation of the heat transfer coefficients of (a) hot air flow supplied by the heater and (b) heat sink liquid (liquid nitrogen and ice-water)

We have complied the data and relations required to calculate the heat transfer coefficients of (a) hot air flow supplied from the heater (h_0) and (b) heat sink liquid (h_{sink}) (liquid nitrogen and ice-water) of the model discussed in section 3.2. The properties of air for five settings of the heater (Table A.1) and the corresponding values of the Reynolds number (Re), Prandtl number (Pr) and Nusselt number (Nu) (Table A.2) utilized to calculate the values of h_o have been taken from Bergman et al. (2011). Values of h_{sink} for the ice-water and liquid nitrogen routes (Table A.3) associated with the present experimental configuration have been taken from Bergman et al. (2011) and others. At the end of this appendix, we have also compiled the values of the properties related to the calculation of non-dimensional parameters (M^+, P^+, and t^+) utilized in Chapter 3 (Table A.4) from Tables A.1, A.2, A.3 and mentioned sources.

A.1. Determination of the heat transfer coefficient associated with the hot air flow within the rectangular cross-section of current experimental configuration (h_0)

The Dittus-Boelter correlation and subsequent equations have been taken from Bergman et al. (2011) and utilized in order to compute the heat transfer coefficient of hot air flow for five settings of the heater:

$$Nu = 0.023Re^{0.8}Pr^{0.4} \qquad \text{(A.1)}$$

$$\frac{h_o D_h}{k} = 0.023\, Re^{0.8}\, Pr^{0.4}$$

$$h_o = 0.023Re^{0.8}Pr^{0.4}\frac{k}{D_h} \tag{A.2}$$

In equations A.1 and A.2, Nu, Re, Pr, k and D_h designate the Nusselt number, the Reynolds number, the Prandtl number, thermal conductivity of the hot air and hydraulic diameter of the test section, respectively. Starting with measured values of air velocity and temperature, the intermediate properties, dimensionless numbers and the heat transfer coefficients corresponding to five settings of the heater have been determined in Tables A.1 and A.2.

A.2. Determination of the heat transfer coefficient associated with the ice-water and liquid nitrogen sinks (h_{sink})

In present study, we have used the following conditions and equations for the case of an immersed vertical plate, taken from Bergman et al. (2011) in order to calculate the Nusselt number and the coefficient of heat transfer associated with the ice-water and liquid nitrogen sinks:

$$\frac{lh_{sink}}{k_{sink\,fluid}} = Nu_l = CRa_l^n \tag{A.3}$$

$$\frac{lh_{sink}}{k_{sink\,fluid}} = C\left(\frac{g\beta(T_S-T_{sink})l^3}{\nu\alpha}\right)^n \tag{A.4}$$

$$h_{sink} = C\left(\frac{k_{sink\,fluid}}{l}\right)\left(\frac{g\beta(T_S-T_{sink})l^3}{\nu\alpha}\right)^n \tag{A.5}$$

In equations (A.3) to (A.5), l, Ra, $k_{sink\,fluid}$, g, β, T_s, T_{sink}, ν and α designate length of the immersed vertical plate, the Rayleigh number, thermal conductivity of the sink fluid, gravitational acceleration, volumetric thermal expansion coefficient of sink fluid, surface temperature of the vertical plate, temperature of the sink fluid, kinematic viscosity and thermal diffusivity of the sink fluid, respectively.

For the ice-water sink, from Table A.3, $Ra_l = 1.262\times10^8$ ($<10^9$) and the resultant natural convection flow is laminar. Values of parameters C and n are 0.59 and 0.25, respectively and equation (A.5) becomes

$$h_{sink} = 0.59\left(\frac{k_{sink\,fluid}}{l}\right)\left(\frac{g\beta(T_S - T_{sink})l^3}{\nu\alpha}\right)^{0.25} \tag{A.6}$$

For the liquid nitrogen sink, from Table A.3, $Ra_l = 7.41\times10^{10}$ ($>10^9$), the resultant natural convection flow is turbulent. Values of parameters C and n are 0.1 and 1/3, respectively and equation (A.5) becomes

$$h_{sink} = 0.1\left(\frac{k_{sink\,fluid}}{l}\right)\left(\frac{g\beta(T_S - T_{sink})l^3}{\nu\alpha}\right)^{1/3} \tag{A.7}$$

The diameter of the copper rod used in the present experimental configuration in order to transfer heat to sink was 1.5 inches (0.0381 m). Assuming that during both solidification routes, the thermal boundary layer will never exceed this diameter, we have approximated the immersed vertical cylinder as an immersed vertical plate according to the suggestion of Kang et al. (2014) and Bejan (2003) and used equation (A.3).

A.3. Evaluation of the non-dimensional parameters corresponding to the one-dimensional model of the specimen processing of Chapter 3

Values of the parameters related to evaluating the non-dimensional parameters that correspond to the one-dimensional model proposed for processing of solid specimen (M^+, P^+ and t^+) in Chapter 3 are summarized in Table A.4.

Table A.1. Air temperature, air velocity and associated properties of air corresponding to five settings of the heater taken from Bergman et al. (2011).

Heater setting	Air temperature, T_∞ (^{o}C)	Air velocity, u (m/s)	Thermal conductivity, k (W/mK)	Specific heat, C_p (J/kgK)	Dynamic viscosity, μ (N.s/m^2)	Kinematic viscosity, ν (m^2/s)
Fan-low, Thermostat setting - 5	34.2	0.3	0.02683	1007.288	187.9984×10^{-7}	16.614×10^{-6}
Fan-low, Thermostat setting - 6	37	0.3	0.02704	1007.4	189.32×10^{-7}	16.896×10^{-6}
Fan-low, Thermostat setting - 7	38.5	0.3	0.027151	1007.46	190.028×10^{-7}	17.0469×10^{-6}
Fan-low, Thermostat setting - 8	38.7	0.3	0.0271658	1007.468	190.1224×10^{-7}	17.067×10^{-6}
Fan-high, Thermostat setting - 8	42.5	0.2	0.027447	1007.62	191.916×10^{-7}	17.4473×10^{-6}

Table A.2. Heat transfer coefficients of hot air flow (h_o) for five settings of the heater with air properties taken from Table A.1 (equations taken from Bergman et al., 2011).

Heater setting	Reynolds number, $Re = uD_h / \nu$, $D_h = 0.254$ m*	Prandtl Number, $Pr = C_p\mu / k$	Nusselt number, Nu	Heat transfer coefficient, h_o (W/m^{2}K)
Fan-low, Thermostat setting - 5	4586.49	0.7058	16.997	1.7953
Fan-low, Thermostat setting - 6	4509.94	0.7053	16.765	1.7847
Fan-low, Thermostat setting - 7	4470.02	0.70511	16.644	1.7791
Fan-low, Thermostat setting - 8	4464.75	0.70508	16.628	1.778
Fan-high, Thermostat setting - 8	2911.62	0.70455	11.8	1.275

* D_h is the hydraulic diameter [m] of the wind tunnel used for processing the specimen (Figure 3.2)

Table A.3. Values of h_{sink} for the ice-water and liquid nitrogen sinks (values taken from Bergman et al., 2011 and others).

Properties & parameters	Parameter values	Ice-Water	Liquid Nitrogen	Remarks
Surface Temperature of the copper rod, T_s (ºC)	25			As the copper rod is at 25 ºC (approximated room temperature) at initial time, this value has been assigned to the copper surface temperature.
Temperature of the fluid in the heat sink, T_{sink} (ºC)		0	-195.657 (Moussa et al., 1966)	
Specific heat, C_p (J/kg.K)		4189	2055.45 (Wiebe and Brevoort, 1930)	Properties have been calculated at 12 ºC for water and at around -196 ºC for liquid nitrogen.
Thermal conductivity, k (W/mK)		0.59	0.1393 (Jensen et al., 1980, Powers et al., 1954)	
Dynamic viscosity, μ (N.s/m^2)		1.225×10^{-3}	1.65×10^{-3} (Jensen et al., 1980, Förster, 1963)	
Density, ρ (kg/m^3)		999.526 (Kell, 1967)	808 (Gilmore and Donabedian, 2003)	
Volumetric thermal expansion coefficient, β (K^{-1})		1.141×10^{-4}	0.00753 (Air Products Industry Co., Ltd., http://www.apithailand.com/nitrogen.html)	
Thermal diffusivity, α (m^2/s)		1.40911×10^{-7}	8.3875×10^{-8}	
Kinematic viscosity, v (m^2/s)		1.225×10^{-6}	2.042×10^{-6}	

Prandtl number, Pr		8.81	24.345	
Immersed length of the copper rod in the fluid, l (m)	0.092			
Gravitational Acceleration, g (m/s^2)	9.81			
Rayleigh number, Ra_l		1.262×10^8 (laminar flow)	7.41×10^{10} (turbulent flow)	
Nusselt number, Nu_l		62.53	420.02	
Coefficient of heat transfer, h_{sink} (W/m^{2}K)		401	635.96	

Table A.4: Values of the parameters related to the calculation of non-dimensional parameters (M^+, P^+, and t^+) from Tables A.1, A.2 and mentioned sources.

Properties	Values
Overall heat transfer coefficient for Octadecane samples, $h_{o\ octadecane}$ (W/m^{2}K)	1.7953
Overall heat transfer coefficient for eicosane samples, $h_{o\ eicosane}$ (W/m^{2}K)	1.778
Coefficient of heat transfer for the ice-water heat sink, $h_{sink\ (ice\text{-}water\ solidification)}$ (W/m^{2}K)	401
Coefficient of heat transfer for the liquid nitrogen heat sink, $h_{sink\ (liquid\ nitrogen\ solidification)}$ (W/m^{2}K)	635.96
Height of the liquid eicosane samples, H (m)	0.009525
Depth of the aluminum molds, l_{Al} (m)	0.0047625
Length of the copper rod, l_{cu} (m)	0.184
Thermal conductivity of copper rod, k_{Cu} (W/mK) (Bergman et al., 2011)	403.2
Thermal conductivity of Aluminum molds, k_{Al} (W/mK) (Bergman et al., 2011)	238.47
Thermal conductivity of liquid eicosane samples, k_l (W/mK) (Nabil and Khodadadi, 2017, Stryker and Sparrow, 1990, Yaws, 1995)	0.148
Density of solid pure eicosane, ρ (kg/m^3) (Nabil and Khodadadi, 2017, Stryker and Sparrow, 1990)	840
Latent heat of eicosane, L_f (J/kg) (Nabil and Khodadadi, 2017, Hale et al., 1971)	247,000
Density of octadecane, ρ (kg/m^3) (Águila et al., 2018)	834
Thermal conductivity of liquid octadecane, k_l (W/mK) (Motahar et al., 2014)	0.151
Latent heat of octadecane, L_f (J/kg) (Ho and Gao, 2009)	243,100
Specific heat of solid eicosane, C_p (J/kgK) (Nabil and Khodadadi, 2017, Humphries and Griggs, 1977)	1920